Institut für Strömungsmechanik und
Hydraulische Strömungsmaschinen

Diffuser Augmented Hydrokinetic Turbines and their Application in Rivers

C. Mastaller

Universität Stuttgart

Mitteilung Nr. 48 | 2023

Diffuser Augmented Hydrokinetic Turbines and their Application in Rivers

Von der Fakultät Energie-, Verfahrens- und Biotechnik
der Universität Stuttgart zur Erlangung der Würde
eines Doktors der Ingenieurswissenschaften (Dr.-Ing.)
genehmigte Abhandlung

Eingereicht von
Christa Maria Mastaller
geb. Stadler
aus München

Hauptberichter: Prof. Dr.-Ing. Stefan Riedelbauch
Mitberichter: Prof. Dr.-Ing. Ewald Krämer

Tag der mündlichen Prüfung: 12.5.2023

Institut für Strömungsmechanik und Hydraulische
Strömungsmaschinen der Universität Stuttgart

2023

ISBN 978-3-948328-07-8

Universität Stuttgart
Institut für Strömungsmechanik und
Hydraulische Strömungsmaschinen
Pfaffenwaldring 10
D-70550 Stuttgart

Tel: +49-711-685-63260
Fax: +49-711-685-53255
Email: sekretariat@ihs.uni-stuttgart.de
http://www.ihs.uni-stuttgart.de

D 93 Stuttgart

Druck und Bindung: Druckerei Kormann, Geislingen an der Steige

Es is scho ois gsogt woarn, aber no ned von am jeden.
Karl Valentin

Vorwort

Das Schreiben von Texten jeder Art gehört ganz sicher nicht meinen Talenten und erfüllt mich auch nicht im geringsten mit Freude. So war das stundenlange Rumformulieren für mich auch die größte Hürde bei dieser Arbeit, noch dazu, da es meistens am fortgeschrittenen Abend stattfand, wenn die Kinder im Bett waren. Dass ich diese Arbeit trotzdem fertig gestellt habe, liegt zum einen daran, dass ich mich sehr für das Thema meiner Arbeit begeistert habe und die Arbeit deshalb unbedingt zu einem guten Ende führen wollte. Zum anderen und vor allem liegt es an der tollen Unterstützung zahlreicher Menschen, die mich während dem Schaffensprozess begleitet und davor bewahrt haben, die Nerven zu verlieren. Um mich bei diesen Menschen zu bedanken, überwinde ich hier ein letztes Mal während dieser Arbeit meine Aversion gegen das Schreiben:

Zunächst ein großes Dankeschön an meinen Doktorvater Prof. Stefan Riedelbauch, der trotz zwischenzeitlich deutlicher Probleme und Widrigkeiten das Projekt Kanada nicht vollständig aufgegeben hat und mir somit die Chance gegeben hat mich in diesem spannenden Themenfeld nach Herzenslust auszutoben. Auch für Ihre Betreuung und Unterstützung während meiner gesamten Zeit am Institut möchte ich mich herzlich bedanken. Vielen Dank an Prof. Krämer für den Mitbericht und die sehr gewissenhaften Anmerkungen zu meiner Arbeit.

Ein weiteres großes Dankeschön geht an Albert: Danke, dass du mich mitgenommen hast bei deinem Herzensprojekt kinetische Turbinen und mir so viel darüber beigebracht hast. Danke, dass du immer und jederzeit für meine Fragen und Probleme (nicht nur die fachliche) ein offenes Ohr hattest, auch noch lange nachdem du dich in den wohl verdienten Ruhestand verabschiedet hast.

Danke an alle Mitarbeiter mit denen ich während meiner Zeit am Institut zusammenarbeiten durfte, das stundenlange Sinnieren über die verschiedensten Probleme an diversen Tafeln oder das gemeinsame Betrachten von deutlich divergierenden Residuen aber auch das ein oder andere Feierabend- oder Korrekturbier wird mir auf ewig in Erinnerung bleiben. Ganz besonders bedanken möchte ich mich bei dir Jonas, vielen Dank für ALLES. Deine fachliche Beratung und die vielen Gespräche und Telefonate mit dir waren Gold wert und haben mir oft den dringend nötigen Motivationsschubser gegeben. Du bist ein wahrer Fluid-Magier. Alex, vielen Dank für die Elternzeitvertretung - ohne dich hätte ich nie so eine tolle Maschine zum Untersuchen gehabt [101]. Danke auch für das Korrekturlesen, ich hoffe du hast davon keine schlechten Träume gekriegt. Es war schon manchmal straff sich hinzusetzten und einen sinnvollen Umgang mit Fehlermeldungen wie “1.0 = 1.0 Think about it...” zu finden. Danke Stefan, dass du mit mir durch diese Vorhölle gegangen bist und auch für die sonstig OpenFOAM- Unterstützung. Einiges davon wird einen

ehrenvollen Platz auf meinem Dachboden finden... Danke auch an die Jungs von den Boulder-Brothers Simon, Hansi und nochmal Jonas für die abendliche Zerstreuung beim Überwinden der Schwerkraft. Danke an Olli, Sicherheitssalamander und gute Seele des Instituts, zu wissen dass du einem in jeglicher Art von Notfällen zur Steite stehst war ein sehr gutes Gefühl.

Ein weiterer großer Dank geht an meine Eltern, die mir und meinen Geschwistern von klein auf vermittelt haben, dass naturwissenschaftliche und technische Skills kein bevorzugtes Geschlecht kennen. Dieses Einstellung hat es mir sicher leicht gemacht meine Talente gut zu nutzen. Auch wenn ihr sicher nicht immer genau verstanden habt, was ich da mache, habe ich mich immer bestens Unterstützt aber nie unter Druck gesetzt gefühlt von euch <3. Mama, vielen Dank für die liebevolle und flexible Kinderbetreuung, die einen großen Beitrag zur praktisch Umsetzung dieser Arbeit geleistet hat. Auch an Omma Susanne vielen Dank, dass du oft kurzfristig eingesprungen bist, wenn Not am Mann war. Liebe Anne von der Kita, vielen Dank, dass du so toll bist und sich der kleine Mann so wohl bei dir gefühlt hat. Das hat mir den Abschied leichter gemacht und ich konnte mich während der Arbeitszeit gut auf diese Arbeit konzentrieren.

Miran, es war sicher nicht immer leicht, dass ich über lange Zeit abends nur physisch neben dir auf der Couch gesessen bin, mit dem Kopf aber immer ganz weit weg war. Danke für dein Verständnis, deine Unterstützung und dass du nie den leisesten Zweifel an der Sinnhaftigkeit dieser Unternehmung geäußert hast und dich am Schluss sogar noch beim Korrekturlesen durch die Arbeit gequält hast. DANKE (That's what she said). David und Laura ihr hab mich super-effizient gemacht, weil ihr so toll seid, dass ich möglichst wenig Zeit mich euch verpassen wollte <3.

Trotz meiner Schreibaversion ist dieser Text jetzt doch überraschend lang geworden... Final bleibt nur noch zu sagen: DIDIT

Abstract

Hydrokinetic turbines are suitable for exploiting unused potential for electrical energy generation in rivers, since they can be used comparatively simple also in sensitive areas. When applied in rivers, the rotor diameter and thus also the power of such a turbine is often limited by a low flow depth. Therefore, it is advisable to equip the rotor with a diffuser at such locations. A large diffuser opening to the sides can increase the projected area of the machine and thus the power.

In order to determine the exact power for such a diffuser augmented hydrokinetic turbine at a potential site an advanced turbine model for 2d shallow water simulations is developed in this work. This requires a deep understanding of this particular turbine type, which is obtained by detailed numerical investigations of several different diffuser geometries. Also site effects, such as the blockage effect of kinetic turbines in narrow channels and sheared flow effects, are investigated in detail by means of numerical 3d flow simulations.

All findings from these studies are included in the development of the advanced turbine model. Regarding the model implementation in the 2d shallow water solver also the blockage effect in the 2d model has to be considered. Among other things, this effect causes the high sensitivity of the model to the dimensioning of the turbine cell.

The final turbine model is applied to simulate turbines in different rectangular channels and at a potential site in Montreal, Canada. The results are compared with results of corresponding 3d simulations to successfully verify the model. Finally, the model is applied to evaluate the arrangement of five diffuser augmented hydrokinetic turbines. A total hydraulic power of the turbine park of around 1.8 MW is determined. This could supply around 635 Canadian households with electricity.

Kurzzusammenfassung

Um bisher ungenutztes Potential zur Erzeugung elektrischer Energie in Flüssen nutzbar zu machen, bieten sich kinetische Strömungsturbinen an, da sie relativ unkompliziert auch in sensiblen Bereichen eingesetzt werden können. Bei einer Anwendung in Flüssen sind der Rotordurchmesser und damit auch die Leistung oft durch eine geringe Fließtiefe limitiert. Deshalb bietet es sich an solchen Standorten an, den Rotor mit einem Diffusor auszustatten. Durch eine starke Diffusoröffnung zu den Seiten können die projizierte Fläche und somit die Leistung erhöht werden.

Um die genaue Leistung an einem potentiellen Standort für eine ummantelte kinetische Turbine bestimmen zu können, wird in dieser Arbeit ein erweitertes Turbinenmodell für 2d Flachwassersimulationen entwickelt. Hierfür ist ein tieferes Verständnis dieses speziellen Turbinentyps erforderlich, welches durch die numerische Untersuchung zahlreicher verschiedener Diffusorgeometrien erlangt wird. Auch Standorteinflüsse, wie der Verblockungseffekt von kinetischen Turbinen in engen Kanälen und die vertikale Geschwindigkeitsverteilung, werden detailliert mithilfe von numerischen 3d Strömungssimulationen untersucht.

Alle Erkenntnisse aus diesen Studien fließen in die Entwicklung des erweiterten Turbinenmodells ein. Bei der Implementierung des Turbinenmodells im Flachwasserlöser muss zudem der Verblockungseffekt im 2d Modell berücksichtigt werden. Dieser führt unter anderem dazu, dass das Modell sehr sensibel auf die Dimensionierung der Turbinenzelle reagiert.

Das fertige Turbinenmodell wird zur Simulation von Turbinen in verschiedenen Rechteckskanälen und an einem potentiellen Standort in Montreal, Kanada, angewandt. Die Resultate werden mit den Ergebnissen entsprechender 3d Simulationen verglichen und so das Modell erfolgreich verifiziert. Schließlich wird das Modell zur Evaluierung der Anordnung von fünf ummantelten kinetischen Turbinen angewandt, wobei eine hydraulische Gesamtleistung des Turbinenparks von ca. 1.8 MW bestimmt wird. Damit könnten rund 635 kanadische Haushalte mit Strom versorgt werden.

Contents

List of Variables

Latin Letters

a	$-$	induction factor
A	m^2	area
B	m	width
c	$-$	constant
c_D	$-$	drag coefficient
c_P	$-$	power coefficient
c_T	$-$	thrust coefficient
D	m	diameter
f	$-$	manipulation factor
F_s	N	support force
g	$\mathrm{m/s}^2$	gravitational acceleration
h	m	height, depth
h_0	m	bathymetric bed elevation
h_{total}	m	absolut water level
hU	m^2/s	specific discharge
k	$-$	loss coefficient
k_s	m	sand grain roughness
L	m	length
M_z	Nm	torque
n	$\mathrm{s/m}^{1/3}$	Manning roughness coefficient
n	$-$	normal vector
n	rpm	runner speed
P	W	power
p	$\mathrm{N/m}^2$	pressure
Q	m^3/s	discharge
q	$-$	mass flow ratio
r, R	m	radius
S	N	momentum source term
t	s	time
T	N	thrust
$\overline{u}$	m/s	depth-averaged velocity
u_∞	m/s	upstream undisturbed velocity
$u_{\infty,t}$	m/s	upstream undisturbed velocity in sheared flow

u_h	m/s	velocity in hub height
u_d	m/s	velocity averaged across rotor height
u_v	m/s	velocity averaged across rotor area
u^+	–	dimensionless velocity
u, v, w	m/s	velocity components
x, y, z	m	coordinates
y^+	–	dimensionless wall distance

Greek Letters

α	–	aspect ratio
β	°	flow angle
γ	–	diffuser area ratio
Δ	–	difference
ϵ	–	channel blockage ratio
η_r	–	rotor efficiency
κ	–	von Kármán constant
ν	m^2/s	kinematic viscosity
ρ	kg/m^3	density
τ	–	thrust ratio
τ	N/m^2	shear stress
$\tau_{b,i}$	N/m^2	soil friction
ω	rad/s	angular velocity

Indices

AD	actuator disk
ax	axial
BC	boundary condition
bed	bed roughness
betz	according to Betz-Limit
c	channel
calc	calculated from turbine model
cell	turbine cell value
d	diffuser exit
dev	deviation in velocity profile
ds	downstream
hub	hub height
mag	magnitude
max	maximum

mech	mechanical
r	rotor
s	sheared flow
t	turbine
total	total (rotor + diffuser)
w	wake flow
∞	infinit flow conditions

Superscripted indices

$+$	upstream of rotor
$-$	downstream of rotor

Abbreviations

ABL	Atmospheric Boundary Layer
AD	Actuator Disk
ADCP	Acoustic Doppler Current Profiler
AMSL	Above Mean Sea Level
BLC	Boundary Layer Control
CFD	Computational Fluid Dynamics
CV	Control Volume
DAT	Diffuser Augmented Turbine
DAWT	Diffuser Augmented Wind Turbine
GGI	General Grid Interface
LES	Large Eddy Simulation
LMADT	Linear Momentum Actuator Disk Theory
M	Million
MP	Mixing Plane
NACA	National Advisory Committee for Aeronautics
RANS	Reynolds Averaged Navier Stokes Equations
SST	Shear Stress Transport
SWE	Shallow Water Equations
TRN	Transient
UTM	Universal Transverse Mercator
VoF	Volumen of Fluid
1d	one-dimensional
2d	two-dimensional
3d	three-dimensional

1 Introduction

Driven by the transition towards sustainable energy production renewable energies receive increased attention in research and development but also in public discussion. A very well-tried and highly developed technology with low carbon footprint (during operation), a high overall efficiency and a long runtime is conventional hydro power. This technology uses the potential energy between two water bodies. In most cases the potential has to be generated artificially by damming a river or channel. For storage power plants the water body is stored by large damming structures, generating a large head and storage volume. Those plant types are usually located in the upper course of rivers, mostly in alpine regions. In middle and lower courses of the river run-of-river power plants are more common. They are characterized by a low head and thus a smaller damming structure but a high flow rate.

However, the interruption of a natural river course by a damming structure has a large impact on the river as a natural habitat for fauna and flora. The disturbance of the ecological passability influences fields like fish migration, natural sediment transport, flow velocity, oxygen content and seasonal run-off fluctuations (alluvial forest). Furthermore, large damming structures are often a major impact in landscape and in some cases even require the resettlement of people. All those factors lead to a controversial discussion of conventional hydro power.

In 2000, the ecological status of watercourses was assessed for the first time at European level through the introduction of the European Water Framework Directive. It states that the member countries have to focus on protecting and improving the status of aquatic ecosystems and related terrestrial ecosystems and wetlands with regard to their water balance. A good ecological state has to be reached within 15 years and a degradation of the current state is prohibited. This target can be reached through measures like bypass waters, fish ladders or fish elevators. Also the introduction of small or micro hydro power technologies like partly bypassed power plants (*Schachtkraftwerk* [87], *Das bewegliche Wasserkraftwerk* [46]), gravitation water vortex power plants [65] and Archimedes' screw turbines [75, 90] can help to generate electrical energy in a more ecologically sustainable way.

Nevertheless, the most effective way to preserve the river's passability is to avoid transverse damming structures. Hydrokinetic turbines are a good way to achive this and still use a river's energy. The operation principle is based on the conversion of kinetic flow energy rather than the potential energy. This approach is similar to conventional wind turbines and eliminates the need for damming, which makes them also interesting for the application in tidal currents.

For this type of energy conversion the Betz Limit defines a theoretical maximum for possible extraction of kinetic energy from the flow: Only about 59% of the available

kinetic energy can be extracted from the flow [11]. Furthermore, those turbines usually do not block the entire flow cross section. Therefore, a large amount of river run-off, and thus energy, is bypassing the turbine without being utilized. Due to these two facts, hydrokinetic turbines cannot adequately replace conventional power plants in terms of power output. Moreover, some concerns have been raised regarding the fish-friendliness of hydrokinetic turbines, in particular mechanical damage from blades, negative impact through rotor noise and orientation problems caused by the magnetic field of the generator. However, many studies show that these impacts are observed to be very low [1, 17, 18, 91]. Generally, hydrokinetic energy is well predictable, environmentally and ecologically friendly with minimal visual impact and very low carbon emission [41].

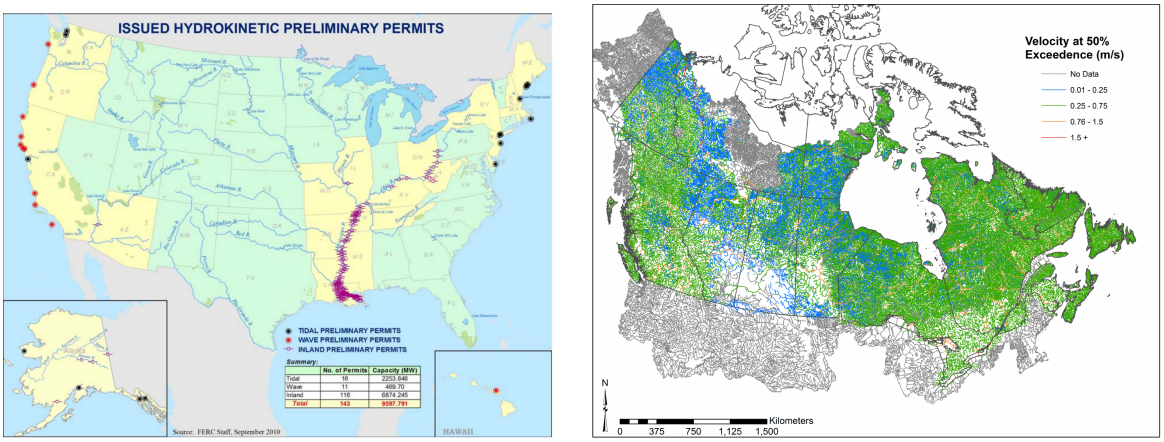

(a) Preliminary permits for hydrokinetic projects issued by the U.S. Federal Energy Regulatory Commission as of September 2010 [17]

(b) Velocity map for Canadian water bodies - 50% exceedance probability [14]

Figure 1.1: Hydrokinetic Energy Potential in North America

Hence, hydrokinetic river turbines may give access to the energy potential of river sections where the construction of a conventional hydro power plant is not possible for ecological, environmental or geographical reasons. Also in densely populated areas, which may not be flooded, unused energy potential can be exploited with this technology. Furthermore, those turbine types are suitable for energy generation in remote areas and for decentralized energy supply. This makes hydrokinetic river turbines particularly interesting for developing and emerging countries with large river systems, where they may replace diesel and fuel generators with little effort under suitable boundary conditions [4, 91, 104]. As those turbines may be arranged in a large number (e.g. in turbine parks) and the development is mostly site-independent a serial production may reduce costs.

With regard to site assessment for kinetic turbines, a high flow velocity is desirable. Furthermore, a sufficient flow depth has to be considered in order to provide enough space for a large rotor. In Europe and especially in Germany conditions for a

feasible operation of hydrokinetic turbines can hardly be met [2]. The potential for hydrokinetic turbines is very low here. The situation is different in North America, were the United States provide good conditions for hydrokinetic energy recovery in rivers (3,000 MW [27] - 12,500 MW [9]). As shown in Figure 1.1a the U.S. Federal Energy Regulatory Commission (FERC) permitted hydrokinetic river projects in the range of 7,000 MW in 2010, mainly in the Mississippi River and in Alaska [17, 50]. With around 340 GW also Canada shows a large potential for the use of kinetic energy in rivers [14, 86]. A map of the available kinetic energy in Canadian water bodies is shown in Figure 1.1b. For further promising regions, especially in emerging countries, detailed potential analyses are not yet available.

1.1 State of the Art

The development of hydrokinetic river turbines is a complex issue. For a successful design and project planning many correlations have to be considered. The most important design considerations are summarized by Laws [60] and shown in Figure 1.2.

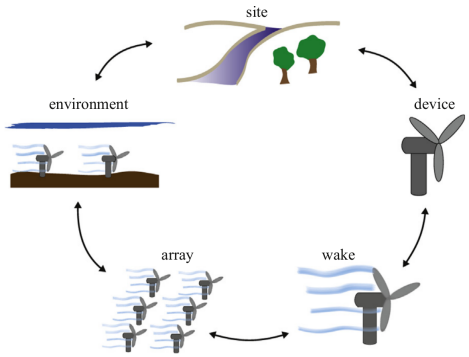

Figure 1.2: Design considerations for hydrokinetic turbines from [60]

The start point in turbine development is a detailed site evaluation in order to determine the relevant boundary conditions and estimate the expected power output. In this step, also the basic design parameters are defined. All those data are used for the detailed turbine design, which nowadays is often supported by numerical methods. Sometimes, automatic optimization tools are used to achieve optimum results in the design process [82, 101]. With the finalized design the wake flow - the response of the machine on the working fluid - may be estimated numerically or experimentally. In a next step possible park arrangements are investigated considering the interaction between several turbines. Also the interaction between the machine(s) and the turbine site has to be evaluated. Depending on the results the turbine design may have to be adapted. In the following, the relevant technical literature is reviewed with regard to all those different steps and aspects in the turbine design process. A more detailed analysis and performance comparison of the different diffuser geometries gathered in this literature review is presented later in this work.

1.1.1 Hydrokinetic Turbine Devices

Regardless of their application as tidal-current or river-stream turbine hydrokinetic turbines may be classified by the orientation of their axis of rotation [54], as illustrated in Figure 1.3.

The most common turbine type is the horizontal axis turbine, which usually consists of a single rotor comparable to classical wind turbines. In this case, the rotational axis is parallel to the main flow velocity vector (see Figure 1.3a). The rotor converts the kinetic energy of the flow through the lift force generated by the profiled rotor blades similar to aircraft wings [60]. Placed around a fixed rotational axis, the lift force is transformed to rotational energy. The main advantages of horizontal axis turbines is that they provide a rather large flexibility through blade pitching with regard to overspeed protection and efficient operation. Moreover, the optimum performance of those turbines is achieved at competitively high rotor speeds, which allows to use small and cheap generators. An additional advantage is that an annular ring augmentation can be applied due to the round projected rotor surface [54]. On the other hand, axial turbines are strongly dependent on the direction of flow. Therefore, they are more suitable for locations with steady and uniform flow direction. Furthermore, the generator has to be placed underwater, which leads to high costs in development, production and maintenance.

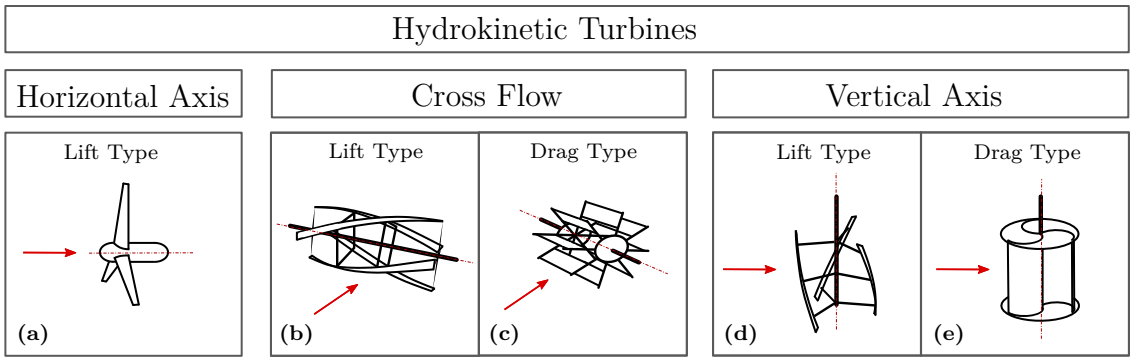

Figure 1.3: Overview over different types of hydrokinetic turbines

Vertical axis turbines are characterized by an axis direction perpendicular to the water surface and the main flow direction as illustrated in Figure 1.3d and 1.3e. For cross flow turbines the rotor axis is parallel to the water surface and orthogonal to the main flow direction (see Figure 1.3b and 1.3c). Both turbine types can be subdivided into lift type and drag type turbines. The blades of the lift type turbines are profiled to generate the necessary lift force. The most prominent example in this family is the Darrieus-Rotor. Drag type rotors use the resistance of the blades to generate the rotational energy similar to cup anemometers used for wind speed measurements. Those blades are commonly shaped in a simple two dimensional geometry (Savonius-Rotor). For vertical axis turbines, it is possible to place the generator above the water surface and thus save costs. Also the simple blade shape can contribute to economic efficiency. Moreover,

those turbine types are independent of the flow direction. On the other hand, some of the cross flow and vertical axis turbines require a starting mechanism due to a low starting torque. In addition, the maximum achievable efficiency is generally low compared to horizontal axis turbines [43, 54, 104]. Besides the subdivision from a hydrodynamic point of view for hydrokinetic turbines presented here, a classification according to generator type, mounting system or field of application is also possible.

According to Khan, horizontal axis turbines are the most common hydrokinetic turbine types [54]. For those machine types the Linear Momentum Actuator Disk Theory (LMADT) introduced by Lanchester and Betz provides good results for a first estimation of turbine power output under the assumption of an infinitely large flow field around the machine [16]. This 1d theory, which is based on the conservation of mass, energy and momentum, states that only a part of the available kinetic energy may be extracted from the flow. The residual energy is required to further transport the fluid downstream of the rotor. The power extracted by the rotor may be determined by the following equation:

$$P = \frac{\rho}{2} A_r \, c_P \, {u_\infty}^3 \tag{1.1}$$

where u_∞ is the infinite undisturbed upstream flow velocity, A_r is the projected rotor area and c_P is the rotor power coefficient. According to the theory, a maximum power coefficient of $c_P = 16/27$ is theoretically possible.

1.1.2 Diffuser Augmented Turbine Devices

From Equation 1.1 it can be derived that the main basic design parameter to increase the generated power is the projected rotor area A_r. For an application of hydrokinetic turbines in rivers, the rotor diameter and thus the area is limited by the flow depth (see Figure 1.4a). The space limitation can be overcome by augmenting the rotor with a diffuser. This allows increasing the projected area to the sides as the diffuser exit is not necessarily circular. Figure 1.4b shows this advantage of the so-called diffuser augmented turbines in limited space.

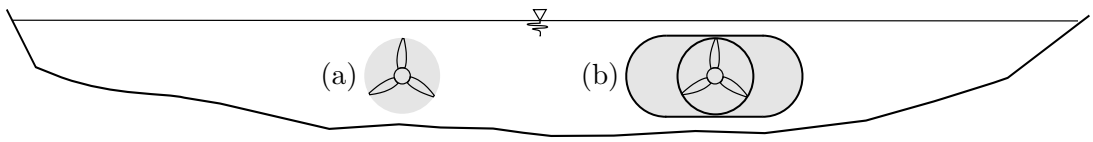

Figure 1.4: Projected area of (a) single rotor turbine and (b) diffuser augmented turbine

The application of diffusers for hydrokinetic turbines has several further advantages: The suppression of the tip vortex leads to a reduction of flow losses, but also the noise emission is reduced. Furthermore, the diffuser increases the mass flow capacity and pressure difference at the rotor. Alternatively, the size of the rotor can be significantly

decreased for a similar projected area of the total machine leading to a higher rotor speed and hence a reduction of the generator costs. Moreover, diffuser augmented turbines are less sensitive to inclined flow angles [21].

However, a diffuser is a large building structure with a large projected area and thus a large flow resistance. This leads to increased demands in terms of stability and mounting. In general, diffuser augmented turbines require increased technical and financial effort and it must be carefully weighted whether this is worthwhile. Furthermore, the concept is very sensitive from the hydrodynamical point of view, as the mass flow capacity of the machine is highly depending on the efficiency of the diffuser. Consequently, a disadvantageous design can disturb the operation principle of a diffuser augmented turbine and significantly reduce its performance. For this reason, important design parameters identified in relevant literature will be reviewed more closely in the following.

As for most kinetic energy converters, early research on diffuser augmented turbines was performed in the field of wind turbines. Some of the first to work on this problem intensively were Lilley and Rainbird [62]. They presented a theoretical approach to determine the augmentation of power obtained by using a diffuser. They were already able to identify important design parameters such as the diffuser expansion ratio and the external shape of the diffuser at the exit by means of their theoretical considerations. Since then, many researchers tried to analytically solve the momentum theory for diffuser augmented turbines [15, 22, 44, 61, 78, 92, 102]. Finally, all of them had to rely on theoretical assumptions or empirical or experimental data in order to describe characteristic fluid dynamical attributes of the diffuser. Depending on the theoretical approach attributes like diffuser efficiency, inlet efficiency, exit pressure, back pressure and/or thrust ratio are used. In some cases calculations based on unloaded flow augmentation (empty diffuser without rotor) are used to predict the performance of diffuser augmented turbines (e.g. [44]).

One of the first to perform experimental research on diffuser augmented wind turbines was Igra [47–49]. He examined various diffuser concepts. An early design consists of a straight wall diffuser with differently shaped intakes. He tried to reduce the diffuser length by placing ring-shaped wings at the rear end of the diffuser [47]. In a next generation he decided to shape the whole diffuser as a circular NACA wing profile in order to generate a high lift force. As for these designs flow separations occurred, bleeding channels were introduced to accelerate the boundary layer flow. This provided a significant improvement [49]. As an alternative to this complex construction, Igra combined previous designs by equipping the wing-shaped diffuser with a flap at the diffusers rear end [48]. In his extensive research, Igra covered all relevant design options for diffuser augmented axial kinetic turbines. Those can be divided into **single-stage** and **multi-stage** concepts. Single-stage diffusers tend to flow separation at the diffuser walls. This may be suppressed by **boundary layer control (BLC)**. For single-stage concepts this can be achieved by bleeding or a large gap between rotor and the shroud. Multi-stage concepts automatically include boundary layer control through the gaps between the different stages.

Single-Stage Diffusers:

An overview of the different single-stage diffuser designs summarized in the following are schematically illustrated in Figure 1.5.

In the field of single-stage diffuser development Lewis et al. performed experiments on a straight-line contour diffuser. During the test series the diffuser area ratio was changed by varying its length at a fixed diffuser angle [61]. The straight-line diffuser design was taken up by Gaden and Bibeau, who numerically investigated different diffuser geometries varying the area ratio and diffuser opening angle [33]. Ohya et al. considered the diffuser shape at the outlet to be of major importance [71]. They developed a straight-line diffuser which is characterized by an extensive flange fixed at the trailing edge. The size of this flange also leads to a large projected machine area and hence a large area ratio. In a later study Ohya and Karasudani concentrated on the experimental investigation of diffusers with more moderate area ratios, varying the flange dimensions [70]. Also the diffuser contour was changed to a curved more compact shape called *wind-lens*.

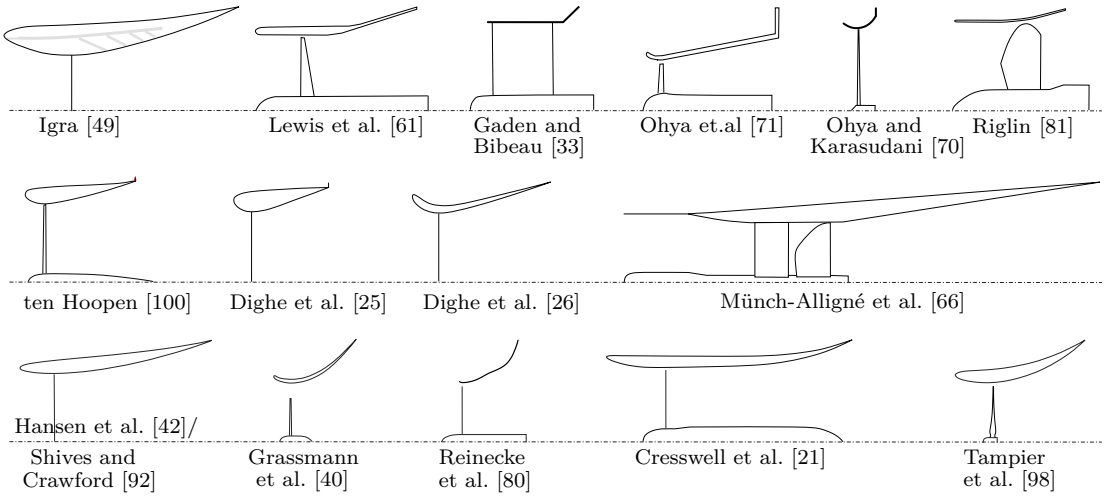

Figure 1.5: Overview of single-stage diffuser geometries from literature

Hansen et al. and later Shives and Crawford rather followed the example of Igra applying wing-shaped diffuser contours based on the NACA profile series [42, 92]. Both used numerical flow simulations. Shives and Crawford investigated different diffusers for tidal turbines, where the variation of the NACA profiles lead to varying area ratios and outlet angles of the diffuser. They observed a higher performance, but a reduced diffuser efficiency for an increase of area ratio. Similar to Hansen et al. they introduced a small gap between actuator disk and diffuser, observing that this improves the performance by acting as boundary layer control. Grassmann et al. also considered a large rotor gap (35% the rotor radius) [40]. This allowed them to apply a large area ratio to their wing-shaped diffuser without observing flow separation at the diffuser walls from the CFD results. The advantageous effect of the rotor gap was also used by Reinecke et al. for the design of a diffuser augmented ocean current turbine [80].

They performed an automatic optimization of the diffusers contour based on B-splines keeping the area ratio constant. Through the optimization a good improvement compared to a straight line diffuser could be reached. In their CFD simulations they used an actuator disk for modeling the rotor. Still the results showed good agreement with the experimental results from the model test. The boundary layer control through the tip gap jet was also used by Cresswell et al. [21]. The diffuser for tidal turbines is wing shaped with moderate area ratio. They also investigated the influence of yaw flow on diffuser augmented turbines (DAT). Tampier et al. separately investigated the performance of a bare rotor and a bare diffuser in a numerical model [98]. Finally they set up a model including both the rotor and the diffuser including a rotor gap. In the separate diffuser simulation flow separations at the diffuser walls occurred. For the combined simulations the backflow zone moved downstream of the hub. The authors concluded that an isolated view of rotor and diffuser is not possible without further consideration.

The diffuser concept called *DonQi Urban Windmill* presented by ten Hoopen consists of a circular airfoil geometry [100]. He focused on the experimental analysis of the benefits provided by vortex generators placed at the trailing edge of the diffuser. It turned out that the vortex generators cause a slight improvement in performance. Dighe et al. used the *DonQi Urban Windmill* design as reference [25]. At first they experimentally and numerically investigated the effect of using flaps (spoiler) at the diffuser outlet. They observed a significant positive influence on the performance caused by the flap but also an increase in total drag. In a next step the diffuser design was manually optimized using numerical flow simulations [26]. They could show that the performance significantly increases when increasing the duct profile camber, leading to a larger redirection of the flow at the diffuser exit.

The diffuser design presented by Riglin et al. was developed for hydrokinetic river turbines. He compared experimental and numerical tests on the full turbine geometry including blades with good agreement [81]. Münch-Alligné et al. developed a straight wall single-stage diffuser for a river channel. They used numerical simulations for the evaluation of the turbine performance. The machine was simulated in-situ, with a pressurized fixed water surface on the one hand and considering the interaction between turbine and water surface by using a multi-phase flow simulation on the other hand [66].

Multi-Stage Diffusers:

Figure 1.6 provides a summarizing overview over the various multi-stage diffusers published in technical literature.

Parallel to the development of single-stage diffusers, the research in the field of multi-stage diffusers was pushed by the Grumman Aerospace Corporation, namely by Oman, Foreman and Gilbert [73]. They published an analytical framework and experimental investigations on different concepts of single-stage and multi-stage diffusers for wind turbines. Within their work, also the application of flange-like flaps at the diffuser outlet was tested. Besides the boundary layer control, those flaps were identified as an important design parameter. During the experiments the pressure

drop at the rotor was simulated by screen meshes. The work at Grumman Aerospace on diffuser augmented wind turbines continued for a long period leading to many publications, such as [31, 35–37, 74]. A group of New Zealand scientists picked up the Grumman concept and together with Foreman developed the *Vortec 7* turbine [77]. This diffuser was further improved by Phillips using numerical and experimental methods [78]. He finally presented three adapted geometry versions, of which the last one is characterized by a significant increase of the diffuser stages. Also Dighe et al. based their work on a previous diffuser design [24]. They used the idea of Igras wing-shaped diffuser with a flap wing at the rear diffuser end [48] and combined it with the findings for single-stage diffusers presented in [26].

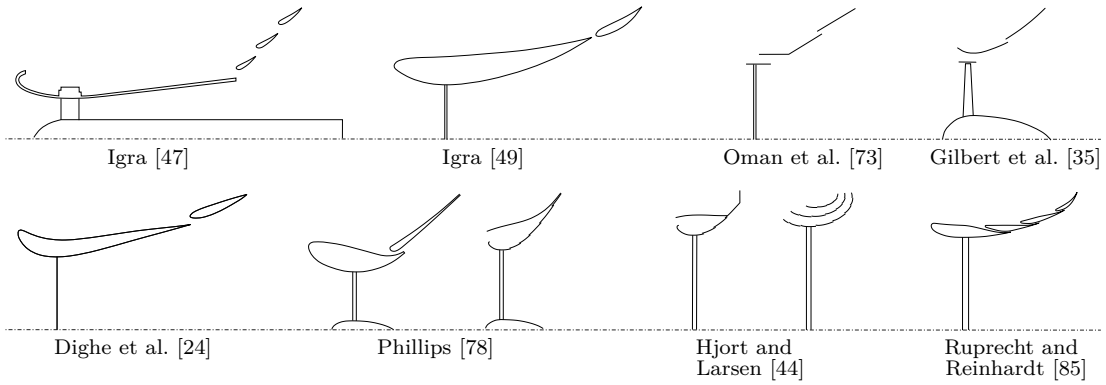

Figure 1.6: Overview of multi-stage diffuser geometries from literature

Ruprecht and Reinhardt developed a multi-stage diffuser for tidal current energy application [85]. Their diffuser concept was manually optimized using numerical flow simulations. Also Hjort and Larsen picked up the idea of boundary layer control through a large amount of diffuser stages and further developed the geometries presented by Ohya [70] and Philipps [78]. By introducing a multi-stage and multi-layer diffuser they could reach outstanding results in performance in relation to the projected machine area using numerical simulations [44].

Non-Circular Diffusers:

As already mentioned, the main benefit of a diffuser augmentation for kinetic river turbines is the fact that the projected machine area, respectively the diffuser exit area, does not necessarily have to be circular. All the publications analyzed previously discuss rotationally symmetric diffuser designs. Literature on non-circular diffuser concepts is barely available. However, two corresponding projects could be identified: Ruopp et al. developed a single-stage diffuser for a kinetic river turbine with a nearly rectangular diffuser exit area [84]. Large vents at each of the diffuser sidewalls provide an active boundary layer control. Furthermore, the diffuser is equipped with a spoiler at the exit. Detailed numerical investigations of the geometry showed good agreement with prototype measurements performed at the St. Lawrence River in Montreal, Canada, where the machine has been running since 2010 [84]. A further example for non-axis-symmetric diffusers is provided by Sierra-Del Rio et

al. They developed a two-stage diffuser, where the first stage consists of an annular hydrodynamic profile and the second stage is a diffuser opening exclusively to the sides. The geometry including a three-bladed rotor was evaluated using numerical flow simulations. Compared to a single rotor turbine, a significant improvement in performance could be observed [23].

Besides those two scientific publications there are several more or less active projects on non-circular diffuser turbines for river use by private companies, such as the river turbine developed by the German pump manufacturer KSB AG [57, 58], the Strom-Boje [5, 6] and multi-stage kinetic turbine by Smart Hydro [94]. Unfortunately, there are no scientific publications on those projects available. An overview over the different concepts of non-circular diffusers is given in Figure 1.7.

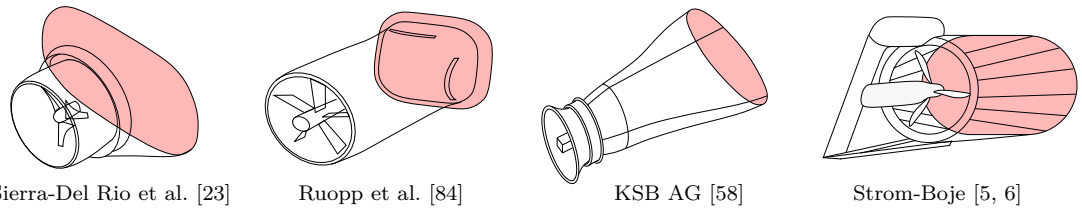

Sierra-Del Rio et al. [23] Ruopp et al. [84] KSB AG [58] Strom-Boje [5, 6]

Figure 1.7: Overview of not axis-symmetric diffuser geometries from literature

Despite the specific diffuser concepts, it is generally agreed in technical literature that a diffuser augmentation of a single rotor leads to an increase of turbine power. Furthermore, the scientific community agrees that with increasing area ratio, also the performance increases. However, Khan has already noted: "Nevertheless, detailed investigation on optimal size, shape and design is still an unsolved problem." [54].

1.1.3 Impact of Site Effects for River Applications

As already observed by Laws [60], turbine design is an important, but not the only relevant point for a hydrokinetic turbine project. Also the interaction of the machine with the environment plays a major role. Usually, for the machine design process ideal numerical or experimental boundary conditions are assumed. At potential turbine sites, other conditions may prevail. Especially with regard to a river application, the assumption of an infinitely large far-field is not given, since the flow depth is in most cases limited. The effect of cross section blockage through the turbine plays a major roll. Also the arrangement of several turbines in a cross section (turbine park) and the interaction between turbine and water surface, which are special cases of the blockage effect, are relevant topics. Furthermore, the upstream flow velocity is usually not constant but can be influenced by a high roughness river bed leading to a sheared flow profile. All those different site effects have to be investigated and considered (see Figure 1.8). Since hydrokinetic river turbines are still rather a peripheral subject in research, relevant literature from wind turbine research is also discussed in the following in case the results seem to be transferable.

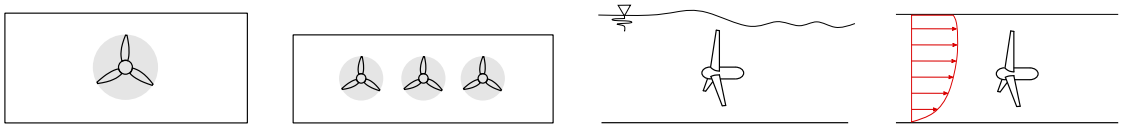

Figure 1.8: Overview of different impact factors at river sites

Influence of Channel Blockage:

The channel blockage phenomenon was analytically investigated and discussed in detail by Garrett and Cummins [34]. Their approach is based on an adapted formulation of the LMADT for an ideal actuator disk operated in a limited channel cross section. They were able to derive a theoretical correlation: the machine performance increases significantly with increasing channel blockage. Also Houlsby et al. presented an extensive theoretical discussion on channel blockage through kinetic turbines based on the LMADT [45]. They considered three different scenarios: an actuator disk in a finite, pressure constrained flow field, an actuator disk in a finite parallel sided tube and an actuator disk in an open channel flow including the free water surface. Nishino and Willden [68] numerically examined the theory presented by Garrett and Cummins. They observed a good agreement between theory and numerical simulations using the standard k-ϵ-model. The results changed significantly for a high blade-induced and free-stream turbulence caused by turbulent mixing effects downstream of the actuator disk.

Sørensen et al. investigated the interaction between rotors or propellers and channel side walls for model test results in narrow wind tunnels [95]. They derived an equation to determine an equivalent free flow velocity as a function of the projected rotor area, the area of far-wake and the channel cross section. By means of this equivalent velocity the quantities observed in the blocked channel flow may be corrected using the principle of kinematic similarity. This model is based on the one-dimensional momentum theory and was validated through axis-symmetric CFD simulations using the actuator disk method. Also Bahaj et al. used this approach for their turbine blockage correction [7]. In their case the equivalent free flow velocity may be determined by the thrust coefficient and the far-wake area.

Schluntz and Willden numerically investigated different rotor designs including the turbine hub using a RANS-based blade element method to model the rotor [89]. The different rotors were located in channels with various cross sectional areas and different aspect ratios. They observed that it is advantageous to adjust the rotor design to the specific blockage situation. However, the increase in power determined in their work is less than the values predicted by the 1d theory. The reason for this is most probably the influence of the hub. Also Kinsey and Dumas performed a detailed numerical investigation of channel blockage through kinetic turbines whereby they resolved the blade geometry of a horizontal axis turbine on the one hand and a crossflow turbine on the other hand [55]. They observed that for aspect ratios smaller than three, turbine type and aspect ratio are not dominating the observed correlation. Generally, horizontal axis turbines were identified to be less sensitive to varying aspect

ratios. Within their work it was furthermore observed that the theoretical correction presented by Bahaj et al. [7] showed good results for axial turbine types but also the blockage correction for cross flow turbines was acceptable. Tampier and Zilic de Arcos analyzed a number of different theoretical blockage correction approaches from literature using results from numerical flow simulations of a blade resolved horizontal axis rotor in different channel cross sections [99]. The different approaches were observed to vary strongly in quality. The best results for blockage correction were observed when using the approaches provided by Soerensen et al. [95] or Bahaj et al. [7].

Also blockage effects of diffuser augmented turbines in channels are a research topic in technical literature. Again engineers from Grumman Aerospace, namely Loeffler and Steinhoff, were one of the first to perform detailed investigations [63]. They used the method of multiple images for the computation of interference effects at wind tunnel walls for experiments with ducted rotors. The blockage ratio is defined as ratio between diffuser outlet diameter and the wind tunnel cross section in this case. Belloni numerically investigated the blockage effect in narrow channels for a bare turbine (actuator disk) and a bi-directional diffuser augmented turbine [10]. She observed that a bare and a ducted turbine are both affected in a nearly similar way by blockage effects.

In the course of a detailed investigation of his diffuser augmented turbine Reinecke performed a numerical study on the turbine blockage of three different channel geometries [79]. However, he could only observe a minimal influence of blockage ratio on the turbine performance which is a significant deviation from the LMADT and Belloni's results. The reason for this deviation could be that a constant disk load was assumed in the study and thus the influence of the blockage effect on the optimum operation point was neglected.

Considerations on turbine park arrangements are a special cases of blockage effects. A large number of publications are available on the investigation of arrays of single rotor turbines, such as [67, 69, 103]. For diffuser augmented turbines Goltenbott et al. published a study on very densely arranged turbines [38]. However, the turbine park literature is not analyzed in detail, as for this work only a small number of turbines is planned to be installed. Also the interaction between the water surface and kinetic turbine is well investigated [45, 56, 76, 105] but also this effect is not considered in detail here, as it is directly modeled by the shallow water solver.

Influence of Shear Flow:

A further environmental impact is the variation of flow velocity over the flow depth. This so-called sheared flow velocity profile shows large gradients, especially in shallow waters, as the roughness of the river bed has a strong influence on the overall velocity distribution. Still most of the relevant literature on sheared flow conditions for kinetic turbines is published in the context of wind turbines and the atmospheric boundary layer profiles (ABL) which are typical for atmospheric flows.

De Vries discussed the influence of the wind velocity profiles occurring due to the surface roughness of the ground [22]. He suggested averaging the varying wind velocity over the height of the rotor in order to determine the annual energy flux. Two different ways for the mathematical description of the wind profile were suggested: a power-law and a logarithmic formula, whereas he preferred the first one.

In their work, Wu and Porté-Agel performed a series of LES simulations on a single horizontal axis wind turbine in ABL flows characterized by different bottom roughness investigating the influence on the turbine wake flow [106]. To model the rotor an actuator-disk model considering rotation was used. They found out that a rough terrain leads to a faster wake recovery compared to a smooth terrain. The basic effect could be isolated by using different turbulence intensities at an inlet boundary with similar velocity profile and roughness. It was observed that the higher inlet turbulence causes a considerable influence on the wake flow.

Also Nishino and Draper numerically investigated three different inlet boundaries for a wind park arrangement: a low turbulence inlet with constant inlet velocity, a high turbulence inlet with constant inlet velocity and a high turbulence inlet with a sheared flow distribution [67]. Similar to Wu and Porté-Agel [106] they could conclude that the influence of a high level of ambient turbulence is more dominant for the development of the wake flow and the power coefficient than the velocity distribution. For both high turbulence inlet conditions a significant increase in power coefficient occurred when referring it to the upstream velocity averaged across the disk area. Contrary to this, Bartl et al. noticed that the upstream turbulence, as well as the sheared flow inlet does only have a very minor influence on the power coefficient, when referring it to the velocity in hub height during experimental investigations of different inlet conditions for a single rotor wind turbine [8].

In the research on tidal turbines in sheared flow Mason-Jones et al. [64] performed a detailed investigation on the influence of a profiled velocity distribution compared to a constant velocity on the performance of a horizontal axis rotor. In the numerical model the rotor geometry was fully resolved. They were able to prove that the power curves for the two different inflow conditions are almost identical when using the volume-averaged velocity over the rotor area for the determination of the power coefficient of the sheared flow results.

Fleming et al. numerically and experimentally investigated a single rotor tidal turbine in a sheared flow varying the hub height of the turbine [30]. They suggested a redefinition of reference velocity, considering the level of flow shear (area-average of the velocity cubic over the projected rotor area) which allowed them to eliminate the observed deviations in turbine thrust and performance.

A similar conclusion was drawn by Blackmore et al. during extensive model tests of tidal turbines under different ambient turbulence conditions [12]. They observed that for a low upstream turbulence length scale the averaged velocity over the rotor area provided good results as reference velocity. However, for larger length scales the results were deviating, which could be improved by cubing the velocity before area averaging. In general, they found out that an increase of turbulence length scale of the

ambient turbulence leads to an increase in turbine performance whereas an increase in turbulence intensity reduces it.

For the influence of sheared flow on diffuser augmented turbines no publications could be found.

1.1.4 Site Evaluation Using Shallow Water Equations

In order to analyze the power potential of a potential turbine site, full 3d simulations require a large computational effort. Therefore, 2d solvers based on the shallow water equations (SWE) are often used for those site evaluations. Depth-averaging the flow quantities allows a reduction of the number of spatial dimensions and thus computational effort. However, due to the reduction of dimensions the modeling of kinetic turbines in the flow field is challenging. Basically, there are two approaches to implement such a turbine model: manipulating the water level or increasing the bottom roughness drag coefficient in the turbine cell.

Draper et al. implemented the first approach to their shallow water model [28]. Their turbine model considers channel blockage effects, as well as free surface effects. From the adapted LMADT, a head loss is determined which is induced as relative change in flow depth in the turbine cell. This model is suitable for single turbines as well as for tidal fence applications.

Sutherland et al. developed a SWE turbine model for tidal fences [97]. For their approach the drag is increased in entire cross sections of tidal channels. In this way the energy potential for a whole fence can be determined. Using this model they assessed the tidal potential of the Johnstone Strait, Vancouver Island. A very similar model was used by Karsten et al. to determine the tidal energy potential in Minas Passage, Bay of Fundy [53]. Also Coles et al. used the tidal fence approach to model the energy extraction by a large number of tidal turbines at potential sites around the Channel Islands [20]. In advance, they successfully validated this turbine model for realistic array densities and different bed roughness conditions using experimental model tests [19].

In a further work, Kasten et al. chose a different approach, in which the individual turbines are considered. The resulting flow field from an empty channel 2d numerical simulation was discretized in uniform turbine size cells. From the available energy the most promising turbine locations were identified and the flow in the turbine cells was reduced according to the LMADT. In a next step the mean cross sectional velocity was recalculated. In this way, the individual turbine wake can be considered [52].

Also Lalander and Leijon decided to resolve the kinetic turbines individually in their shallow water model using the Mike3 solver [59]. They increased the drag coefficient in the turbine cells until reaching a fixed total power loss, which was determined from the drag using the LMADT. With this model they could investigate the influence of a number of kinetic turbines on the upstream water level of a river. However, they

faced problems with the turbine model with regard to the correct determination of the drag coefficient.

Joly et al. applied and tested the turbine model provided by the shallow water solver Telemac-2D [51]. Also this model can represent individual tidal turbines by increasing the bed friction. For the correct determination of the turbine drag through the LMADT the upstream undisturbed velocity is determined by accessing the flow informations in an upstream cell.

In his work, Ruopp enhanced the openFoam solver shallowWaterFoam for a feasible application in tidal site assessment [82, 83]. Also his turbine model relies on an increased drag coefficient in the turbine cell. However, he solved the problem of the unknown upstream undisturbed velocity by applying a continuity equation in the turbine cell considering the induction factor and the sheared flow profile.

1.2 Previous Work

This work was inspired by a previous research and development project. Within the scope of the project a horizonal axis hydrokinetic river turbine for a specific type of sites was to be developed and investigated. As an exemplary site, the St. Lawrence River in the region of the old port of Montreal, Canada, was chosen (see Figure 1.9a). Here, comparatively high flow velocities of up to 4 m/s are locally achieved at comparatively high flow depths. Due to the urban character of the location, the use of conventional hydropower for an exploitation of the energy potential is not possible. All those factors predestine this project area for the use of hydrokinetic turbines. The large width of the St. Lawrence stream even would theoretically allow the installation of a turbine park. Within the project framework, detailed hydraulic data of the site, such as bathymetry, velocity measurements and run-off data are available. Since 2010, a kinetic turbine designed during a previous project is operated and monitored in the project area [84].

The concept of the turbine had to be developed particularly on the site requirements. The predecessor diffuser augmented turbine presented by Ruopp [84] and illustrated in Figure 1.7 was the basis for the new turbine design. However, based on the evaluation of relevant literature a multi-stage diffuser concept was chosen. In order to optimally utilize the available space it was decided to reach the whole diffuser opening to the sides. The resulting concept was a 3-stage diffuser with an extensive diffuser exit area four times larger than the projected rotor area. The rotor was defined to consist of four blades and is kept in place by two supporting blades at the upstream and two supporting blades at the downstream part of the hub.

Based on these design boundary conditions, the detailed turbine design was determined through a fully automatic optimization as part of the work presented by Tismer [101]. Similar to Tampier et al. [98] he observed the necessity to consider all hydraulically relevant turbine components, including rotor blades, support structures and all diffuser stages in the design process. The optimization chain consisted of an

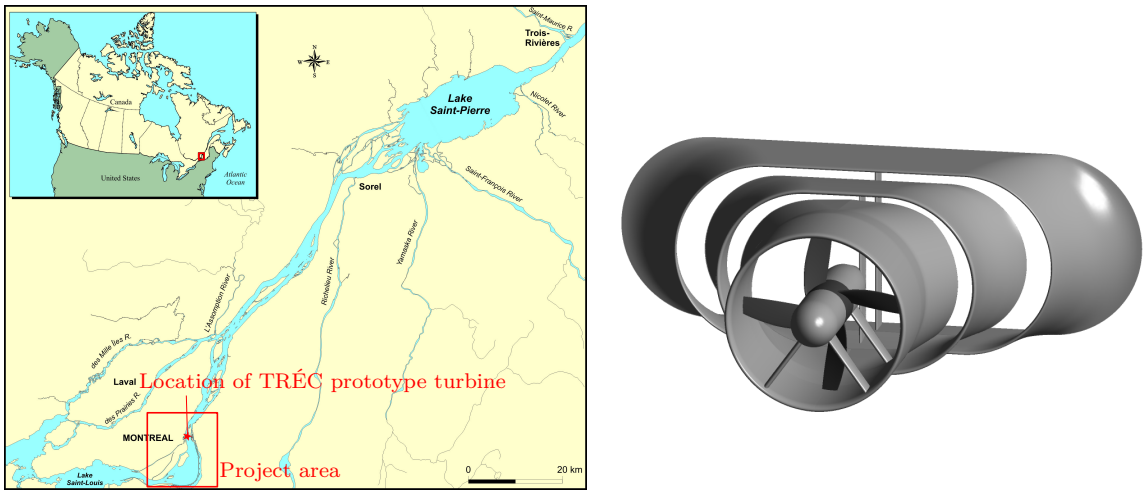

(a) Project area (Map from [39])

(b) Geometry of GenIHS DAT

Figure 1.9: Project framework

automatic generation of the whole turbine geometry followed by a fully automatic hybrid meshing of the solution domain including the far field around the kinetic turbine. This mesh was used for a numerical flow simulation of the entire geometry. The blade geometry and the contours of the individual diffuser stages were optimized simultaneously leading to 27 degrees of freedom in total [101]. The resulting geometry of the GenIHS hydrokinetic river turbine is presented in Figure 1.9b.

1.3 Research Objective

In order to determine the performance of the newly developed GenIHS turbine in-situ, a site evaluation is necessary. For this purpose, the solver developed by Ruopp and the associated turbine model is used [82, 83]. However, this turbine model was originally developed for single rotor turbines in an almost infinitely large flow field.

Since these conditions cannot be met for the current project, the main objective of this work is to develop an appropriate turbine model for diffuser augmented turbines in rivers. The major steps of the development are shown in Figure 1.10 and described in the following.

In order to mathematically describe diffuser augmented turbines in this model in a meaningful and simple way, a good understanding of the turbines' operating principle is required. For this purpose, various sensitive diffuser design parameters, such as area ratio, detailed diffuser shape and boundary layer control, are systematically investigated by means of numerical flow simulations.

Furthermore, the turbine model has to consider site effects which are specific for river applications. Therefore, several simulations with single rotor and diffuser augmented turbines are performed, increasing the complexity of the boundary conditions

representing those site effects. In this way, separate site effects like blockage or sheared flow effects can be isolated and implemented in a meaningful way.

The findings from those investigations are implemented in the existing turbine model. The resulting model consists of a single rotor and a diffuser augmented turbine module and can therefore be variably applied. It is verifyed through numerical 3d models of a single rotor turbine and the diffuser augmented turbine in the project area in Montreal. The final model is applied for the evaluation of a small turbine park arrangement of five diffuser augmented turbines.

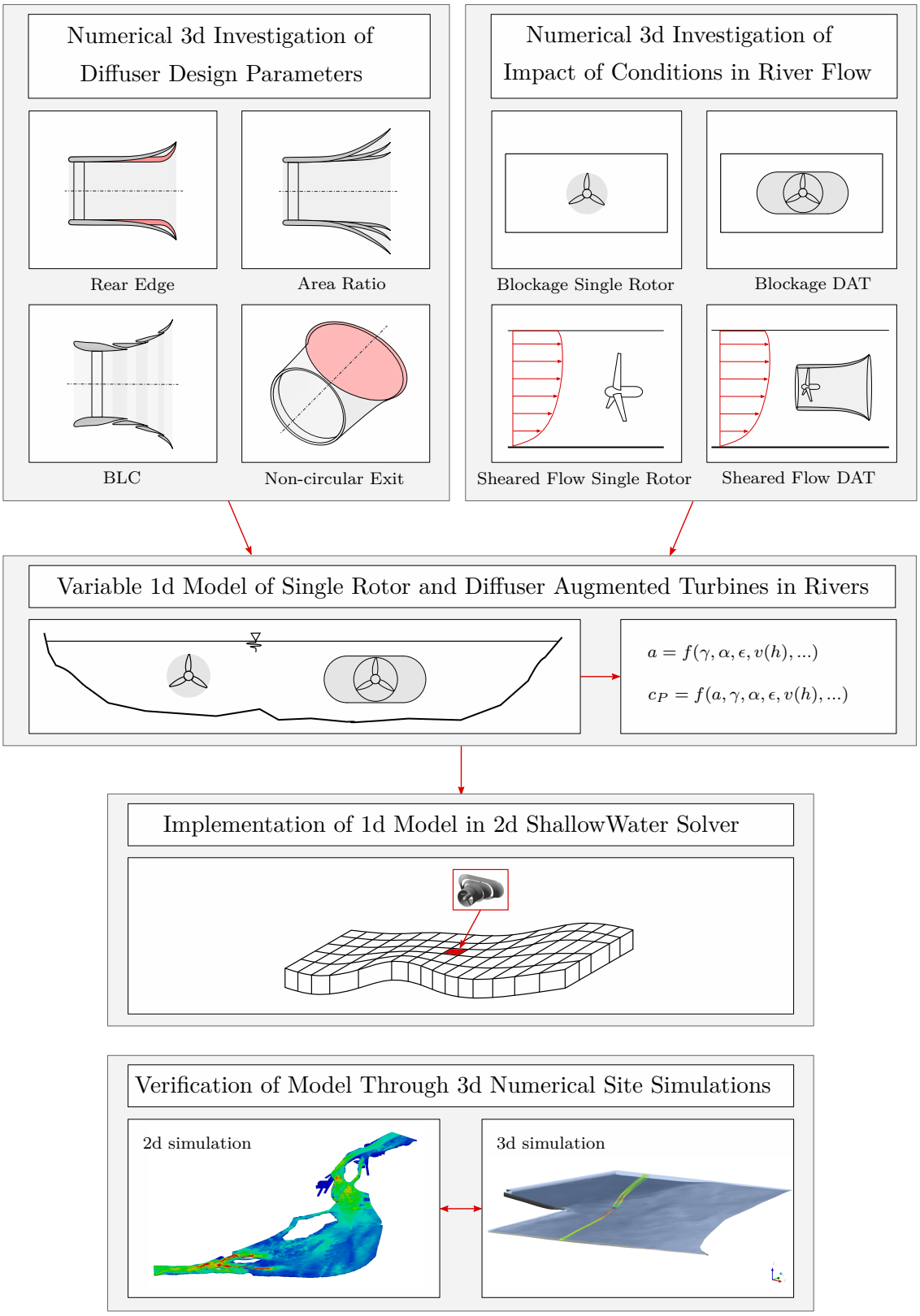

Figure 1.10: Schematic overview of key issues treated in this work

2 Theory on Hydrokinetic Turbines

In order to get an overview over different aspects of hydrokinetic turbines the following chapter presents basic theory but also new theoretical considerations on this field of research.

2.1 The Actuator Disk Theory and Lanchester-Betz-Limit

The basis for all theoretical considerations on kinetic turbines is the linear momentum actuator disk theory (LMADT) and the Lanchester-Betz-Limit. The actuator disk theory, also called momentum theory was introduced by Rankine (1865), Greenhill (1888) and Froude (1889). This approach only considers the energy extraction by the kinetic turbine, regardless of the specific turbine design. The rotor is represented by an infinitely thin disk, acting as momentum source. The model is valid assuming an infinite number of blades, the neglection of all rotation effects and an infinitely large flow field around the turbine [16]. Furthermore, the velocities are assumed to be constant over each reference area.

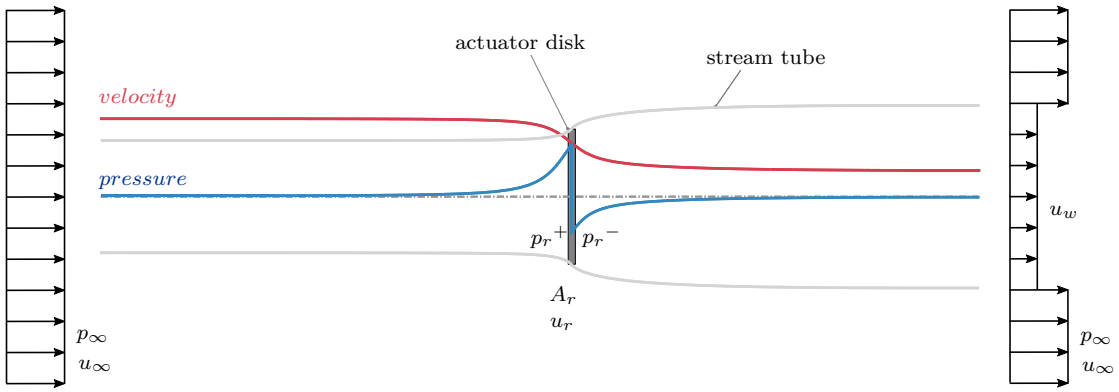

Figure 2.1: Flow pattern at actuator disk

As illustrated in Figure 2.1 the flow is continuously slowed down by the extraction of kinetic energy through the turbine. Through this deceleration, the pressure upstream of the actuator disk increases. In the rotor plane, the momentum source induces a sudden pressure drop. From there on the pressure continuously increases until reaching the ambient pressure level. Considering the conservation of mass along the flow from

the undisturbed upstream flow (∞) via the rotor plane (r) to the downstream wake flow (w) a stream tube may be derived. This stream tube widens towards the rotor plane as the flow velocity decreases. Downstream of the rotor, the flow continues to slow down and the cross-sectional area of the stream tube widens. This may also be represented by Equation 2.1 defining the conservation of mass:

$$\rho A_\infty u_\infty = \rho A_r u_r = \rho A_w u_w \tag{2.1}$$

where u_∞ is the undisturbed upstream velocity, u_r is the velocity in rotor plane and u_w is the wake velocity. The axial flow induction factor a describes the deceleration of the flow caused by the rotor:

$$a = 1 - \frac{u_r}{u_\infty} \tag{2.2}$$

Now the LMADT may be derived using the boundaries of the stream tube as control volume applying the conservation of momentum. The rotor thrust T_r, respectively the change in axial force induced by the actuator disk may be calculated as follows:

$$T_r = \rho A_r u_r \left(u_\infty - u_w\right) \tag{2.3}$$

By applying the conservation of momentum to the control volume directly around the actuator disk this force may also be expressed by the pressure difference directly up- and downstream of the rotor:

$$T_r = \left({p_r}^+ - {p_r}^-\right) A_r \tag{2.4}$$

The pressure at the rotor is determined applying the conservation of energy along the stream line from far upstream to the rotor (Equation 2.5) and from far downstream to the rotor (Equation 2.6):

$$\frac{\rho}{2}{u_\infty}^2 + p_\infty = \frac{\rho}{2}{u_r}^2 + {p_r}^+ \tag{2.5}$$

$$\frac{\rho}{2}{u_r}^2 + {p_r}^- = \frac{\rho}{2}{u_w}^2 + p_\infty \tag{2.6}$$

By equating the two energy equations, the following expression for the pressure difference is obtained:

$$\left({p_r}^+ - {p_r}^-\right) = \frac{\rho}{2}\left({u_\infty}^2 - {u_w}^2\right) \tag{2.7}$$

Combining Equation 2.7 and Equation 2.4 and equating it with Equation 2.3 combined with Equation 2.2 leads to:

$$\rho A_r u_\infty (1-a)(u_\infty - u_w) = \frac{\rho}{2}\left({u_\infty}^2 - {u_w}^2\right) A_r \tag{2.8}$$

which is resolved to the following expression for the wake velocity:

$$u_w = (1-2a)\, u_\infty \tag{2.9}$$

The rotor thrust can be expressed by substituting u_w to Equation 2.3:

$$T_r = 2\rho A_r {u_\infty}^2 a\,(1-a) \tag{2.10}$$

The theoretical power of a kinetic turbine in an infinitely large flow field can now be expressed as a function of the rotor thrust determined in Equation 2.10 on the one hand and by the general formulation for the available kinetic energy (Equation 1.1) on the other hand:

$$P_r = T_r u_r = 2\rho A_r {u_\infty}^3 a\,(1-a)^2 = \frac{\rho}{2} A_r {u_\infty}^3 c_P \tag{2.11}$$

This correlation allows the power coefficient of the rotor $c_{P,r}$ to be derived as:

$$c_{P,r} = 4a\,(1-a)^2 \tag{2.12}$$

Accordingly, the thrust coefficient $c_{T,r}$ is:

$$c_{T,r} = 4a\,(1-a) \tag{2.13}$$

The theoretical maximum power coefficient to be achieved in a free flow situation is denoted as Lanchester-Betz-Limit [11]. It is determined by equating the first derivative of the function described in Equation 2.12 to zero:

$$\frac{d\,c_{P,r}}{d\,a} = 4\,(1-a)\,(1-3a) \stackrel{!}{=} 0 \tag{2.14}$$

From this the induction factor at which the maximum occurs is determined to:

$$a\,(c_{P,r,max}) = \frac{1}{3} \tag{2.15}$$

And finally the maximum $c_{P,r}$-value is quantified to:

$$c_{P,r,max} = \frac{16}{27} \tag{2.16}$$

So, according to Lanchester and Betz around 60% of the total kinetic energy in a flow can theoretically be extracted by a kinetic turbine device. For conventional

kinetic turbines, this limit cannot be exceeded. This theory is the very basis for all considerations on kinetic turbines in fluid flows. It can be extended or adapted for several different applications such as the rotor disk model, the vortex cylinder model and the blade element method [16].

2.2 Considerations on Diffuser Augmented Turbines

The LMADT presented previously is valid only for a single free stream rotor in an infinitely large flow field. For diffuser augmented turbines, not all of these assumptions are fulfilled. The basic theory has to be adapted, as the diffuser is redirecting the flow, introducing an additional thrust to the balance of momentum. For this purpose, new definitions and reference planes have to be introduced.

2.2.1 Definitions

In this work, the diffuser exit area A_d (including flanges or brims, if existing) is assumed to be the relevant reference area for diffuser augmented turbines. In most cases this is similar to the projected area of the machine. The power coefficient of the machine is now defined as:

$$c_{P,d} = \frac{P_r}{\frac{\rho}{2} A_d {u_\infty}^3} \tag{2.17}$$

This definition is in contrast to the nomenclature used in several scientific publications presented in Section 1.1.1. However, it is considered reasonable because it allows to rate the machine according to its real dimensions and is therefore more authentic than the more common definition referring to the projected rotor area. A further advantage of this approach is that the performance of a diffuser augmented turbine can be directly compared with the performance of an equally sized single rotor turbine. This is underlined by the following statement by van Brussel: *"Without extra back pressure at the diffuser exit this means that the maximum power coefficient related to the exit area is equal to the Betz maximum* 16/27*"* [102]. The approach to consider the entire machine area is also used by Hjort and Larsen [44].

The overall thrust coefficient $c_{T,total}$ consisting of the sum of rotor and diffuser thrust referred to the diffuser exit area A_d is defined as follows:

$$c_{T,total} = \frac{T_{total}}{\frac{\rho}{2} A_d {u_\infty}^2} \tag{2.18}$$

The share of thrust between rotor and diffuser is defined by the thrust ratio τ according to Lewis et al. [61]:

$$\tau = \frac{T_r}{T_{total}} = \frac{T_r}{T_r + T_d} \tag{2.19}$$

Furthermore, the induction factor is redefined referring to the diffuser exit area. This factor reflects the deceleration of the velocity by the entire machine:

$$a_d = 1 - \frac{u_d}{u_\infty} \tag{2.20}$$

The area ratio γ is introduced as a geometric parameter to describe the diffuser. It is defined as the fraction between diffuser outlet area and the rotor area:

$$\gamma = \frac{A_d}{A_r} \tag{2.21}$$

As for multi-stage diffusers or diffusers with other types of boundary layer control the mass flow is not conserved from the inlet to the exit, the mass flow ratio q is introduced. It is described by the ratio between the mass flow at the diffuser exit and the mass flow through the rotor and therefore indirectly quantifies the mass flow which is entrained by large gaps or vents to the diffuser:

$$q = \frac{A_d u_d}{A_r u_r} \tag{2.22}$$

2.2.2 Adaption of the Actuator Disk Theory

For a theoretical assessment of a single-stage diffuser augmented turbine an approach similar to the basic LMADT is used. The walls of the diffuser are assumed to be friction-less and all kinds of losses in the diffuser flow are neglected. The rotor is modeled through a momentum source similar to the actuator disk theory.

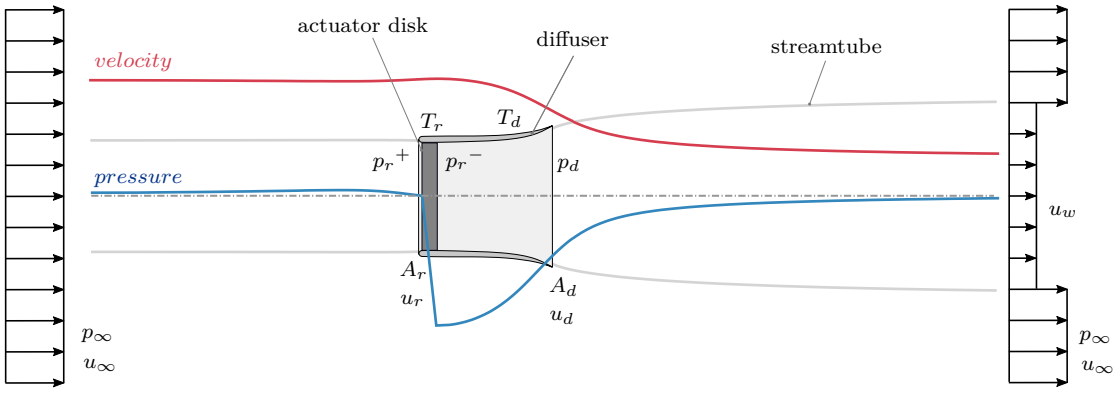

Figure 2.2: Flow pattern at an exemplary diffuser augmented turbine

Figure 2.2 schematically shows the flow pattern at a diffuser augmented turbine. It is recognized that in this case the upstream velocity is not slowed down by the machine when approaching the rotor. Depending on the specific design and operation point even an acceleration of the flow upstream of the rotor is possible driven by the suction effect of the diffuser. The deceleration of the flow due to the energy extraction rather happens in the area of the diffuser exit. Consequently, there is no stagnation pressure occurring in front of the rotor, but the necessary pressure drop across the rotor is achieved by a lower pressure in the diffuser.

The mathematical approach to the problem follows a procedure similar to the basic conventional actuator disk theory. The conservation of mass in the stream tube is applied. In this case, also the mass flow at the diffuser exit is added to the mass balance:

$$\rho A_\infty u_\infty = \rho A_r u_r = \rho A_d u_d = \rho A_w u_w \tag{2.23}$$

Analogous to Equation 2.3, the conservation of momentum is applied to the flow field around the turbine in order to determine the difference in the axial force and thus the machine thrust. However, here the total machine thrust T_{total} consists of rotor thrust and diffuser thrust:

$$T_{total} = \rho A_r u_r \left(u_\infty - u_w\right) \tag{2.24}$$

The rotor thrust is expressed based on the pressure difference upstream and downstream of the rotor but also by rearranging Equation 2.24 using the thrust ratio τ defined above:

$$T_r = \left({p_r}^+ - {p_r}^-\right) A_r = \boldsymbol{\tau} \rho A_r u_r \left(u_\infty - u_w\right) \tag{2.25}$$

Furthermore, the energy along the stream line from upstream through rotor and diffuser to the wake flow has to be conserved. Neglecting all flow losses in the diffuser the energy balance applied in the conventional LMADT (Equation 2.7) is also valid here. Substituting the pressure difference determined by the energy balance to the momentum balance (Equation 2.25) leads to the following equation:

$$\frac{\rho}{2} A_r \left({u_\infty}^2 - {u_w}^2\right) = \tau \rho A_r u_r \left(u_\infty - u_w\right) \tag{2.26}$$

The rotor velocity u_r is expressed as a function of the area ratio γ and the diffuser induction factor a_d by applying the conservation of mass in the diffuser:

$$u_r = \frac{u_d A_d}{A_r} = u_\infty \gamma \left(1 - a_d\right) \tag{2.27}$$

Similar to the derivation of the conventional LMADT, the following expression for the wake velocity u_w far downstream of the diffuser can now be derived from Equation 2.26 and Equation 2.27:

$$u_w = u_\infty \left(2\gamma\tau \left(1 - a_d\right) - 1\right) \tag{2.28}$$

For the special case of a single rotor without diffuser, where $\tau = 1$ and $\gamma = 1$ the resulting expression for the wake velocity is equivalent to the one resulting from the conventional LMADT (Equation 2.9).

Combining Equation 2.25, Equation 2.27 and Equation 2.28 the rotor thrust is expressed in the following way:

$$T_r = \frac{\rho}{2} A_d \, {u_\infty}^2 \, 4\tau \left(1 - a_d\right) \left(1 - \tau\gamma \left(1 - a_d\right)\right) \tag{2.29}$$

Accordingly, the power generated by the ideal rotor in a diffuser augmented turbine is:

$$P_r = T_r u_r = \frac{\rho}{2} A_d \, {u_\infty}^3 \, 4\tau\gamma \left(1 - a_d\right)^2 \left(1 - \tau\gamma \left(1 - a_d\right)\right) \tag{2.30}$$

In combination with Equation 2.17 the power coefficient of the machine may now be determined to:

$$c_{P,d} = 4\tau\gamma \left(1 - a_d\right)^2 \left(1 - \tau\gamma \left(1 - a_d\right)\right) \tag{2.31}$$

The corresponding overall thrust coefficient is:

$$c_{T,total} = 4 \left(1 - a_d\right) \left(1 - \tau\gamma \left(1 - a_d\right)\right) \tag{2.32}$$

Due to its dependence on area ratio and thrust ratio, this analytical description of diffuser augmented turbines is considerably more complex compared to conventional LMADT (Equation 2.12 and 2.13). While the diffuser area ratio γ is a geometric parameter which depends only on the machine geometry, the thrust ratio τ is a fluid mechanical parameter depending on the flow field in and around the machine. To determine the power limit for diffuser augmented turbines analogous to the procedure described in section Section 2.1, Equation 2.31 must be differentiate with respect to a_d. In order to obtain an explicit solution, τ and thus the rotor thrust and the total machine thrust must be known.

The rotor thrust is a known function depending on the diffuser induction factor a_d and τ (see Equation 2.29). The critical point is the determination of the diffuser thrust component. The outer diffuser shell is a solid body in a free flow - a problem which can not be solved directly and is usually approached through potential theory or empirical constants. Furthermore, the flow field around the diffuser and thus the diffuser thrust is not constant but depends on the rotor operation point. This is visualized by the different streamlines in Figure 2.3b. An exemplary dependence of the diffuser thrust and the thrust ratio on the induction factor gained from a laminar simulation of a simple diffuser ($\gamma = 1.5$) is shown in Figure 2.3a. All those

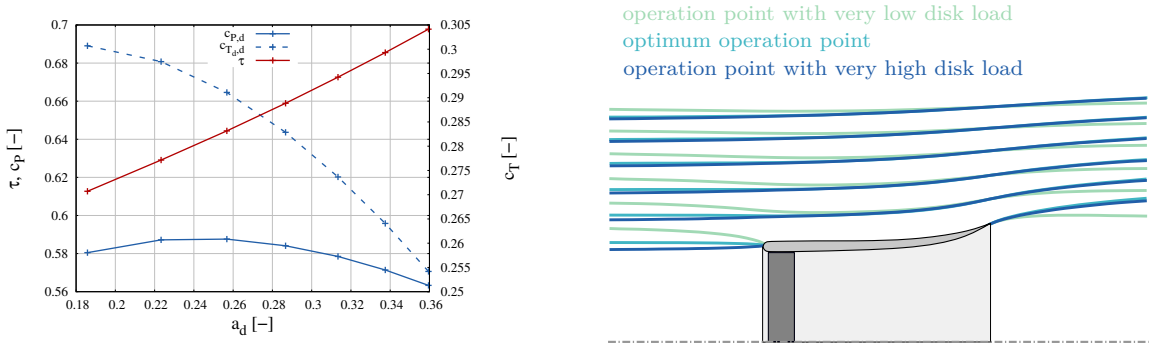

(a) Correlation between thrust ratio, power coefficient and induction factor

(b) Flow field around the diffuser for varying operation points

Figure 2.3: Dependence of thrust ratio on operation point for an exemplary diffuser with $\gamma = 1.5$ (from laminar simulation)

considerations lead to the conclusion that an analytical determination of a power limit for diffuser augmented turbines is not possible which is in accordance with the observations of several researchers such as:

- de Vries: *"The axial momentum equation is not convenient in this case, because the external forces on the diffuser are difficult to estimate."* [22] and
- Phillips: *"Difficulty arises in determining the pressure force on the external surface of the diffuser, without which a solution is not obtainable. This can be seen as the reason why previous authors have used various assumptions or semi-empirical approaches to evaluate the DAWT problem."* [78]

Despite the discussed limitations, the theory derived previously helps to better understand the geometric and hydrodynamic correlations for diffuser augmented turbines. For this purpose Equation 2.31 is plotted for different area ratios in Figure 2.4. It can be seen that there is no explicit power limit for the diffuser power coefficient and high values are theoretically possible. They occur for a low diffuser induction factor (high mass flow capacity) and a comparatively low thrust ratio (small rotor thrust). Furthermore, a clear influence of the area ratio on the power coefficient is visible comparing Figures 2.4a, b and c. The range for potentially high $c_{P,d}$ -values and thus high performance diffusers becomes significantly smaller for an increasing area ratio.

Comparing the theory to the results of the laminar simulation of a simple diffuser (see also Figure 2.3a), which are marked in red in Figure 2.4a, a good agreement is observed. The power coefficient determined in the simulation is only around 2% lower than the one provided by the theory for the respective conditions. However, the theoretical relations only give an indication of the characteristics of a good diffuser, as quite significant effects such as wall friction, turbulence and flow separation regions are neglected. Furthermore, not all regions characterized by a high power coefficient

provide a realistic operation point. For example, an operation at $a_d = 0$ where the exit velocity at the diffuser is equal to the undisturbed upstream velocity is not possible, as no energy can be extracted without a deceleration of the flow. The challenge is to find a suitable detailed diffuser geometry which meets the theoretical requirements.

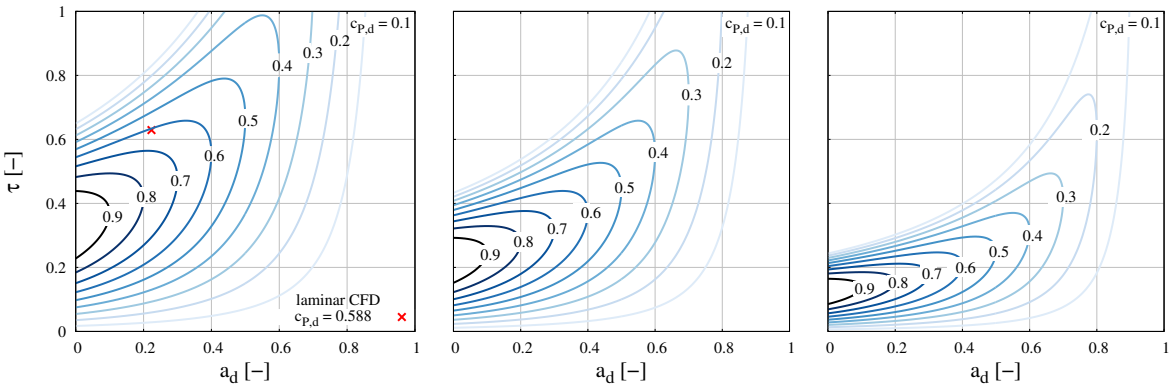

(a) Area ratio $\gamma = 1.5$ **(b)** Area ratio $\gamma = 2.25$ **(c)** Area ratio $\gamma = 4.0$

Figure 2.4: Theoretical correlation between diffuser power coefficient, thrust ratio and induction factor for different diffuser area ratios (from Equation 2.31)

2.2.3 Boundary Layer Control

The theoretical considerations presented above assume a single-stage diffuser concept. However, as described in Section 1.1.1, several publications in technical literature recommend the so-called Boundary Layer Control to increase the performance of diffusers. It can be implemented by a large rotor gap, by axial slots in the diffuser walls or through a multi-stage concept. This design method accelerates the flow at the inner diffuser walls and, ideally, prevents flow separation. The concept is schematically illustrated in Figure 2.5.

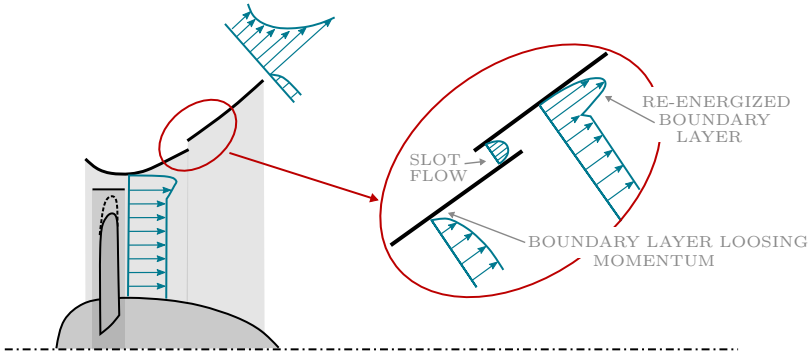

Figure 2.5: Concept of Boundary Layer Control from Gilbert et al. [35]

Applying this design concept, the disadvantages such as the loss of mass flow in the rotor gap and the increase in back pressure in the diffuser have to be weighted against the advantage of a homogeneous, well-attached diffuser flow. Due to the additional input of mass, momentum and energy into the diffuser flow, an analytical approach to the problem is even more complicated than for simple diffuser concepts.

2.3 Blockage Effects

One assumption for the validity of the LMADT is an infinitely large flow field around the turbine. This can be approximated for many applications of kinetic turbines such as wind turbines or tidal turbines. Operating kinetic turbines in rivers, the channel cross section can be very small in relation to the machine size, and the blockage effects cannot be neglected. The influence of this blockage effect on the turbine performance is analytically investigated and discussed in detail by Garrett and Cummins [34] and presented in the following. They adapted the LMADT to the redefined boundary conditions and introduced the blockage ratio as fraction between the projected rotor area A_r and the channel cross section A_c:

$$\epsilon = \frac{A_r}{A_c} \tag{2.33}$$

Their theory provides the following correlation between the power coefficient $c_{P,\infty}$ for a kinetic turbine in an infinitely large flow field and the power coefficient influenced by the channel blockage:

$$c_{P,c} = \frac{c_{P,\infty}}{(1-\epsilon)^2} \tag{2.34}$$

Consequently, for a constant turbine size the turbine power increases as the channel cross section decreases. According to Garrett and Cummins also the corresponding optimum operation point is influenced. The channel induction factor a_c is derived accordingly:

$$a_c = \frac{a_\infty + \epsilon}{1+\epsilon} \tag{2.35}$$

This means that the optimum turbine operation point is shifted to smaller rotor velocities in narrow channels. As both power coefficient and induction factor are influenced by the channel blockage also the disk load has to be adapted:

$$c_{T,c} = \frac{c_{T,\infty}\,(1+\epsilon)}{(1-\epsilon)^2} \tag{2.36}$$

The accuracy of this approach in direct comparison to numerical simulations is demonstrated by Nishino and Willden [68]. Still, they observed that the exact shape of

the channel cross section is not considered by the theoretical approach and therefore has only limited validity for channels with a very large aspect ratio $\alpha = B_c/h$.

It has to be mentioned here that several other theories for the consideration of blockage effects exist in relevant literature (see Section 1.1.3). However, most of them were developed for the correction of results of wind tunnel experiments [7, 95]. For this work, the approach of Garrett and Cummins is chosen because of its good accuracy in combination with its simplicity.

2.4 Sheared Flow Conditions

For sheared flow conditions, the upstream undisturbed flow velocity is not constant over the flow depth. A meaningful reference velocity has to be identified, in order to predict the turbine performance correctly for a given power coefficient. Various possible approaches on this problem are published in relevant literature.

The easiest way is to use the flow velocity in hub height u_h which is quite common in wind turbine applications [8, 106]. A further approach is to determine the depth-averaged velocity across the vertical diameter of the rotor u_d [64, 82]. Also an area-average or volume-average of the undisturbed velocity profile across the projected turbine area u_v provides promising results [12, 30, 64, 67]. The different approaches are illustrated in Figure 2.6. However, research has not come to a clear conclusion which reference velocity eliminates the influence of sheared flow conditions best.

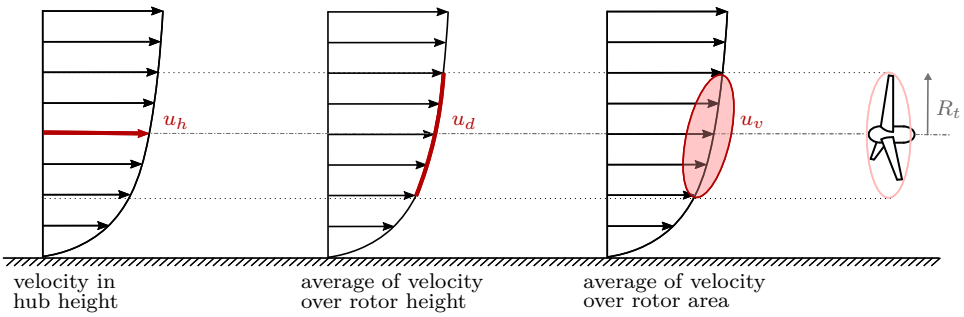

Figure 2.6: Illustration of different approaches for determinig the reference velocity for sheared flow conditions

3 Relevant Numerical Methods

For the various problems investigated in this work, different numerical methods are applied. The detailed diffuser and site effect investigations are performed using 3d numerical solvers based on the Navier-Stokes-Equations. For the large scale site evaluations a shallow water solver is used, which is based on a depth-averaged version of the Navier-Stokes-Equations. In order to model the rotor, high bottom roughness or the entire kinetic turbine specific modeling approaches are applied which are described in detail in the following.

3.1 The Simple Actuator Disk Model

The concept of the actuator disk theory is already presented in the previous chapter. It may be numerically implemented using a momentum source. According to the LMADT, a constant momentum has to be specified for this source. For actuator disk simulations, modeling an unshrouded rotor, the momentum source has to be infinitely thin. In this case, stability problems can be observed at the outer radial boundaries of the disk caused by large gradients in pressure and velocity. Within this work, a constant quadratic loss coefficient k_{AD} is applied to model the loss of momentum at the disk:

$$S_i = \frac{\rho}{2} k_{AD} A_r |u| u_i \tag{3.1}$$

By varying the loss coefficient, the disk load and thus the turbine operation point is adjusted. For the unshrouded rotor simulations an adapted version of the simpleFoam solver in foam-extend-4.1 is used, which is able to handle a 2d momentum source. Using this rotor model for numerical simulations of single actuator disks considering turbulence provides a slightly higher power coefficient than predicted by the LMADT and laminar simulations [33, 96].

The simple actuator disk model can also be applied for modeling the rotor of diffuser augmented turbines. In this case the momentum source does not necessarily have to be two-dimensional as the rotor is shrouded. The use of this model in diffuser augmented turbine research is quite common, not only in numerical [26, 33, 42, 92], but also in experimental investigations where screen meshes or gauze are used to simulate different disk load coefficients [35, 49, 61, 73, 78].

Regardless of a single rotor or shrouded rotor application, the simple actuator disk model is based on the assumption of swirl-free wake flow. Especially in the diffuser

design process, this assumption can cause problems, as it suggests flow conditions in the diffuser that will never occur when using guide vanes and runner blades.

For all numerical 3d turbine investigations, including the studies on flow conditions in rivers, five different disk loads and thus operation points are simulated for each setup. From the simulation results the optimum operation point is determined by fitting a cubic function. This procedure is very extensive, but indispensable for a precise investigation of the different examined phenomena.

3.2 Modeling High Bed Roughness

A sheared flow velocity distribution is generally caused by a no-slip condition defined at wall boundaries. The detailed velocity profile developing in the flow is depending on the degree of wall roughness. In rivers this roughness is commonly very high. An exemplary time-averaged vertical velocity distribution measured at the Montreal project area is shown in Figure 3.1a.

According to the boundary layer theory the boundary layer flow is divided into a thin viscous sublayer and a logarithmic turbulent boundary layer [88]. In order to describe them, the dimensionless wall distance y^+ and the dimensionless velocity u^+ are introduced. The viscous sublayer is located in the region of $y^+ < 5$, the logarithmic turbulent boundary layer in the region $30 < y^+ < 500$. In between, there is a buffer layer (see Figure 3.1b).

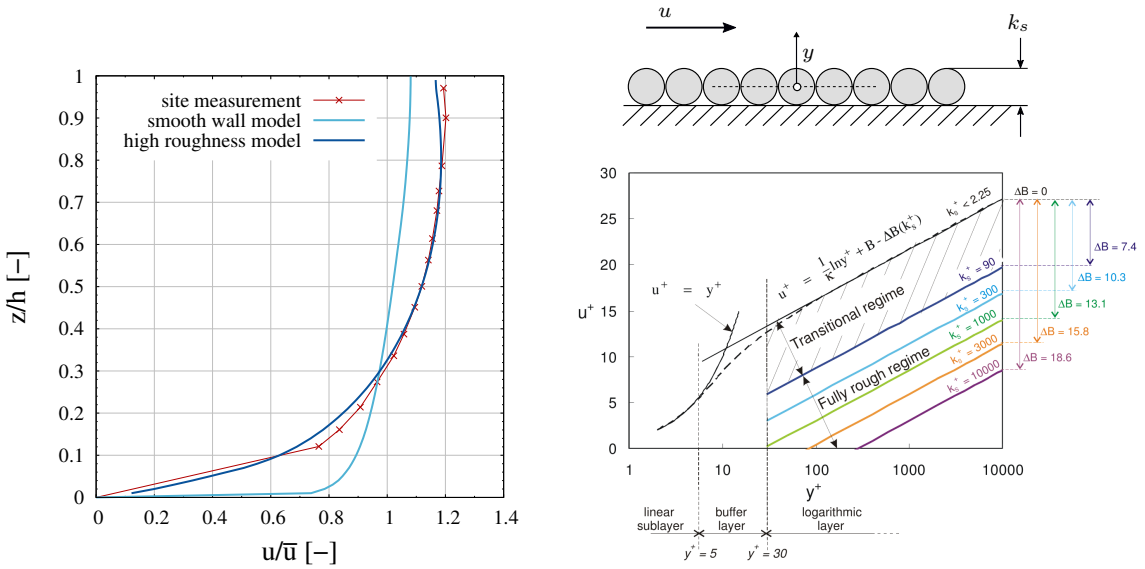

(a) Comparison of different methods **(b)** Scheme of sand grain roughness model [3, 13]

Figure 3.1: Numerical modeling of high bed roughness

Numerically, the velocity profile of the turbulent boundary layer can be fully resolved. In this case the cell closest to the wall must be located inside the region of the linear

sublayer. Since this layer is usually very small, a very fine mesh is required. In order to save computational effort, the Law of Wall can be applied to model the boundary layer flow for coarser meshes. The common wall treatment was originally developed for smooth surface boundaries.

However, a high roughness can be modeled using a sand-grain-based roughness modification [3, 13]. In this case, the Law of Wall is extended by the shift term ΔB, which is a function of the dimensionless sand grain roughness height ${k_s}^+$. Through this term the dimensionless wall velocity is artificially decreased with increasing wall roughness. The profound principle is illustrated in Figure 3.1b. To consider the blockage caused by large sand grains, it is recommended to place the wall physically at 50% height of the roughness elements as illustrated at the top of Figure 3.1b. Furthermore, the distance of the cell closest to the wall should not be smaller than the roughness height [3]. For a high roughness this is possibly in the range of several decimeters. This condition is in conflict to the required resolution of the boundary layer flow. The problem is discussed in detail by Blocken et al. [13]. They suggest a coarse dimensioning of the cell closest to the wall in the upstream and downstream regions of their solution domain and a fine resolution only in the central area of interest. However, due to the described inconsistencies, this approach is not reliable.

A further approach to model high bottom roughness is to geometrically resolve the roughness elements. This requires very detailed bathymetric data as well as a high mesh resolution. This approach is computationally very expensive even for small solution domains.

In case that the bed roughness elements are very large compared to the flow depth Olsen and Stokseth suggest to use a porosity model. Within this method, an additional source term is introduced, which specifies a loss depending on the flow depth and controling the vertical velocity distribution. However, this approach is expected to influence the turbulence in the free flow [72]. For this reason, the porosity model is not directly suitable for the investigation of kinetic turbines in sheared flow conditions.

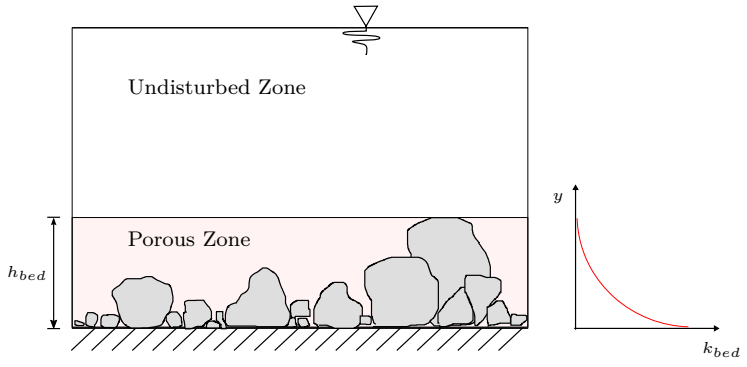

Figure 3.2: Schematic illustration of new high roughness model

In this work, an approach closely related to Olsens and Stokseths work is chosen. The additional porous roughness source is not applied to the entire channel geometry, but

only to a specific zone directly above the river bed. Thus, the turbulence in the main flow is not affected. In the porous layer an isotropic resistance loss coefficient k_{bed} is chosen. As a rough river bed usually consists of a dense region of fine-grained sediment at the bottom and less dense regions of coarser sediment in the higher regions the loss coefficient is defined to be decreasing with increasing wall distance (see Figure 3.2). In order to accurately model the profile measured at the potential project area the following function is empirically determined:

$$k_{bed} = b\, y^{-2} \tag{3.2}$$

where y is the absolute wall distance from the bottom. The constant b is varied with the thickness of the porous zone h_{bed}. It is chosen in a way that the loss coefficient at the top of the porous zone is 0.2 m^{-1} for every layer thickness. Hence, the integral loss coefficient is increasing with increasing roughness height. The lower boundary of the porous zone is defined as smooth wall. An exemplary resulting velocity profile is plotted in dark blue in in Figure 3.1a.

An additional challenge when modeling high roughness flow is the correct definition of the inlet boundary. It was observed that when specifying a fixed velocity distribution (e.g. determined theoretically or obtained from site measurement data) the velocity profile specified at the inlet changes in flow direction [13]. The reason for this is the discontinuity between the inlet boundary condition and the bottom wall boundary condition. This can be prevented by generating the inlet velocity profile numerically.

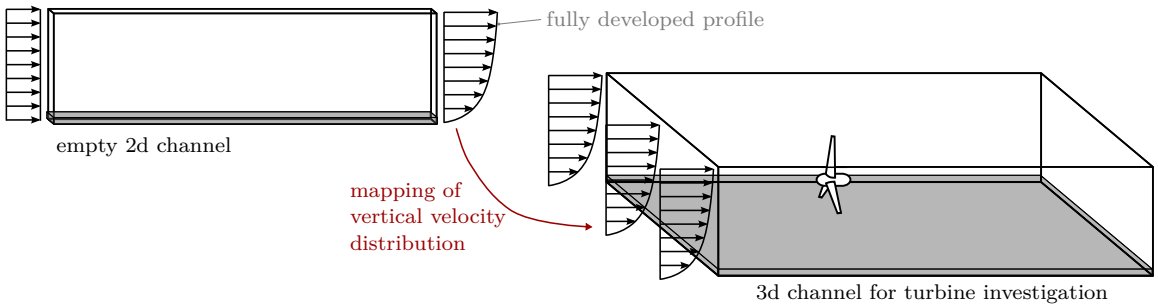

Figure 3.3: Illustration of the procedure to generate a fully developed velocity profile

For this purpose, a very long 2d empty channel (around 2 km length) is generated, where a constant velocity is defined at the inlet. The bottom and the top boundary condition of this channel have to be defined identical to the boundary conditions in the actual 3d simulation. The flow in the channel is assumed to be fully developed from the point on where the vertical velocity profile does not change in axial direction. The fully developed velocity profile from the 2d simulation - including the turbulent quantities - is mapped to the inlet boundary of the actual 3d simulation. The procedure is summarized in Figure 3.3. It can also be applied for a smooth wall boundary or every other bed roughness model and has to be performed separately for every variation of channel roughness and flow depth.

3.3 The Shallow Water Equations

The shallow water equations are derived from the Reynolds-Averaged Navier-Stokes-Equations assuming a hydrostatic pressure distribution. They are applied for problems where the horizontal extension of the computational domain is significantly larger than the flow depth and the horizontal velocity components are significantly larger than the vertical component. Under these conditions, the vertical dimension of the flow field is not spatially resolved and the problem can be solved in two dimensions. This means that the vertical velocity component is neglected and the horizontal flow quantities are depth-averaged resulting in the following conservation equations:

The continuity equation:

$$\frac{\partial h}{\partial t} + \frac{\partial h\bar{u}}{\partial x} + \frac{\partial h\bar{v}}{\partial y} = 0 \tag{3.3}$$

The momentum equations:

$$\frac{\partial h\bar{u}}{\partial t} + \bar{u}\frac{\partial h\bar{u}}{\partial x} + \bar{v}\frac{\partial h\bar{u}}{\partial y} = -gh\frac{\partial\left(h_0 + h\right)}{\partial x} + \frac{1}{\rho}\frac{\partial h\bar{\tau}_{xx}}{\partial x} + \frac{1}{\rho}\frac{\partial h\bar{\tau}_{xy}}{\partial y} - \frac{\tau_{b,x}}{\rho} \tag{3.4}$$

$$\frac{\partial h\bar{v}}{\partial t} + \bar{u}\frac{\partial h\bar{v}}{\partial x} + \bar{v}\frac{\partial h\bar{v}}{\partial y} = -gh\frac{\partial\left(h_0 + h\right)}{\partial y} + \frac{1}{\rho}\frac{\partial h\bar{\tau}_{yx}}{\partial x} + \frac{1}{\rho}\frac{\partial h\bar{\tau}_{yy}}{\partial y} - \frac{\tau_{b,y}}{\rho} \tag{3.5}$$

Here h is the flow depth and h_0 is the position of the bottom or the bathymetric bed elevation (see Figure 3.4).

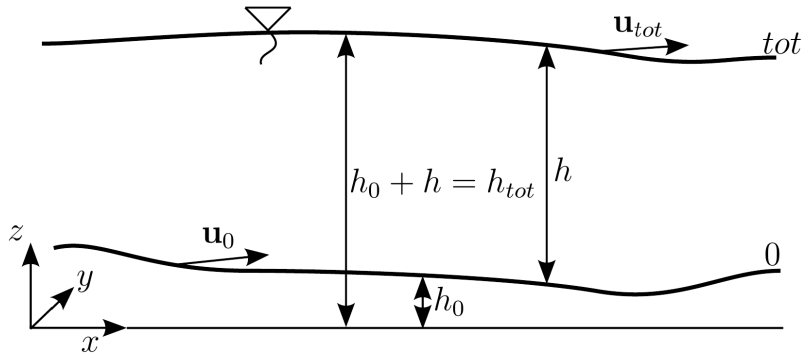

Figure 3.4: Definitions for shallowWaterFoam from [82]

Depending on the detailed application, various source terms can be added to the basic equation, modeling phenomena like the Coriolis force or the surface tension caused by wind. For this work only the soil friction $\tau_{b,i}$ is considered to be relevant. It is defined as:

$$\tau_{b,i} = c_D \rho \bar{u}_i |\bar{u}_i| \tag{3.6}$$

The drag coefficient c_D may be obtained from Equation 3.7 using the Manning roughness coefficient n, which is determined through calibration or from empirical tables.

$$c_D = \frac{n^2 g}{h^{1/3}} \tag{3.7}$$

There are various possibilities for modeling turbulence in shallow water solvers. However, also the turbulent quantities must be depth-averaged. In this work, the depth-averaged zero-equation turbulence model according to Smagorinsky is applied for turbulence modeling [93]. The turbulence model and the soil friction model were implemented in the basic openFOAM solver shallowWaterFoam by Ruopp [82].

3.4 Existing Turbine Model for Shallow Water Solvers

For site evaluations in large scaled tidal flow fields Ruopp also developed a kinetic turbine model for his advanced shallow water solver [82, 83]. The basic modeling concept is to increase the drag coefficient in the soil friction model (Equation 3.6) at the turbine site in order to simulate the energy extraction by the turbine. It is assumed that the drag in the 2d turbine cell is equal to the actual 3d rotor thrust (Equation 2.13). Consequently, the 2d drag coefficient $c_{D,t}$ is derived from the LMADT:

$$c_{D,t} = \frac{A_r 4a\,(1-a)\,\overline{u}_{\infty,t}{}^2}{2A_{cell}\overline{u}_{cell}{}^2} \tag{3.8}$$

In this equation, the upstream undisturbed velocity $\overline{u}_{\infty,t}$ is unknown. For its determination, the solver must either access the flow quantities of an upstream cell or the upstream undisturbed velocity has to be calculated from the velocity in the actual turbine cell. The model presented by Ruopp applies the latter method.

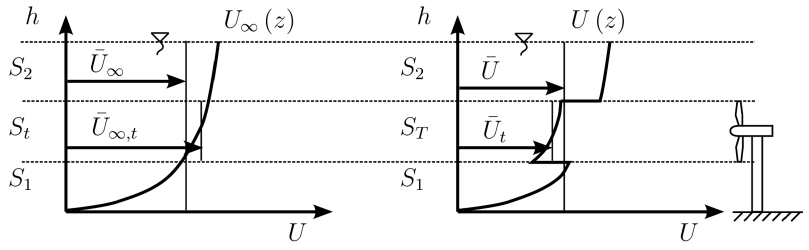

Figure 3.5: Deceleration model for the upstream undisturbed velocity determination [82]

For this approach, a vertical velocity distribution according to the 1/7-Power law is assumed. This undisturbed velocity profile is decelerated over the height of the turbine $2R_t$, whereby the rest of the profile is not affected by the rotor. The principle

is illustrated in Figure 3.5. Integrating over this disturbed velocity profile, a relation between the mean velocity in the turbine cell $\overline{u}$ provided by the solver and the upstream velocity averaged over the height of the rotor $\overline{u}_{\infty,t}$ may be derived:

$$\overline{u}_{\infty,t} = \frac{h\overline{u}\left[\left(\frac{h_{hub}+R_t}{h}\right)^{8/7} - \left(\frac{h_{hub}-R_t}{h}\right)^{8/7}\right]}{2R_t\left[1 + a\left[\left(\frac{h_{hub}-R_t}{h}\right)^{8/7} - \left(\frac{h_{hub}+R_t}{h}\right)^{8/7}\right]\right]} \tag{3.9}$$

The resulting power of the kinetic turbine is determined from the 2d drag coefficient and the undisturbed reference velocity:

$$P_t = \rho A_{cell}\, c_{D,t}\, \overline{u}_{cell}{}^2\, (1-a)\; \overline{u}_{\infty,t} \tag{3.10}$$

This turbine model is used as basis for the advanced turbine model considering river site effects and diffuser augmented turbines, which is developed in the course of this work.

4 Numerical Investigation of Diffuser Augmented Turbines

This chapter provides a detailed study of different diffuser attributes and concepts under ideal flow conditions in an infinitely large flow field using numerical flow simulations (Ansys CFX and openFoam). Finally, the automatically optimized GenIHS diffuser geometry is examined in detail. The results help to better understand the working principle of diffuser augmented turbines. This is a necessary basis for the developemnt of a flexible 1d turbine model.

4.1 Detailed Investigation of Different Diffuser Attributes

In order to perform a systematic examination of the diffuser design, the technical literature is evaluated for relevant references. The following sensitive diffuser attributes could generally be identified from this review:

- The shape of the diffuser at the exit [25, 35, 44, 62, 70, 71, 73, 92]
- The diffuser area ratio [33, 61, 62, 92]
- The concept of boundary layer control [24, 35, 44, 85, 92]

In the following, these three design parameters are therefore examined in more detail. Furthermore, the performance of diffusers with non-circular exit area is evaluated as this design concept is expected to be advantageous for an application in limited flow depth. All the investigated parameters are illustrated in Figure 4.1.

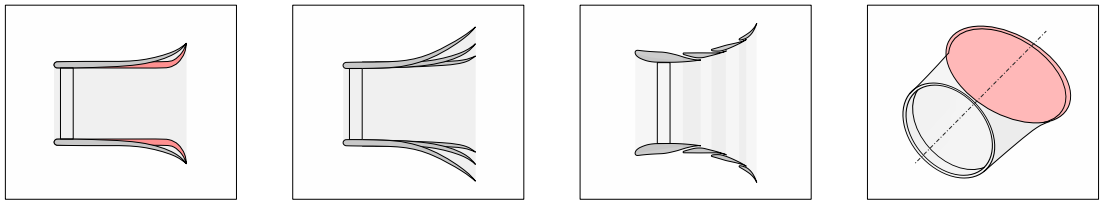

Figure 4.1: Overview over investigated diffuser attributes

4.1.1 Simulation Setup

All diffuser geometries are investigated in a very large solution domain in order to avoid interactions with the domain boundaries and minimize blockage effects. For the rotationally symmetrical diffuser geometries it is reasonable to reduce the solution domain to a section of 10° of the geometry in order to minimize the computational effort. For the investigations of the non-circular diffusers, axis symmetric boundary conditions are applied and the solution domain is reduced to a quarter of the full geometry. An exemplary domain geometry for a rotationally symmetrical diffuser is shown in Figure 4.2a.

At the inlet the constant axial velocity $u_\infty = 4\ \frac{\mathrm{m}}{\mathrm{s}}$ is defined and at the outlet a constant static pressure is set. The radial domain side walls are assumed to be free slip walls. The diffuser walls are defined as smooth walls. The respective viscous sublayer is modeled through a wall model. The applied meshes resolve the wall flow with $30 < y^+ < 300$. The k-ω-SST-Model is used to model the turbulence. For each diffuser geometry the solution domain is discretized through a block structured hexahedral mesh. An exemplary mesh resolving a multi-stage diffuser is shown in Figure 4.2b. In general, steady state flow conditions are assumed.

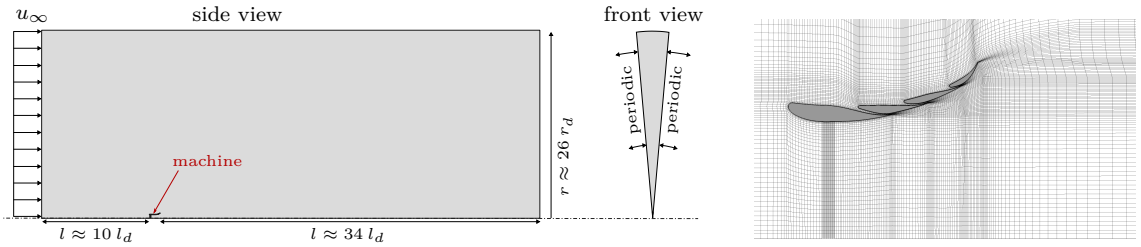

(a) Solution domain and boundary conditions

(b) Mesh around a diffuser

Figure 4.2: Simulation setup for the investigation of diffuser augmented turbines

For the investigation of the diffuser design parameters the rotor geometry is not directly resolved but modeled through an actuator disk (see Section 3.1). In order to determine the optimum operation point, the disk load is varied. In this way five operation points are simulated for each diffuser geometry. From the results, a cubic function is determined by curve fitting. Calculating the first derivative of this function provides the maximum power coefficient and the respective induction factor.

4.1.2 Basic Diffusers

A basic “first guess” diffuser geometry is derived from the shape of the stream tube around an actuator disk at optimum operation point. The inner contour of the diffuser follows the stream tube upstream of the disk, which is gained from CFD results. The basic idea is that the diffuser outlet is equivalent to the single actuator disk, as illustrated in Figure 4.3.

The inner contour is thickened and the diffuser is equipped with an elliptical leading edge. The variable wall thickness results in a sharp trailing edge. As the deceleration of the flow by the rotor is $u_r/u_\infty = 2/3$ for an optimum operation according to the LMADT, the area ratio of the basic diffuser is $\gamma = 1.5$. In accordance to general diffuser design guidelines (conventional hydropower) an overall opening angle of less than 8° is applied to ensure stable flow conditions in the diffuser [85].

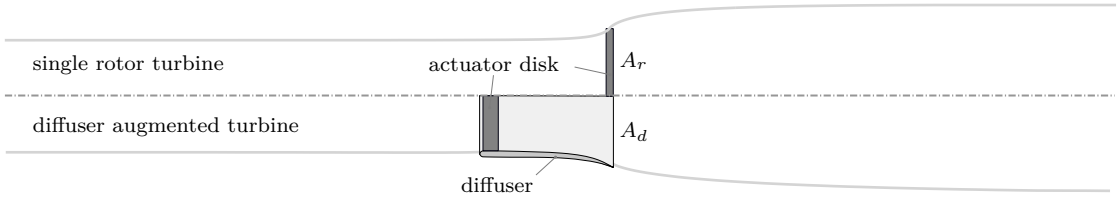

Figure 4.3: Schematic illustration of the derivation of a diffuser design from the stream tubes around an ideal actuator disk

The resulting diffuser version **V0** is presented in Figure 4.4a. With this design, a maximum power coefficient of $c_{P,d} = 0.555$ at an induction factor of $a_d = 0.3$ is achived. The diffuser shape looks very similar to the geometries presented by Hansen et al. [42] and Shives and Crawford [92] and also the performance is in a similar range.

4.1.3 Diffuser Shape at the Rear Edge

For the investigation of the significance of the diffuser shape at the outlet, the basic diffuser geometry **V0** is scaled in axial direction. This leads to different exit angles at the rear edge of the diffuser for a constant diffuser area ratio of $\gamma = 1.5$. The different geometry variants are presented in Figure 4.4a.

As shown in Figure 4.4b the basic diffuser **V0** provides the lowest power output of the investigated diffusers. With increasing redirection of the flow at the exit the diffuser performance increases until reaching a maximum of $c_{P,d} = 0.633$ for the diffuser version **V3**. For this geometry, the flow is redirected sharper through the contour of the diffuser than by mere deceleration at a single rotor which leads to a power coefficient above the Betz limit. Furthermore, an additional thrust force is absorbed by the diffuser. Consequently, a larger widening of the downstream stream tube is achieved for the optimum operation point increasing the mass flow capacity and the upstream catchment area of the machine. With increasing flow deflection, also the size of the flow separation zone at the diffuser outlet increases (see Figure 4.4a). This results in a decrease of back pressure and hence of available turbine “head” as already observed by Gilbert et al. [35]. When a certain size of the flow separation zone is exceeded, the positive effect is surpassed by the negative effect of the blockage of the effective exit area through the stagnation and back flow regions. This may be observed for geometry version **V4** where the overall turbine performance decreases significantly. The effect observed in this study is known as spoiler or flange effect. An

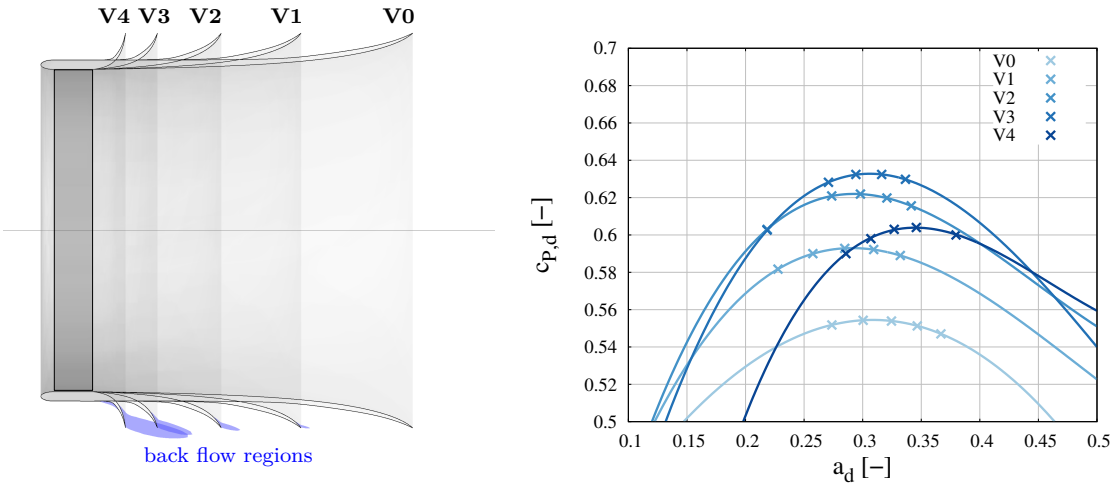

(a) Overview of different geometries **(b)** Diffuser power curves

Figure 4.4: Influence of the flow angle at the diffuser outlet

opposite effect can be observed regarding a perfectly cylindrical shroud without any redirection of the flow ($\gamma = 1$). In this case the streamlines follow the geometry and hardly widen. This leads to a very low power output, as observed by [33] (see also Figure 4.6a).

4.1.4 Diffuser Area Ratio

In order to examine the influence of the area ratio on the turbine performance, the diffusers presented in the previous section ($\gamma = 1.5$) are compared to diffusers with an area ratio of $\gamma = 2.25$ and $\gamma = 4.0$. These diffusers are manually optimized, testing and comparing around ten geometry versions for each area ratio. The best diffuser geometries for each area ratio are presented in Figure 4.5.

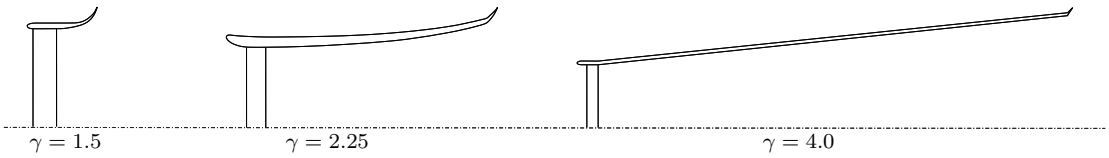

Figure 4.5: Overview over best single-stage diffuser geometries designed in this work

The resulting diffuser power coefficients $c_{P,d}$ as a function of the area ratio are presented in Figure 4.6a by the black dots. A clear correlation can be observed: for an increasing diffuser area ratio the maximum achievable diffuser power coefficient decreases. Also the corresponding diffuser induction factor a_d is obviously influenced by the area ratio. As shown in Figure 4.6b for an increasing area ratio the induction

factor increases, which means that the optimum operation point is shifted to a smaller machine discharge.

In order to verify the observations from this study, geometries and performance data published in relevant literature are reinterpreted according to the definitions presented in Section 2.2.1. Most of the considered geometries are illustrated in Figure 1.5. At this point a certain inconsistency in the gathered data must be discussed. In some cases geometric diffuser attributes like the diffuser outlet area are not clearly stated in the publications and had to be recalculated or measured from sketches. Furthermore, all the data were collected using very different investigation and evaluation methods. Some of the investigations were performed based on experiments, whereas other authors used numerical methods. Also within those two methods there are large differences in methodology, e.g. in the treatment of the rotor or the consideration of the hub. In some cases the authors used rotor models like a screen mesh or the actuator disk model. Others considered the runner blade geometry and specified the performance coefficient based on the shaft power (e.g. [61, 70, 100]). Nevertheless, the collected data give a good general overview.

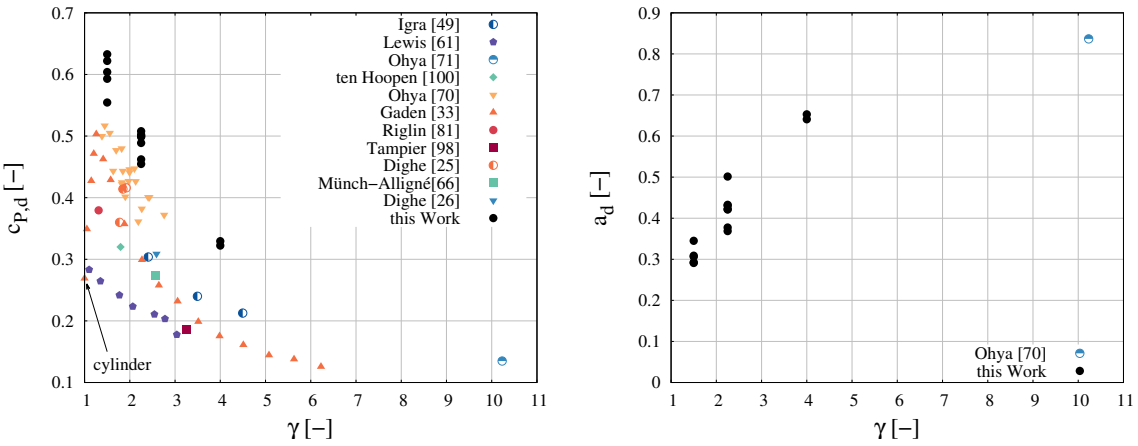

(a) Diffuser power coefficient **(b)** Diffuser induction factor

Figure 4.6: Influence of the area ratio for single-stage diffusers

The reevaluated data from literature are shown in Figure 4.6 represented by the multicolored markers. They support the theory that there seems to be an upper limit for the diffuser power coefficient depending on the diffuser area ratio. To find an explanation for this, the flow fields around the different diffusers are analyzed in Figure 4.7. They show the normalized axial velocity and the stream tube close to the optimum operation point. It can be observed that for large area ratios relatively high velocities occur in the rotor plane. Assuming that - similar to single rotor turbines - the ideal deceleration by a diffuser augmented turbine a_d is in the range of 1/3, these high flow velocities may be explained applying the continuity equation in the diffuser. Furthermore, despite the conservative diffuser opening angle of less than 8° (leading to the large diffuser lengths), larger zones of low flow velocity (colored in dark blue in Figure 4.7) can be observed for diffusers with large area ratios. The fast flow in the

rotor plane does not follow the diffuser contour and detaches from the diffuser walls. The occurring zones of low velocity and flow separations block the effective diffuser outlet area and significantly reduce the mass flow capacity. This can also be observed from the shape of the downstream stream tubes, which do not widen for a large area ratio.

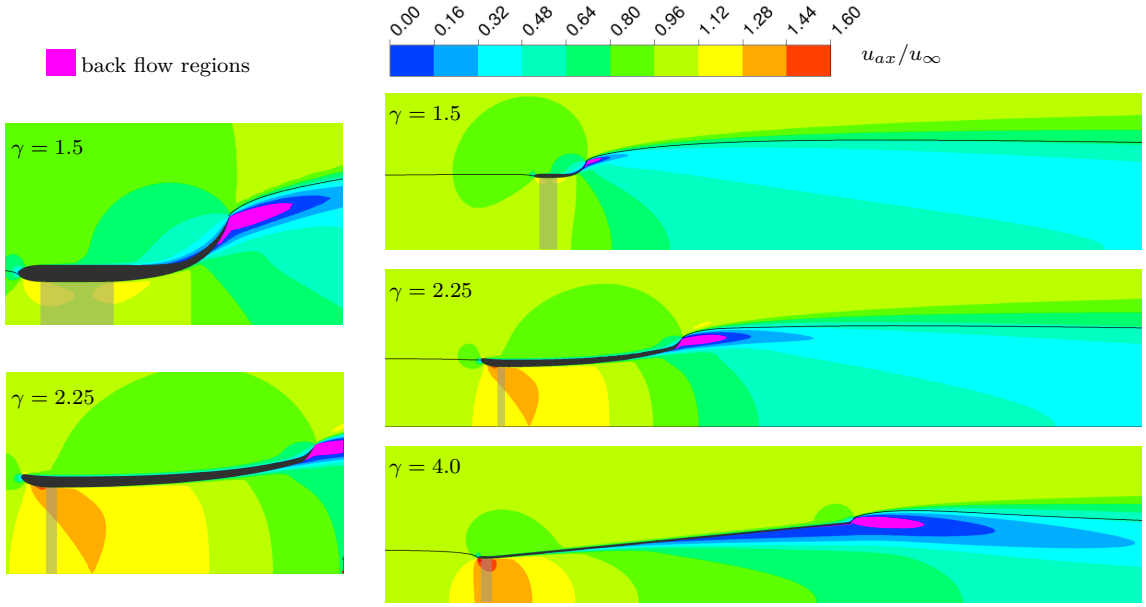

(a) Detail **(b)** Overview

Figure 4.7: Axial velocity field around single-stage diffuser augmented turbines with different area ratios

In order to identify the cause of this effect and to prove that the zones of low velocity are not directly caused by the diffuser bypass flow, a separate simulation is set up: The diffuser geometry with $\gamma = 4.0$ is modeled as conventional draft tube, ending in a very large reservoir. The inlet boundary condition is defined at the draft tube inlet and the velocity distribution resulting from the free flow simulation is mapped. The simulation setup is illustrated in Figure 4.8a.

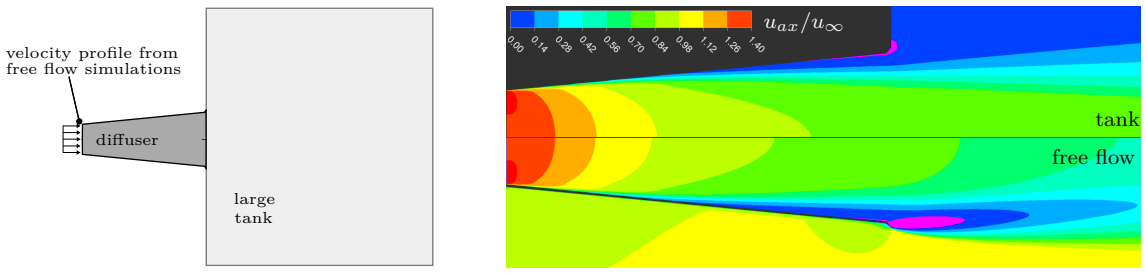

(a) Simulation setup **(b)** Resulting axial velocity fields

Figure 4.8: Comparison of diffusers ($\gamma = 4$) in conventional and in free flow conditions

Regarding the resulting flow fields in Figure 4.8b it can be observed that the zones of low velocity are not caused by the bypass flow but also occur for a similar conventional draft tube. However, for conventional hydropower applications those separations do not significantly influence the mass flow rate and thus the turbine power. In case of a hydrokinetic turbine, where the flow has the possibility to bypass the machine, the separations are blocking the effective outlet area and decrease the mass flow capacity of the diffuser. Therefore, an optimum induction factor of $a_d \approx 1/3$ and hence a good overall power coefficient can not be reached for single-stage diffusers with large area ratios.

4.1.5 Diffusers with Boundary Layer Control

As already discussed in Section 1.1.1 and 2.2.3 technical literature recommends the application of any form of boundary layer control (BLC) in order to avoid the problems identified in the previous section and increase the performance of diffuser augmented turbines. This may be implemented for example by considering a large rotor gap (e.g. [21, 40, 42, 80, 92]), bleeding (e.g. [49]), diffuser vents (e.g. [84]) or a multi-stage diffusers concept (e.g. [24, 35, 44, 47, 73, 85]).

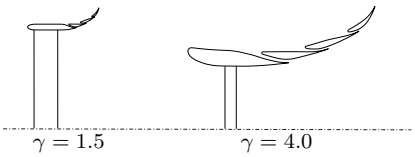

Figure 4.9: Overview over multi-stage diffuser geometries designed in this work

In order to examine if the correlation between overall power coefficient and area ratio is influenced by boundary layer control, the multi-stage diffuser presented by Ruprecht and Reinhardt [85] is re-investigated, not considering the runner blades and hub. Besides this geometry, having an area ratio of $\gamma = 2.25$, two further diffusers based on Ruprecht's and Reinhardt's concept are designed, having an area ratio of $\gamma = 1.5$ and $\gamma = 4.0$. These geometries are presented in Figure 4.9.

The resulting performance quantities for the diffusers developed in this work (black dots) as well as for the initial design published by Ruprecht and Reinhardt (orange triangle) are shown in Figure 4.10a. For a direct comparison, the data gathered for the single-stage investigation without boundary layer control are represented by the small gray dots. It can be observed that all of the multi-stage diffusers are significantly more efficient. Both the diffuser with $\gamma = 1.5$ and the diffuser presented by Ruprecht and Reinhardt are well above the Betz-Limit. Furthermore, the good results achieved by the geometry with $\gamma = 4.0$ indicate that the limitation of the overall power coefficient through the area ratio discussed in the previous section can be improved through the BLC. Also the mass flow capacity at optimum is clearly increased for those designs (see Figure 4.10b). All these observations prove that the concept generally can improve the diffuser design.

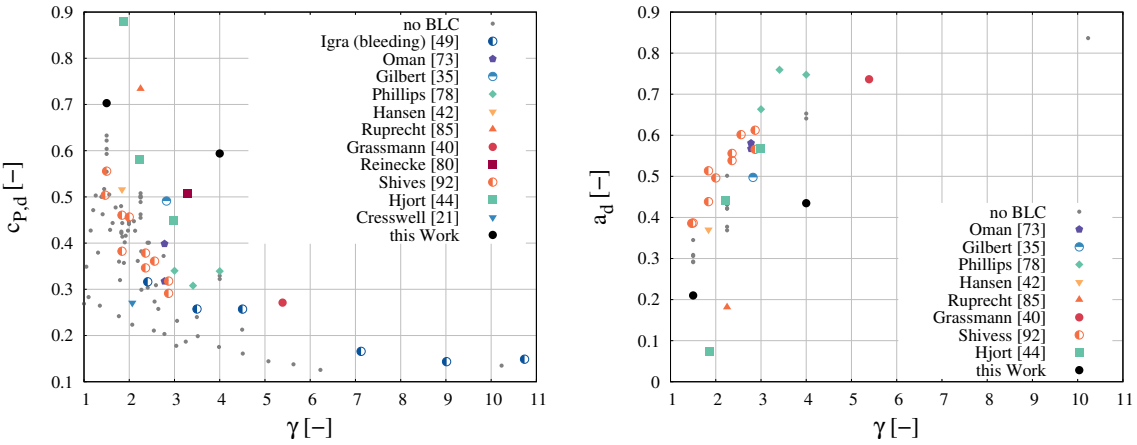

(a) Diffuser power coefficient **(b)** Diffuser induction factor

Figure 4.10: Influence of area ratio using BLC

Again the results are substantiated reevaluating various BLC designs and corresponding performance data from literature and adding them to Figure 4.10a. Many of these geometries are illustrated in Figure 1.5 and 1.6.

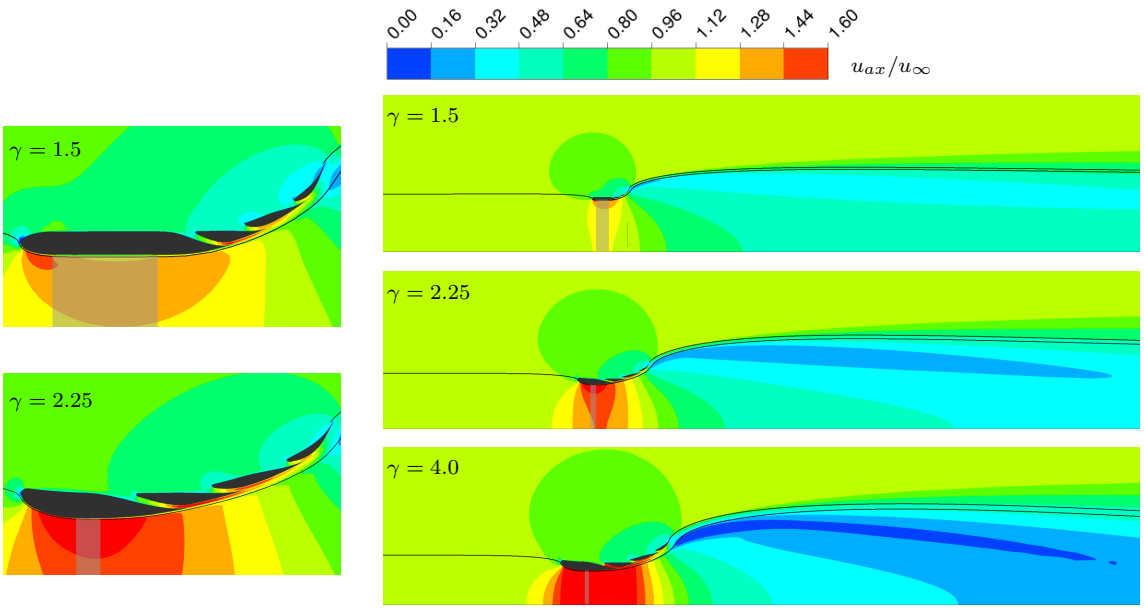

(a) Detail **(b)** Overview

Figure 4.11: Axial velocity field around multi-stage diffuser augmented turbines with different area ratios

With regard to the induction factor, it must be noted that, if at all, the velocity in the rotor plane is specified. Since the continuity in the diffuser is not fulfilled due to the additional mass flow through the vents, the velocity at the diffuser outlet and thus a_d cannot be determined precisely from this. Nevertheless, since the vents are

usually quite small, this approach is considered sufficient for a rough estimate and a qualitative evaluation.

Also from the gathered literature data a general improvement through the concept of the boundary layer control may be observed. The main reason for this is the prevention of the flow separations by re-energizing the wall boundary layer, which may be observed from the resulting flow fields in Figure 4.11a. As consequence, the mass flow capacity of the diffuser is increased and the flow follows the contour leading to a homogeneous velocity distribution in the diffuser and a large expansion of the downstream stream tube (see Figure 4.11b). This is reflected in a lower diffuser induction factor, as may be seen from Figure 4.10b. Especially the superior designs, like Hjort's [44] and Ruprecht's and Reinhardt's [85] geometry, are characterized by this property. By introducing a multi-stage and multi-layer diffuser Hjort's [44] could reach the highest power output in relation to the projected area found in this literature review.

4.1.6 Non-Circular Diffusers

As discussed in Section 1.1.1 the main advantage of the use of diffuser augmented turbines in rivers is the increase of the possible projected machine area at limited flow depth by opening the diffuser to the sides. However, all the designs investigated in the previous section are rotationally symmetric. The objective of this section is to identify the behavior and performance of diffusers with a non-circular outlet area in direct comparison with rotationally symmetric diffusers.

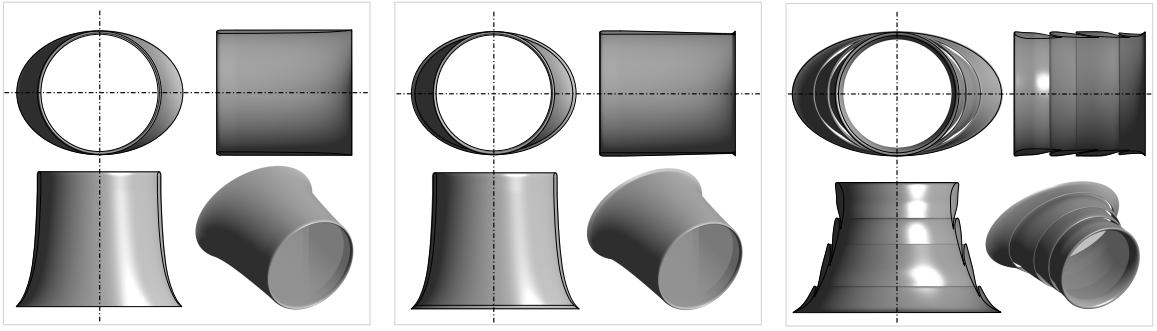

(a) Simple diffuser NC1 **(b)** Spoiler diffuser NC2 **(c)** Multi-stage diffuser NC3

Figure 4.12: Overview over investigated diffuser geomerties with non-circular exit area

For this purpose, the basic diffuser geometry **V0** presented in Section 4.1.2 is again used as a reference. From this geometry two designs with the same area ratio $\gamma = 1.5$ and the same axial length but an elliptic diffuser outlet area are derived. In vertical direction the height of the diffuser in the exit plane does not exceed the size of the machine in the rotor plane. In the first design **NC1**, presented in Figure 4.12a, the top and bottom of the diffuser end completely straight. For the second design **NC2**, presented in Figure 4.12b, a very small spoiler is attached at the diffuser exit to

deflect the flow. This ensures that the outlet area and the overall diffuser height is not increased despite the use of a spoiler. From this design **NC2** two further geometries are derived scaling the diffuser in axial direction by the factor 0.75 and 0.50.

Also from the multi-stage diffuser presented by Ruprecht and Reinhardt a non-circular version is derived. This design **NC3** is presented in Figure 4.12c and has an area ratio of $\gamma = 2.25$. At the last diffuser stage a small spoiler is attached without increasing the height of the diffuser similar to design **NC2**. All the geometries are not optimized automatically but designed based on experience.

The results of the numerical investigations are presented in Figure 4.13. It can be observed that the design **NC1** provides a significantly lower maximum power coefficient compared to the rotationally symmetric basic diffuser geometry **V0**. Using a small spoiler in design **NC2** improves the situation: the power coefficient is 6% higher compared to design **NC1** and also somewhat higher but still not in the range of the good rotationally symmetric designs. Scaling the geometry with a factor of 0.75, it can be observed that the performance is increased. A power coefficient of $c_{P,d} = 0.582$ is achieved. This is possible through a stronger redirection of the flow at the outlet, which is also observed for the rotationally symmetric diffusers in Section 4.1.3. For a stronger scaling of the geometry **NC2** by the factor of 0.5, the performance decreases.

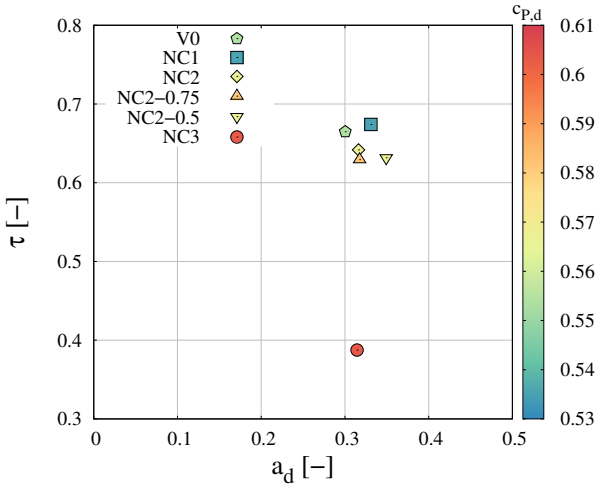

Figure 4.13: Resulting diffuser power coefficients for various non-circular diffusers

Evaluating the multi-stage non-circular diffuser design **NC3** in Figure 4.13 it appears that just from this first-guess geometry a diffuser power coefficient in the region of the Betz limit may be achieved. This design is therefore the most successful of the non-circular geometries presented here. However, compared to the original rotationally symmetrical diffuser presented by Ruprecht and Reinhardt the performance is around 16% lower. It is also obvious that for **NC3** the thrust ratio is particularly low compared to the other non-circular diffuser designs. The reason for this is the larger area ratio leading to a larger projected diffuser area and thus a larger diffuser thrust. The diffuser induction factor is in the same range for all the different diffuser geometries.

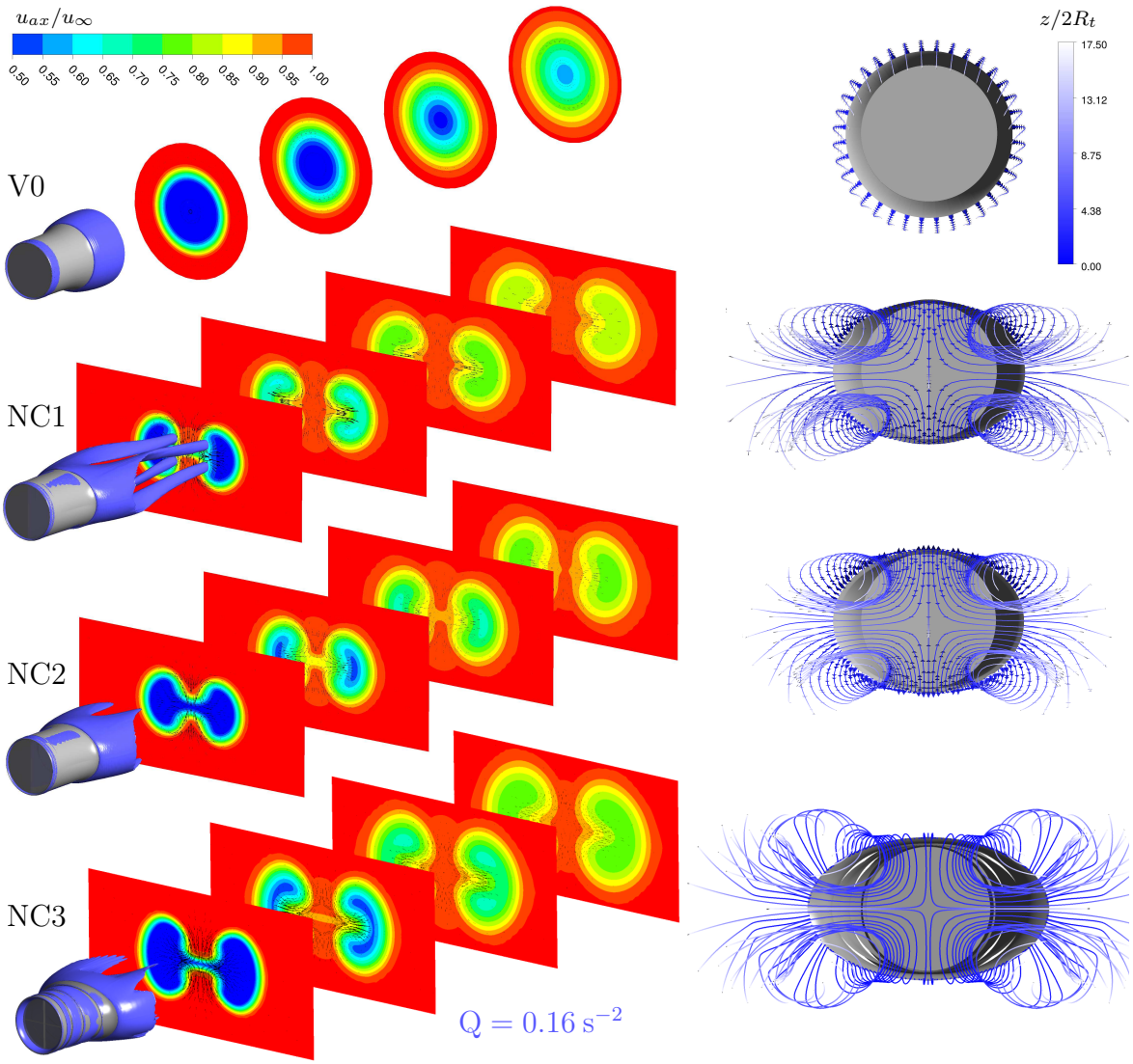

Figure 4.14: Axial velocity in different downstream cross sections (left) and upstream view on streamlines starting at the diffusers rear edge (right) for the non-circular diffusers

Regarding the flow field in several planes downstream of the different diffusers in Figure 4.14 (left) it can be observed that the non-circular diffusers develop two stream tubes widening separately to the sides instead of one extending homogeneously to all sides. From the downstream streamlines starting at the diffusers rear edge in Figure 4.14 (right) it may further be seen that the wake flow is dominated by four vortices, which develop by the inhomogeneous deceleration of the bypassing flow at the diffuser exit. For version **NC2** it can be observed that the two stream tubes are closer. Also the intensity of the vortices is reduced, as visualized by the Q-criterion in Figure 4.14. Examining the flow situation for the multi-stage diffuser **NC3**, it can be noticed that, in contrast to the single-stage geometry variants, the downstream

stream tubes expand not only in horizontal but also in vertical direction. This seems to be advantageous with respect to the power output.

In general, it can be concluded that for non-circular diffusers the irregular deflection of the flow at the outlet makes it more difficult to achieve high power coefficients. Small spoilers on the otherwise flat top and bottom of the diffuser can have a positive effect. Nevertheless, a relatively large area ratio can be applied, especially when using a multi-stage concept. This allows an efficient utilization of the available space for a limited flow depth: for a constant available flow depth, the multi-stage diffuser **NC3** can obtain 1.55 times as much power as the best single-stage machine **NC2-0.75**.

4.2 Investigation of the GenIHS Diffuser Geometry

The design of the advanced diffuser augmented hydrokinetic turbine **GenIHS** developed at the Institute of Fluid Mechanics and Hydraulic Machinery of Stuttgart University is in accordance to all the criteria for a successful diffuser design identified previously. For this diffuser a 3-stage concept was chosen. An area ratio of $\gamma = 4.0$ is achieved by an extreme opening to the sides. The width of the diffuser outlet is three times the rotor diameter. Very large gaps between the diffuser stages ensure a stable wall boundary flow.

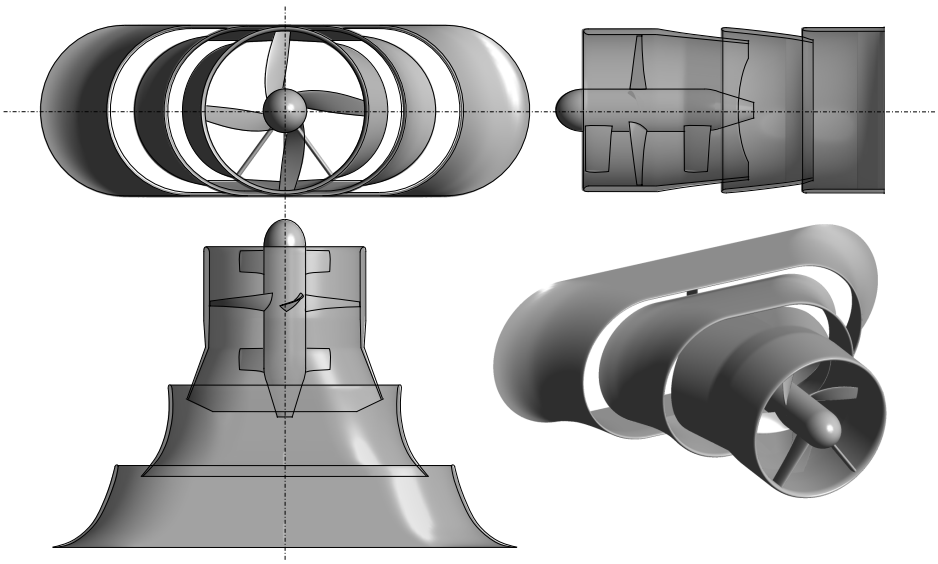

Figure 4.15: Geometry of the GenIHS hydrokinetic turbine

The detailed shape of the diffuser and the runner blades was determined by Tismer using a fully automatic optimization process [101]. Due to the simultaneous optimization, diffuser and blade geometry are perfectly adjusted. The runner consists of four blades running at 90 rpm for optimum operation. The gap between runner and shroud is neglectably small. The hub is fixed by four profiled struts, two upstream and two downstream of the runner. As the second and the third diffuser traverse a

fairly large width, they are each stabilized by one vertical strut in the middle. The final geometry of GenIHS hydrokinetic turbine is presented in Figure 4.15.

4.2.1 Setup for Steady State and Unsteady Simulations

Approach 1 (AD):
For an initial evaluation of the diffuser geometry, a setup similar to the one described in Section 4.1.1 is applied. This means that the actuator disk method is applied to model the rotor. However, all the struts and also the hub are geometrically resolved. The geometry and the expected flow field are axis symmetric for this setup, which enables the reduction of the solution domain to half of the full geometry using a symmetry boundary condition. A steady state flow situation is assumed.

Approach 2 (MP):
In a next step the four rotor blades are geometrically resolved (see Figure 4.16a). The rotor and the stator domain are coupled using a mixing plane approach (also called stage interface) at the upstream and downstream rotor-stator-interface. This means that all flow quantities are circumferentially averaged for the transfer to the neighbouring reference frame. This allows to use steady state conditions in the simulation despite the rotating parts. However, the flow conditions are not axis symmetric in this case. Therefore, the full diffuser geometry is considered in the simulations.

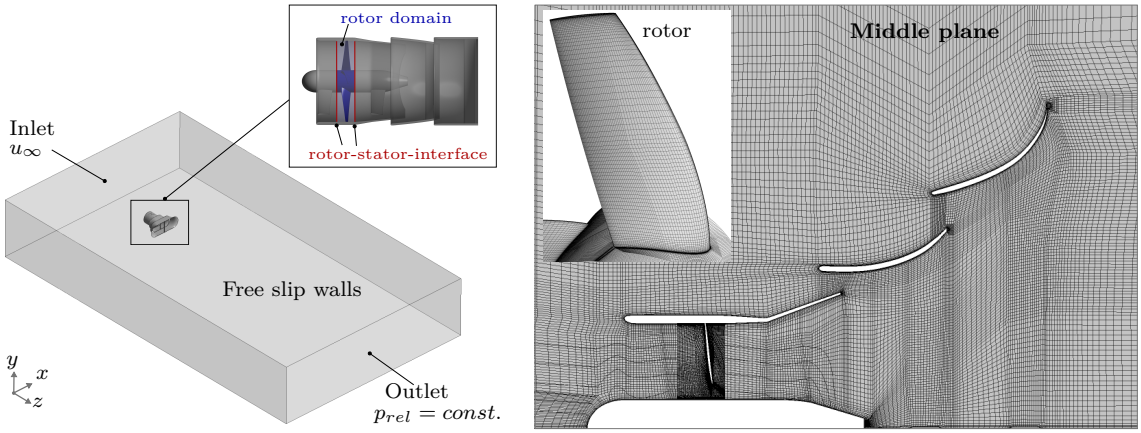

(a) Schematic setup **(b)** Mesh around rotor and in domain middle plane

Figure 4.16: Simulation setup and mesh for the investigation of the GenIHS turbine

Approach 3 (TRN):
For the final and most realistic simulation setup the motion of the rotor is represented by a moving mesh using a sliding mesh approach at the rotor-stator-interfaces. In this case an unsteady simulation is required. A time step of 0.0075 s, which corresponds to a rotation of 4° per time step, is used for time discretisation. As those simulations are quite cost intensive, only three operation points are simulated (85 rpm, 90 rpm

and 95 rpm). Besides the treatment of the rotor, all boundary conditions and models described in Section 4.1.1 are used for the investigations of GenIHS.

The solution domains are discretized by block-structured meshes, which are exemplary shown in Figure 4.16b. The stator domain including the diffuser and the far field is discretized by 10 M elements. The rotor domain resolving the four runner blades consists of 3.5 M elements. The respective viscous sublayer is modeled through a wall model. The applied meshes resolve the wall flow with $30 < y^+ < 300$. The results gained with this mesh are conservative concerning the power prediction (Details on the mesh independence can be found in Appendix D).

4.2.2 Results of the Investigation of the GenIHS Diffuser

The results of the different simulations investigating the GenIHS diffuser augmented turbine are presented in Figure 4.17. It can be observed that for all quantities the results of the actuator disk simulations (AD) and the simulations using the mixing plane approach (MP) agree very well. The maximum hydraulic diffuser power coefficient calculated from the head loss over the rotor is $c_{P,d} = 0.45$.

Resolving the rotor geometrically, it is possible to calculate the diffusers shaft power coefficient resulting from the pressure and shear stress distribution on the rotor blades as follows:

$$c_{P,d,mech} = \frac{\omega M_z}{\frac{\rho}{2} A_d \, {u_\infty}^3} \tag{4.1}$$

For the mixing plane approach the maximum shaft power coefficient is determined to $c_{P,d,mech} = 0.40$. Compared to the curve representing the hydraulic power, the optimum is reached at a lower diffuser mass flow. At this operation point the runner speed is $n = 90$ rpm and the blade efficiency is $\eta_r = 0.9$.

Comparing the results of the steady state simulations to those from the unsteady simulations (TRN) represented by the blue lines in Figure 4.17, it can be seen that all characteristic values are overestimated by the steady state simulations. For the unsteady simulations a maximum shaft power coefficient of $c_{P,d,mech} = 0.38$ is reached. Also the power curve of the hydraulic power is significantly lower (the exact maximum is not determined, as it occurs at a different operation point).

The reason for this can be found in a direct comparison of the respective flow fields in Figure 4.18. It can be seen that for the unsteady simulation the diffuser flow is asymmetric and a back flow zone develops on one side directly downstream of the diffuser. The asymmetric flow field is caused by the residual swirl and the resolved wake flow of the runner blades in interaction with the non-rotationally symmetric components of the turbine, such as diffuser walls and struts. This zone is blocking the outflow reducing the diffusers mass flow capacity and consequently its performance. This effect is not observed for the results of the mixing plane simulations, where the flow field is circumferencially averaged at the rotor-stator-interface and the wake flow

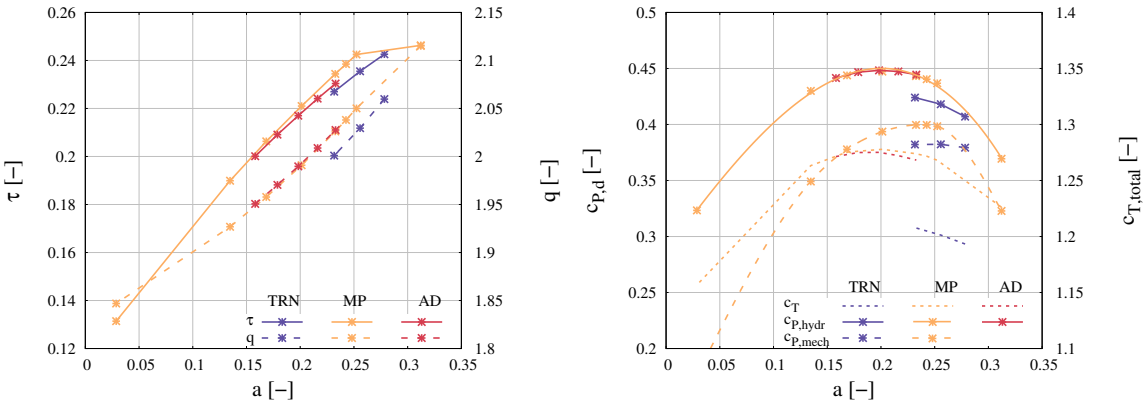

(a) Thrust ratio and mass flow ratio

(b) Diffuser power coefficient and thrust coefficient

Figure 4.17: Resulting characteristic values for GenIHS turbine using different rotor models

of the runner blades in the diffuser is not resolved. The same applies to the results of the actuator disk approach where the runner blades are completely neglected (see Figure D.2 in Appendix D). It can thus be concluded that the wake flow of the runner blades leads to the asymmetric flow field an the significant reduction in overall performance.

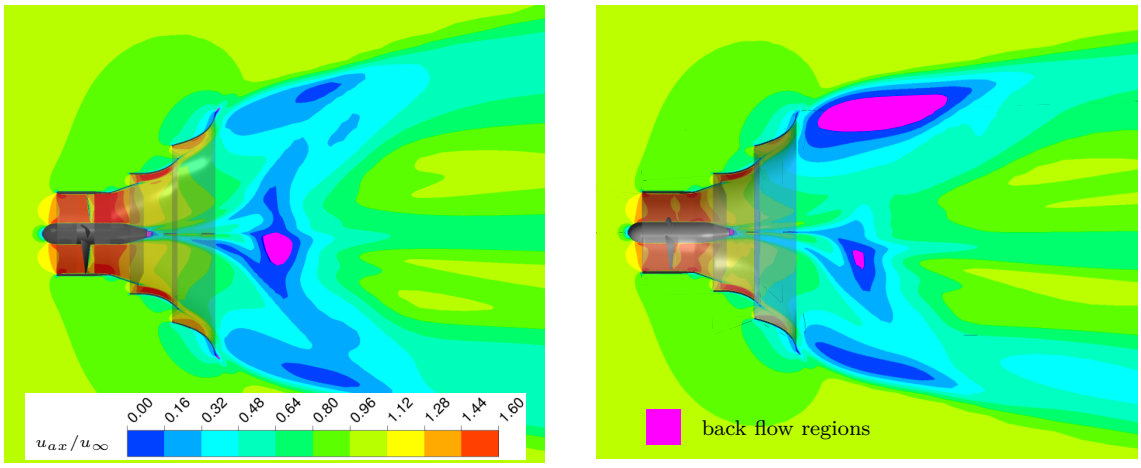

(a) Mixing Plane model

(b) Fully resolved unsteady simulation

Figure 4.18: Axial velocity field around GenIHS turbine in horizontal mid-plane

Regardless of the specific simulation approach, some special attributes of the machine are identified. It is especially remarkable that the ratio between the mass flow at the diffuser outlet and the mass flow through the rotor at optimum operation is $q \approx 2$. Hence, the amount of water flowing through the rotor is similar to the one coming through the vents. This can also be seen from the flow field in Figure 4.18a: the comparatively large vents are perfused at high velocity. Still, the large vents are

successfully preventing flow separations in the diffuser. The downstream flow field is homogeneously decelerated by the diffuser. Furthermore, the thrust ratio τ is very low compared to the previously investigated diffusers. This means that the diffuser thrust is very large compared to the rotor thrust which is mainly caused by the expansive third diffuser stage and the high area ratio.

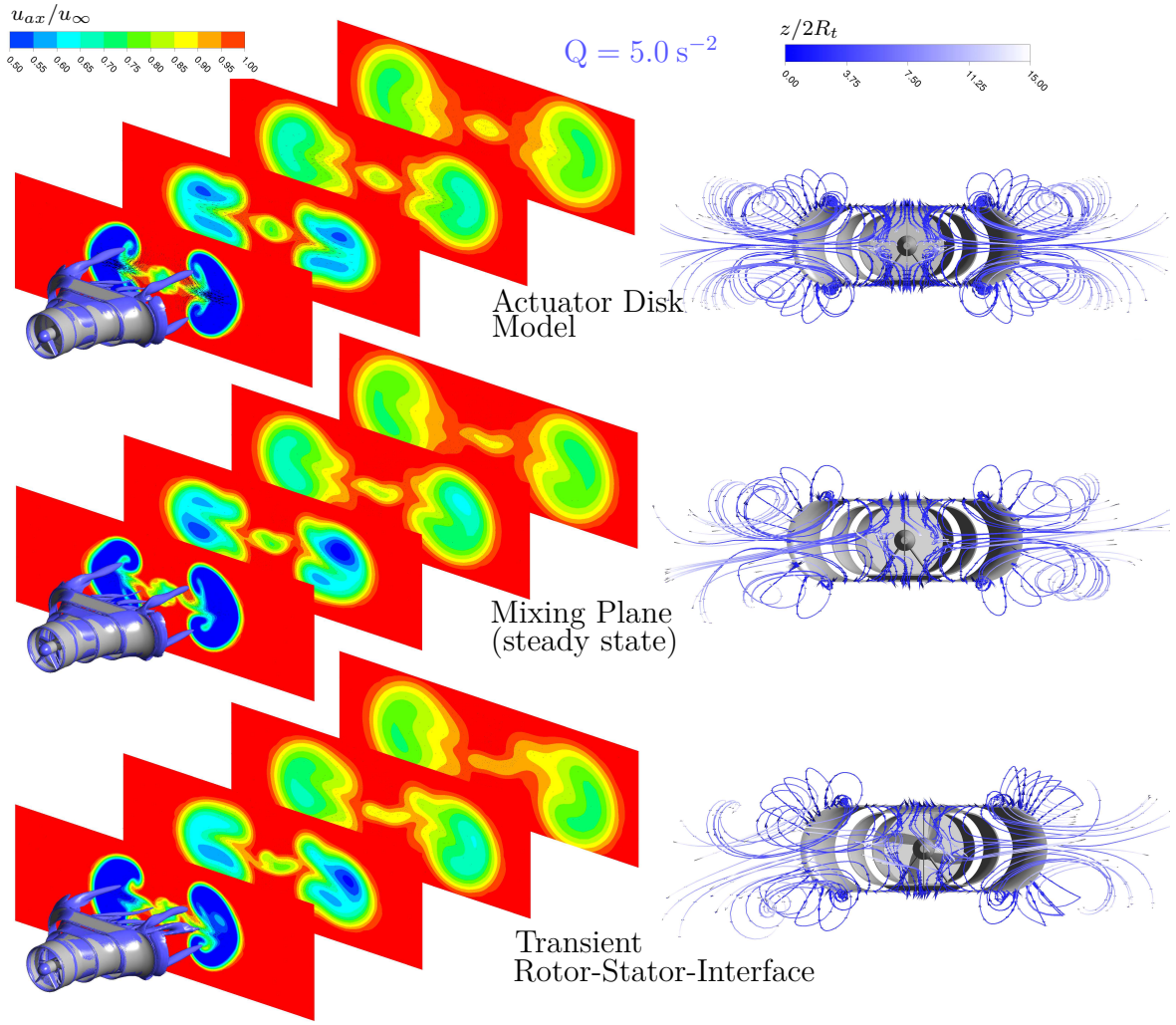

Figure 4.19: Axial velocity in different cross sections downstream of the GenIHS machine (left) and upstream view on streamlines starting at the diffusers rear edge (right) for different rotor modeling methods

Regarding the flow fields in Figure 4.19 it can be noticed that the four downstream vortices identified as characteristic for non-circular diffusers in Section 4.1.6 also occur for this design. The divided downstream stream tube is also very clearly visible. In addition, the wake flow from the hub occurs in the center between the two stream tubes. Similar to the design **NC3**, the stream tube is not only expanding in horizontal but also in vertical direction. On the whole, the performance achieved with the GenIHS

diffuser in combination with the comparatively low required flow depth at a large area ratio is very promising for shallow water applications.

4.3 Evaluation of Consistency between 1d Theory and Numerical Investigations

The various different diffuser geometries designed and investigated in the previous sections are used to evaluate the general 1d theory on diffuser augmented turbines derived in Section 2.2.2. For this purpose, the simulation results are added to the theoretical contour plots and colored according to the diffuser power coefficient determined in the numerical flow simulations. The results are presented in Figure 4.20 for different area ratios.

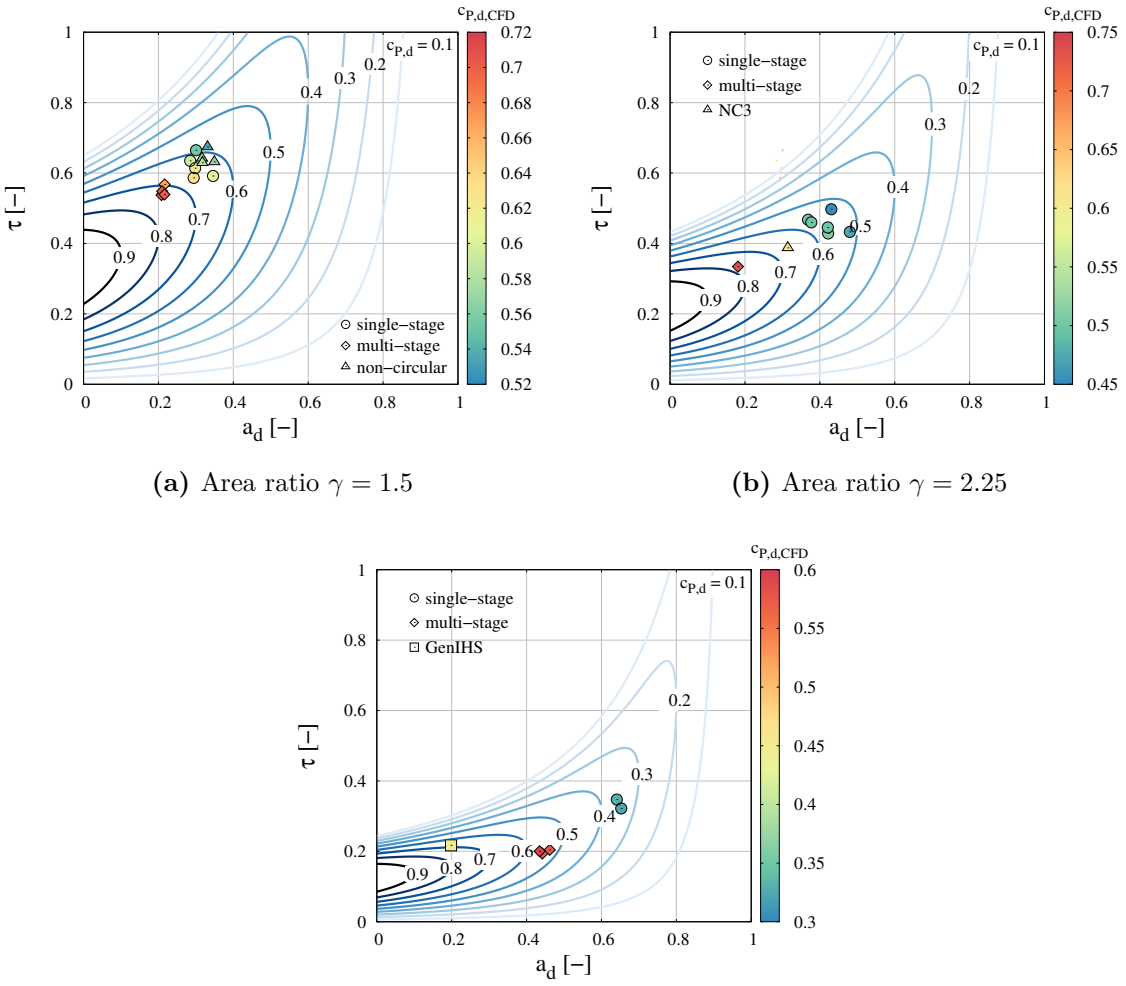

(a) Area ratio $\gamma = 1.5$

(b) Area ratio $\gamma = 2.25$

(c) Area ratio $\gamma = 4.0$

Figure 4.20: Results of CFD simulations in direct comparison to 1d theory (Figure 2.4)

It can be observed that theory and simulation results of different detailed diffuser geometries correspond comparatively well, especially for the single-stage diffusers with an area ratio of $\gamma = 1.5$. Also the results for the geometries with $\gamma = 2.25$ and $\gamma = 4.0$ are found to be in the predicted ranges. However, the precision of the respective $c_{P,d}$ -values is lower under those geometric conditions. The reason for this is probably that for higher area ratios larger flow separation zones develop in the diffuser, a phenomenon which is not covered by the 1d theory. Furthermore, the correlation between power coefficient and area ratio observed in the theory is clearly confirmed by the simulation results for single-stage diffusers.

A consideration of the numerical results of the multi-stage and non-circular diffusers in context with the 1d theory is problematic, as both geometric concepts are not covered by the applied theoretical approach. However, also those data are found in the ranges predicted for the respective area ratios. Furthermore, the simulated diffuser power coefficients are roughly in the theoretically predicted region. Most probably the mass flow and momentum entrainment through the vents are small enough to only play a minor roll in the conservation equations. Moreover, the positive effect of the BLC is clearly visible: by increasing the mass flow capacity, a lower induction factor is reached, leading to a significant increase in performance in theory as well as in praxis.

Among all the results, the GenIHS diffuser is especially remarkable (see Figure 4.20c). Caused by the large gaps between the diffuser stages, which lead to a high mass flow ratio, this geometry operates at a very low diffuser induction factor. According to the theory, a high diffuser power coefficient is possible under this condition in combination with the observed thrust ratio. However, the numerical simulations provide a remarkably lower value. This large deviation is caused by the increased back pressure level in the diffuser due to the large gaps, which is to the expense of the diffuser power coefficient.

Independent from the detailed geometric designs and concepts, Figure 4.20 shows that the resulting characteristic values of most of the diffusers (colored point symbols) can be found at a maximum possible induction factor and thrust ratio for the corresponding constant power coefficient (blue iso lines). This means that if the induction factor can be reduced by increasing the mass flow capacity of a diffuser through an adaption of design parameters, its power coefficient will most probably increase while the thrust ratio is decreasing. In general, it can be concluded that the 1d theory is well suited for analyzing a diffuser geometry, but accurate performance predictions are not possible, as usually thrust ratio and induction factor are unknown.

4.4 Conclusion

A systematic analysis of different geometric attributes of diffuser augmented hydrokinetic turbines is presented. The work is based on the design and numerical investigation of various diffuser geometries. The results are supported by data from literature, which are reevaluated according to the theory that the diffuser exit area is

the relevant geometric reference. This approach allows to identify a clear correlation between the diffuser area ratio and the overall machine power coefficient for the diffusers designed in this work as well as for the diffusers presented in literature. The observed effect may be reduced using boundary layer control, where higher area ratios are possible without observing a dramatic decrease in overall power coefficient. The observed correlations can provide a rough estimation of the performance of diffuser augmented turbines depending on the area ratio.

Considering a non-circular diffuser exit area to increase the projected machine area for shallow water applications significantly changes the downstream flow field. Due to the inhomogeneous deflection at the diffuser outlet, four counter-rotating vortices develop in the wake flow and compared to rotationally symmetric geometries a lower maximum power coefficient is achieved. However, also in this case, a boundary layer control concept can help achieving a larger diffuser area ratio and a higher diffuser power coefficient.

In general, it becomes clear that for a successful diffuser design a balance between a high diffuser power coefficient and a large area ratio is necessary - especially for applications with limited available flow depth. This consideration was successfully implemented in the design of the GenIHS machine. Despite a mid-range power coefficient, it can convert twice as much power as the more efficient single-stage design NC2-7.5 when assuming a similar machine height.

However, it should be noted that the high total thrust occurring especially for diffusers with large area ratio requires a high structural stability of the machine and a large effort ensuring a resistant turbine mounting. Furthermore, especially multi-stage diffusers are expected to be very complex in manufacturing. All of this can lead to high costs, which has to be considered for potential projects.

With regard to the turbine model, the different effects caused by the design parameters show that a detailed mathematical description based only on geometric data is not possible. The observed correlation between power coefficient, induction factor and area ratio can provide the basis for a rough estimation. However, for a precise 1d modeling of diffuser augmented turbines, characteristic diffuser flow quantities determined in 3d simulation have to be used.

5 Numerical Investigation of Hydrokinetic Turbines in River Flow

It is well known that certain site characteristics can have a major impact on the performance and operation point of kinetic turbines. In the following, the influence of the channel cross section and a sheared flow distribution on both single rotor turbines and diffuser augmented turbines is systematically investigated.

For the investigations, a special focus is set on the characteristics of the potential site in Montreal, Canada. The St. Lawrence river in this area is characterized by a large width and a relatively small flow depth. Furthermore, measurements of the vertical velocity distribution indicate a high bed roughness. More details on the hydraulic attributes of the project area are provided in Section 7.1.

5.1 Blockage Effects

As already described in Chapter 2.3 the channel dimensions around a hydrokinetic turbine theoretically have a strong influence on the turbine power. In order to demonstrate the applicability of the theory introduced by Garrett and Cummins [34] for practical use, different hydrokinetic turbines in various channel geometries are investigated in this context.

For the basic investigations, rectangular channel cross sections are chosen. Besides the blockage ratio ϵ also the aspect ratio of the channel $\alpha = B_c/h_c$ is varied in the range between 1 and 20. The latter is particularly interesting as a high aspect ratio is one of the main characteristics of the Montreal site. An overview of the channels with varied aspect ratios is presented in Figure 5.1a and the detailed channel dimensions are listed in Appendix A.

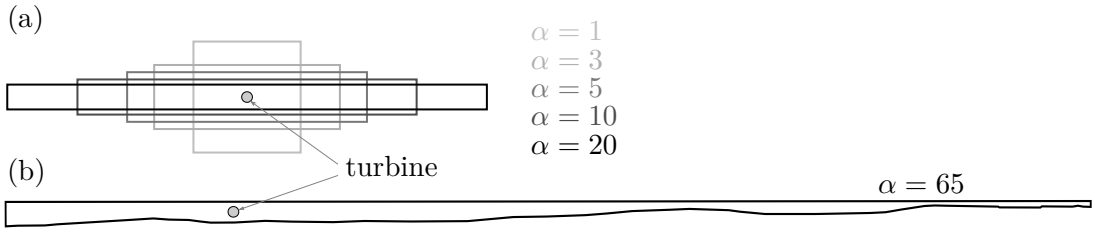

Figure 5.1: Academic (a) and realistic "Montreal" (b) channel cross sections

In addition to those academic channel cross sections also a more realistic channel geometry is considered. The geometry presented in Figure 5.1b is gained by extracting

the river bed geometry from one exemplary cross section of the digital terrain model (DTM) of the St. Lawrence River in Montreal. Hence, it represents the characteristics of the river in the project area very well. This bottom geometry is constant in axial direction. In this non-rectangular channel geometry the aspect ratio is defined as ratio between the width of the cross section and the local flow depth at the turbine position. For the "Montreal" cross section, this value is $\alpha = 65$.

In the following, the partial blocking of those channel geometries by different turbine types is investigated. For a basic investigation a single rotor actuator disk with a radius of $R_t = 2.45$ m is placed in the channels. On the one hand the applicability of the theory presented by Garrett and Cummins [34] is evaluated through this test series. On the other hand it allows to identify a potential influence of the channel aspect ratio on the results. Besides the single rotor turbine also the influence of the blockage effect on different diffuser augmented turbines is investigated. For this purpose the single-stage diffusers **V0**, **V3** and **NC1** and the multi-stage diffusers presented by Ruprecht and Reinhardt [85] and the GenIHS diffuser (without considering struts, support structure and detailed rotor geometry) are used. Details on the diffuser geometries can be found in Chapter 4. For the "Montreal" cross section only the single actuator disk and the GenIHS diffuser are investigated.

5.1.1 Simulation Setup

In order to isolate the effect of the channel blockage without having to consider any other effects (e.g. sheared flow), the channel walls are defined as free slip walls for this investigation. Therefore, for the academic channel geometries a horizontal and a vertical symmetry boundary condition may be applied reducing the solution domain to a quarter of the full geometry. The "Montreal" cross section has to be fully resolved, as the geometry is not symmetric. The respective turbine is placed at an axial distance of 60 m from the inlet in the 300 m long channel. Besides those boundary conditions the setup is identical to the one presented in Section 4.1.1. The constant upstream velocity is 2.69 m/s.

5.1.2 Blockage Effect for Single Rotor Turbines

The results of the investigations are presented in Figure 5.2 showing the power coefficient and induction factor over the blockage ratio. Different channel aspect ratios are represented by differently colored curves. In order to evaluate the theory presented by Garrett and Cummins (Equation 2.35 and 2.36) also laminar simulations are conducted in this context. The results are presented by the green curves in Figure 5.2. It can be observed that the laminar simulations agree quite well with the Garrett and Cummins theory especially regarding the power coefficient. For the induction factor some deviations can be observed for large blockage ratios. Obviously, the influence of the channel aspect ratio is of minor importance in this case.

When considering the turbulence in the numerical model, which is mainly developing at the shear layer along the boundaries of the stream tube the results are very different. For small blockage ratios the deviation from theory and laminar results is largest. Both the power coefficient and the induction factor are determined to be higher in the turbulent simulation. For increasing blockage ratios the turbulent and the laminar results converge. It can be concluded that the turbulence mainly influences the correlation for channels with small blockage ratios.

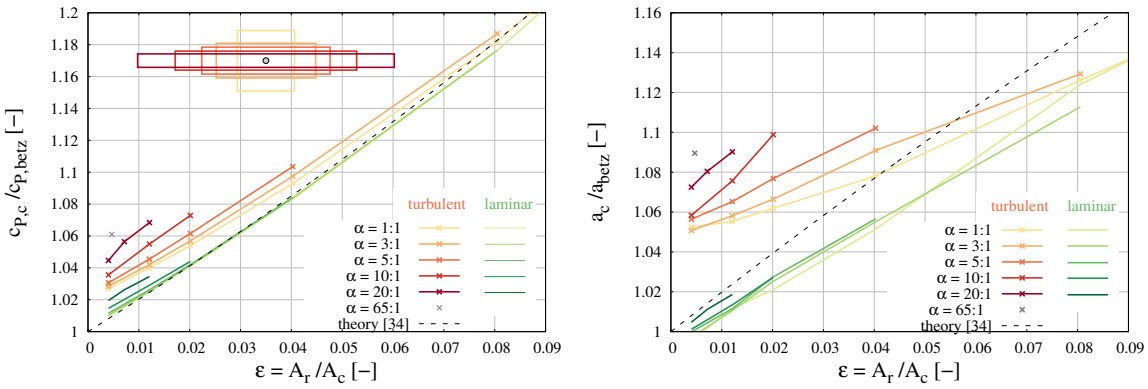

(a) Power coefficient **(b)** Induction factor

Figure 5.2: Influence of different channel geometries on a single rotor actuator disk

Furthermore, it is clearly visible that the channel aspect ratio has a significant influence on the results of the turbulent simulations: the larger the area ratio, the larger the power coefficient and the induction factor. This becomes most obvious for the "Montreal" cross section: in this case the power coefficient is around 6% increased compared to the free flow situation, whereas the theoretical increase for this blockage ratio is around 1%.

All those results indicate that turbulence has a major influence on the channel blockage effects - especially for cross sections with a large aspect ratio. Similar observations were made by Nishino and Willden. They observed that "both c_P and c_T are slightly higher in the narrow rectangular cross section channel than in the square cross-section channel..." [68].

At this point it has to be noted that the results presented in this work differ slightly from the ones published in [96]. The reason for this is that, for the simulations published there, the k-ϵ turbulence model was used. Moreover, not a constant loss coefficient but a constant momentum loss over the actuator disk was assumed.

5.1.3 Blockage Effects for Diffuser Augmented Turbines

Similar to the previous investigation, the diffuser outlet area is again used as a reference area for all dimensionless quantities. Especially for the determination of the blockage ratio, it is important to use the actual projected surface of the entire

machine A_d as this area is effectively blocking the channel. The investigated diffuser geometries as well as two designs studied in the corresponding literature are presented in Figure 5.3.

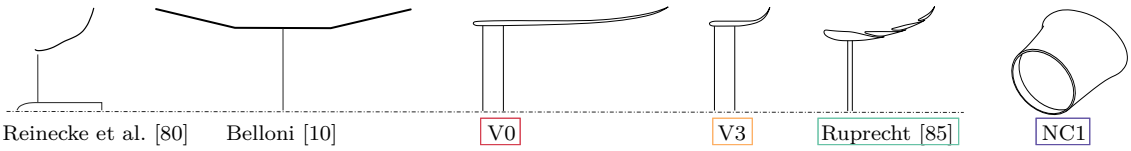

Figure 5.3: Overview of diffuser designs investigated in context of blockage effects in literature and this work

Due to the large number of simulations, a presentation of all results would be too convoluted. Therefore, at first only the results for the channels with an aspect ratio of $\alpha = 3$ and $\alpha = 20$ are discussed. The results, summarized in Figure 5.4a, show a significant deviation among the different diffuser geometries. In general, for a comparatively small aspect ratio of $\alpha = 3$ the influence of the blockage ratio on the diffuser power coefficient is smaller compared to the theory. However, it is apparent that some diffuser geometries behave similarly in those channels. The curves for the basic diffuser geometry **V0** and the one for the non-circular version **NC1** are very close. Both diffusers are characterized by a moderate deflection of the flow at the diffuser's rear edge and a comparatively low power coefficient. The shorter version of the basic diffuser **V3** behaves similar to the multi-stage diffuser presented by Ruprecht and Reinhardt. Also the characteristic of the GenIHS turbine is close to those curves. These three diffusers react with a large increase in performance to a higher channel blockage. It seems that the diffuser's rear edge is more dominant for the blockage effects in channels with moderate aspect ratio than other attributes like boundary layer control or axis symmetry of the diffuser.

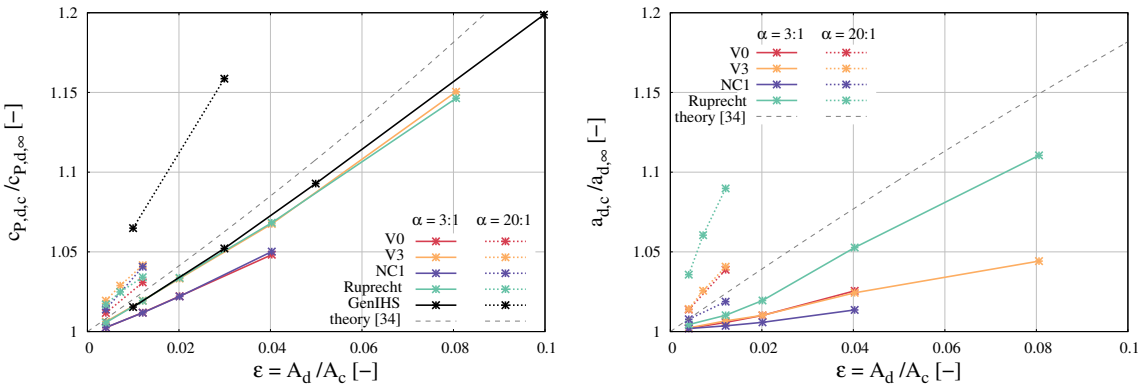

(a) Power coefficient

(b) Induction factor

Figure 5.4: Blockage effect on different diffuser augmented turbines for various channel geometries

For channels with a high aspect ratio of $\alpha = 20$ the results are very different. The increase in performance for all investigated diffusers is larger than the theoretical value. The behavior of the GenIHS diffuser is particularly noticeable in those wide and shallow channel cross sections. Here, a significant increase in performance of up to roughly 15% can be observed. For the other diffusers the effect of increasing performance is less significant.

It can be seen from Figure 5.4b that the induction factor for the optimum operation point is influenced by the blockage effect in a different way. The curves are very different for the various geometries. While for an aspect ratio of $\alpha = 3$ the multistage diffuser from Ruprecht and Reinhardt behaves almost like predicted by the theory, the curve for the elliptical diffuser **NC1** is very flat.

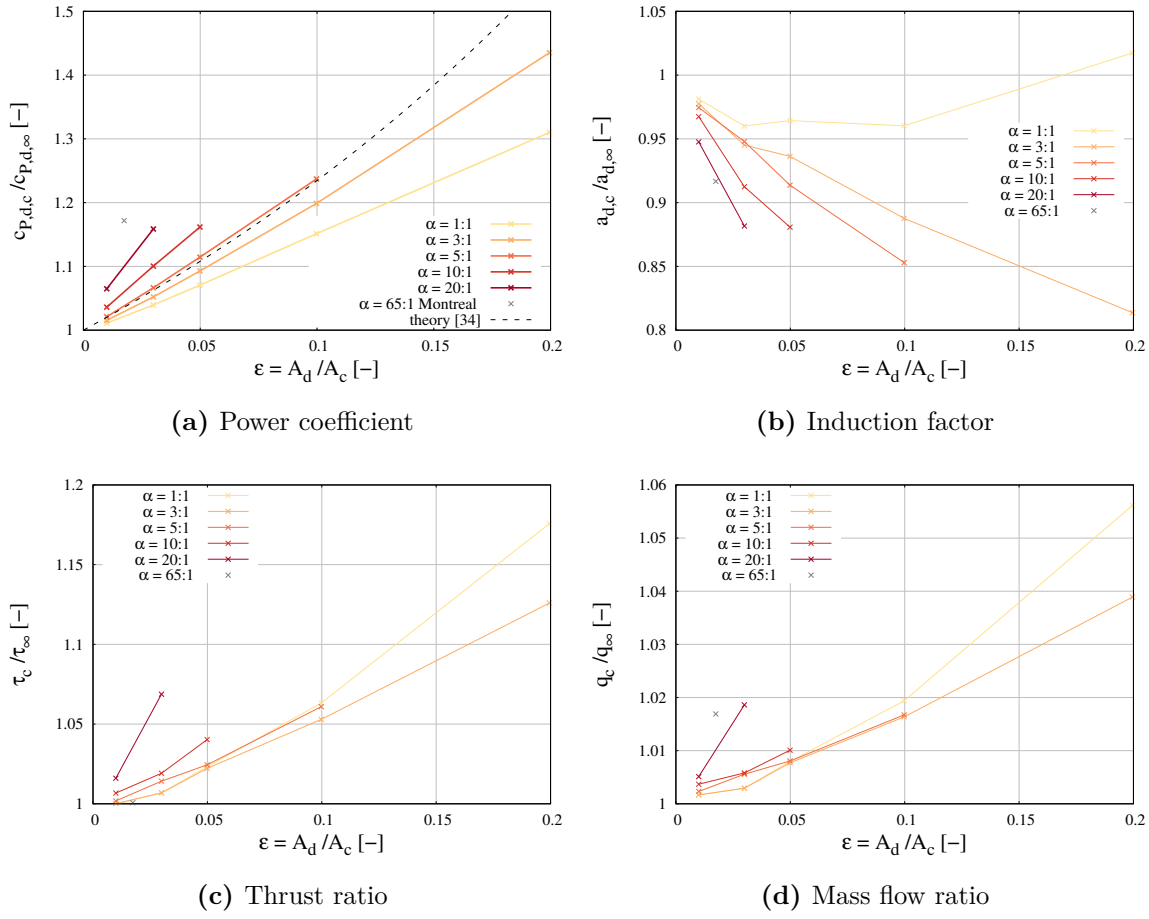

(a) Power coefficient

(b) Induction factor

(c) Thrust ratio

(d) Mass flow ratio

Figure 5.5: Influence of different channel geometries on the GenIHS turbine

Again, the behavior of the GenIHS geometry is particularly remarkable. In contrast to all other investigated turbines the optimum diffuser induction factor decreases with increasing blockage ratio and is therefore not plotted in Figure 5.4b but separately in Figure 5.5b. That means that the optimum is shifted to higher diffuser discharges in this case, which is probably caused by the fact that for this geometry half of the mass flow at the diffuser outlet enters the diffuser through the vents.

Figure 5.5 furthermore allows a detailed analysis of the relevant flow quantities for the GenIHS turbine in all investigated channels. For the power coefficient, a wide spread of the array of curves can be seen in Figure 5.5a. From this it can be concluded that this diffuser geometry is very sensitive with respect to the exact shape of the channel cross section. This is probably caused by the extreme aspect ratio of the diffuser exit. Also thrust and mass flow ratio are influenced by the blockage effect. Both parameters increase with increasing channel blockage as shown in Figure 5.5c and 5.5d. However, it seems that the aspect ratio is of minor importance for those variables. Only for very large aspect ratios the results clearly differ from the trend. The complete results for the other diffuser geometries are listed in Appendix A.

The blockage effect for diffuser augmented turbines was also numerically investigated by Reinecke et al. [79] and Belloni [10] with very contradictory results. The results of those two studies are summarized in Figure 5.6, where the power coefficients are normalized by the value for the lowest presented blockage ratio. Reinecke et al. only determined a very slight influence of the channel blockage on the turbine performance, whereas Belloni observed a behavior close to the theory presented by Garrett and Cummins and consequently also to the observations made in this work. These results underline once again that the prediction of the behavior of diffuser augmented turbines in limited channels is very complex.

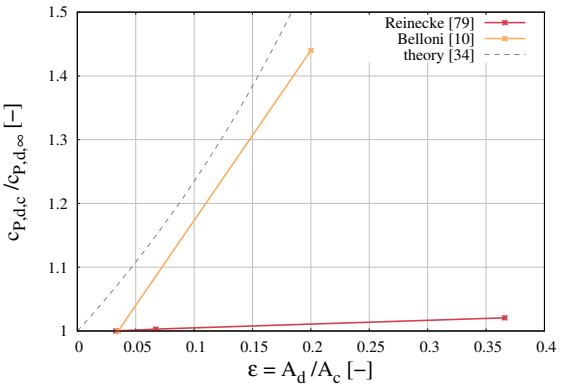

Figure 5.6: Influence of blockage effect on the performance of DATs presented in literature

5.2 Influence of Sheared Flow Conditions

As already explained in Section 3.2, a new method for modeling a high bed roughness is developed and used in this work. For this approach the roughness is represented by a porous zone directly above the bottom and a very realistic velocity profile is generated. In this way the influence of a sheared flow profile on the performance of single rotor and diffuser augmented kinetic turbines can be investigated in detail. The distribution of the vertical velocity profile is modeled to reproduce the conditions at the potential turbine site. In addition, the reaction on several further velocity profiles is investigated in order to determine the sensitivity of the effect.

There are multiple options for interpreting the resulting turbine power with respect to the choice of the reference velocity. In the following investigation the different approaches presented in Section 2.4 are applied and compared in order to identify the most suitable approach. For eliminating the influence of the blockage effect, the results of the following investigations are normalized using the corresponding results from Section 5.1.2 and 5.1.3.

5.2.1 Simulation Setup and Generation of Velocity Profile

For the basic investigation a simple actuator disk with a rotor radius of $R_t = 2.45$ m is used. Furthermore, also the diffuser augmented turbine GenIHS is investigated. The turbines are placed in the channel geometries B2 and D2 (for geometric details see Appendix A). Those channel geometries have already been used in the previous section to analyze the blockage effect. Similar to the setup in Section 5.1 the channel side walls are defined as free slip wall and the turbine is placed in the center of the channel. For shallow water applications this is a meaningful positioning, as it provides enough distance to the water surface (surface waves and ice) but also to the river bed (low velocity and sediment transport). Due to the asymmetric inlet boundary only one symmetry plane (vertical middle plane) is used to reduce the computational effort.

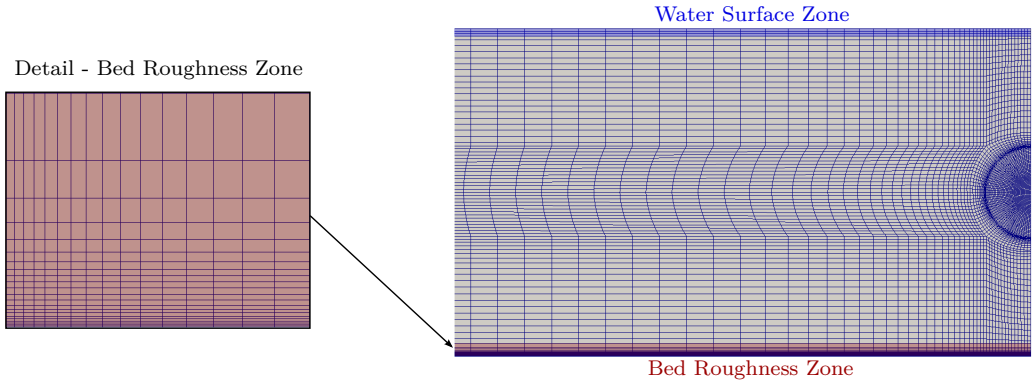

Figure 5.7: Mesh for high roughness simulations

The top boundary condition representing the water surface is defined as free slip wall neglecting the influence of both, the bed roughness and the turbine on the water surface (similar to [30]). For the site measurements a deceleration of the flow velocity towards the water surface can be observed (see Figure 5.8). This is in accordance to many measurements of velocity profiles in open channels published in relevant literature (e.g. [29, 32]). In order to reproduce this in the simulation, a porous zone with constant thickness of 0.4 m and constant loss coefficient of 0.015 m^{-1} in both horizontal directions is defined directly below the top boundary condition.

The bottom roughness is modeled according to the procedure described in Section 3.2. Four different inlet velocity profiles are generated using various roughness heights for a depth-averaged velocity of 2.69 m/s. The corresponding roughness parameters are

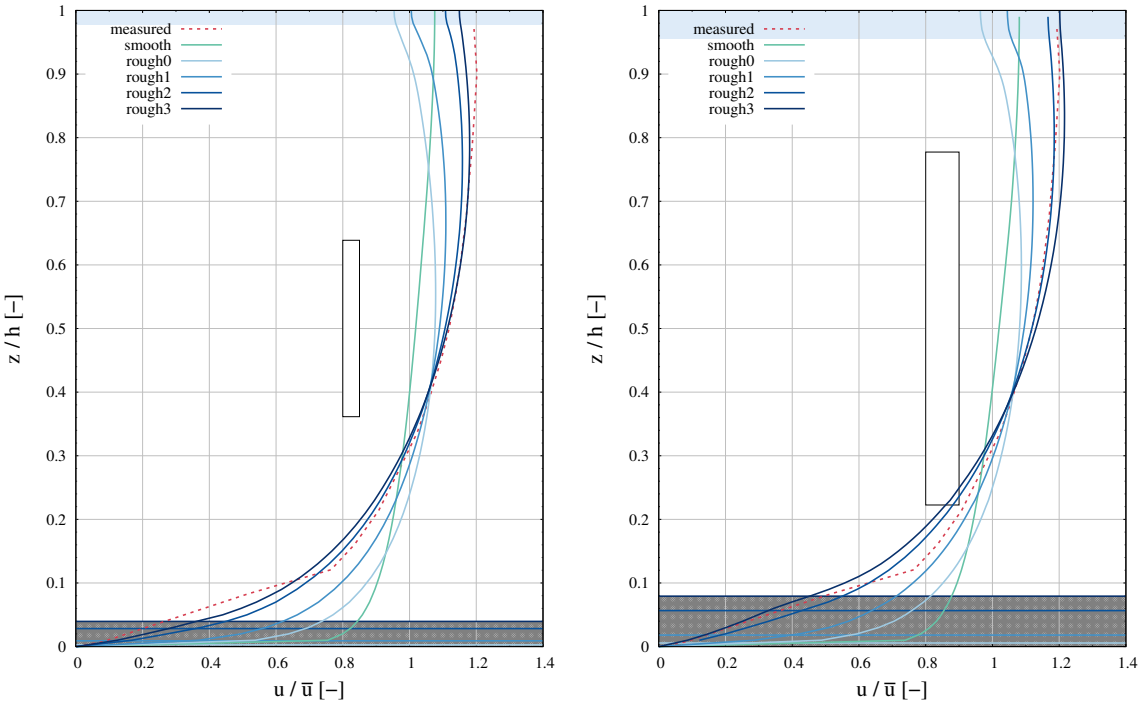

(a) Channel B2 - $h = 17.664$ m **(b)** Channel D2 - $h = 8.832$ m

Figure 5.8: Fully developed velocity profiles for different bed roughness conditions

listed in Table A.2 and the resulting inlet profiles are shown in Figure 5.8. The velocity profile generated by the roughness parameter *rough2* reproduces the distribution measured at the site reasonably well. In addition to the investigations of the turbines in rough channels, investigations were also carried out in channels with a hydraulically smooth bottom wall. Since the investigation of the GenIHS turbine is computationally expensive due to the complex diffuser geometry and the fact that five operation points have to be simulated for each setup, the influence of the sheared flow on this turbine is only investigated in channels with roughness *rough1* and *rough2*.

The structure of the meshes is similar to those applied for the investigations presented in Section 5.1. However, for the sheared flow problem the flow at the bottom boundary condtion has to be resolved in more detail. Therefore, the cell closest to the bottom wall has a dimension of $y^+ \approx 300$ with a hyperbolic growth rate as illustrated in Figure 5.7. This means that the viscose sublayer is not resolved but modeled by a wall model. In total the meshes for the actuator disk simulations consist each of around 1 M cells. For the investigation of the GenIHS turbine the number of mesh cells is around 4 M.

5.2.2 Single Rotor Turbines in Sheared Flow

The results of the simulations modeling an actuator disk in channels of different roughness are presented in Figure 5.9 and 5.10. The coefficients are plotted over u_{dev}

which is defined according to Equation 5.1 as the maximum value of the velocity distribution in relation to the velocity at half flow depth. This value is higher for larger shear and thus higher bottom roughness and offers a description of the profile directly based on measured values and independent of the exact knowledge of the bottom roughness.

$$u_{dev} = \frac{u_{max}}{u\left(z/h = 0.5\right)} \tag{5.1}$$

Marked with red curves, Figure 5.9a shows the resulting power coefficients using the depth-averaged undisturbed upstream velocity $\overline{u}$ as characteristic velocity. It can be observed that in this case the results are significantly increasing with increasing bed roughness. This makes sense, since the velocity in the height of the turbine position increases with increasing roughness. For very high bed roughnesses, it can be observed that the c_P-value is almost 60% larger than for a turbine facing a constant upstream velocity. The results for channel B2 and D2 only show a slight deviation. On the one hand, this proves that the influence of the blockage effect is successfully eliminated by meaningful normalization. On the other hand, it shows that the results are almost independent of the ratio of flow depth and rotor size.

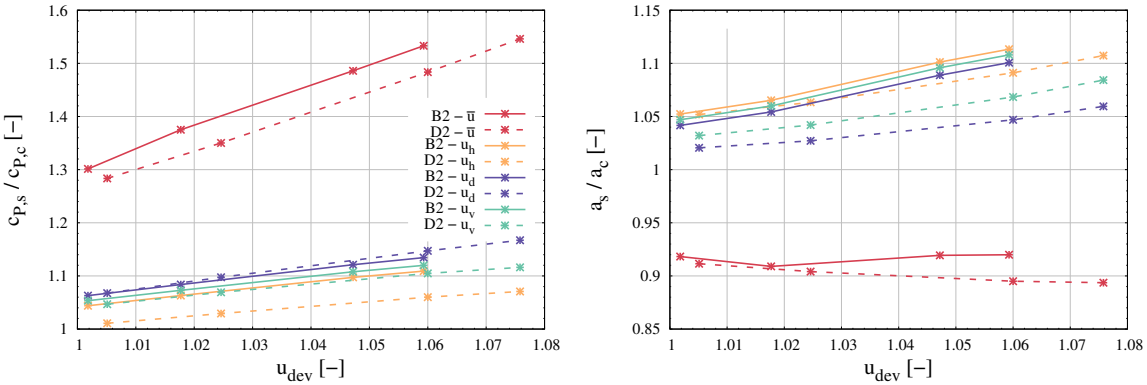

(a) Power coefficient **(b)** Induction factor

Figure 5.9: Influence of porous roughness height on a single rotor actuator disk using different reference velocities

Considering the alternative referencing methods, it becomes apparent that the influence of the sheared flow profile on the results is reduced. Still, the curves do not fully collapse for any of the investigated approaches. An increase in the power coefficient with increasing roughness can also be observed for those post processing procedures. This is possibly caused by the higher turbulence level under such conditions. Nishino et al. [68] and also Blackmore et al. [12] observed that the level of turbulence in the upstream flow field has a significant influence on the performance. Also the results of Flemming et al. indicate that effects other than the change of speed at rotor height must be the cause for the increase of performance [30]. This effect seems to behave straight linear independent from the applied reference velocity.

For a consideration of the sheared flow, the normalization to the depth-averaged velocity over the height of the turbine u_d seems to be the most suitable as it provides results independent from the detailed channel dimensions.

As shown in Figure 5.9b, for the induction factor the results are not that explicit. Related to the depth-averaged velocity $\overline{u}$, it decreases with increasing roughness. For all other evaluation methods, however, the induction factor increases to a similar extent as the power coefficient. Nevertheless, no independence from the channel dimensions can be observed. The choice of the post processing method proves to have more influence for the more shallow channel cross section D2.

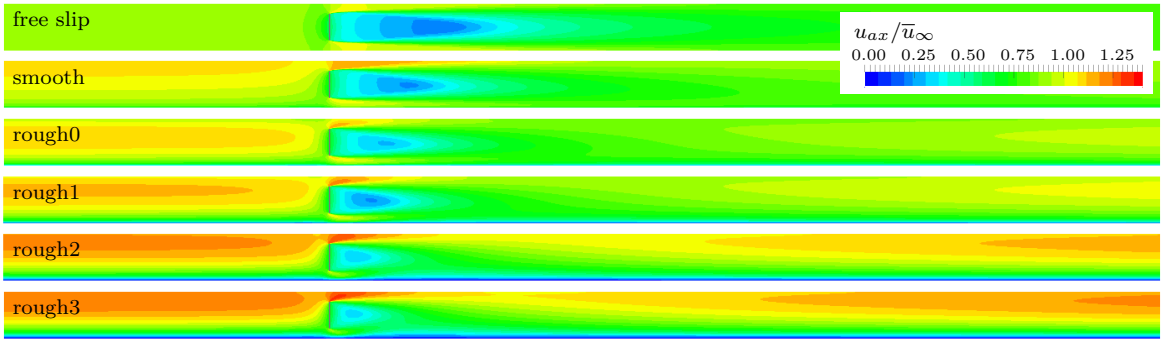

Figure 5.10: Resulting flow fields for actuator disk in channel D2 with varying roughness

Figure 5.10 provides an overview over the flow fields in axial direction in channel D2 for varying channel condition. They each represent an operation point close to the optimum.

5.2.3 GenIHS Turbine in Sheared Flow

The behavior of the diffuser augmented turbine GenIHS in sheared flow is totally different to the one of a single rotor actuator disk. This can be observed from Figure 5.11. When referenced to the depth-averaged undisturbed upstream velocity the power coefficient seems to be independent from the bed roughness but not from the channel dimensions. The performance is increased around 20% compared to a constant upstream flow.

As for single rotor turbines, the influence of shear flow conditions is partially eliminated by using alternative reference velocities for the determination of the power coefficient. Here again, the depth-averaged velocity over the height of the diffuser u_d is promising, since in this case, similar to Section 5.2.2, the results are independent from the channel dimension. For the GenIHS turbine, however, it is apparent that $c_{P,d}$ decreases with increasing roughness. It seems that for this type of kinetic turbine the increased upstream turbulence caused by the increased bottom roughness has a negative effect on the performance.

Table 5.1: Influence of sheared flow on thrust and mass flow ratio

Channel	Roughness	$\frac{q_s}{q_c}$	$\frac{\tau_s}{\tau_c}$
B2	rough1	1.004	0.889
	rough2	1.006	0.867
D2	rough1	0.998	0.856
	rough2	1.012	0.867

For the diffuser induction factor, a strong dependence on the channel cross-section geometry is evident. The influence of the shear flow on the optimum operating point of this diffuser augmented turbine is probably caused by the very large lateral vents through which a large amount of additional mass can enter the diffuser. Since only two bed roughness scenarios per channel are investigated for the GenIHS machine, the detailed shape of the observed curves cannot be determined here. Hence, the correlations presented in Figure 5.11 are not necessarily linear.

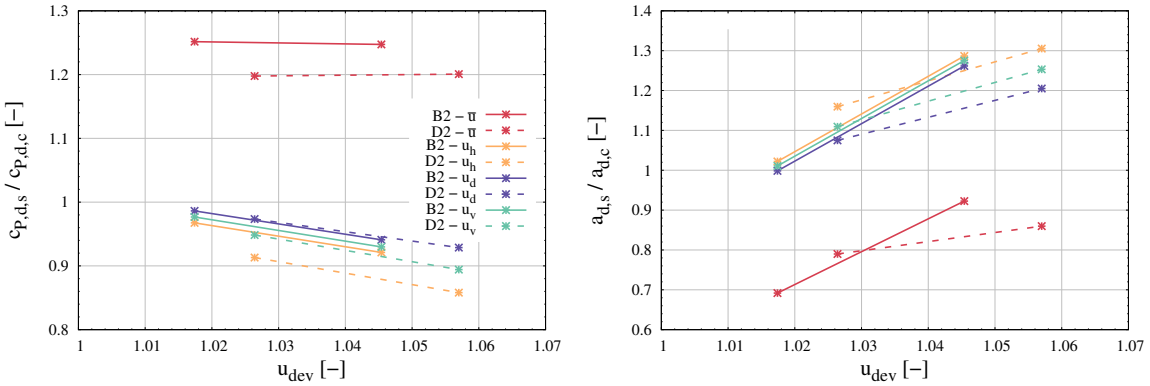

(a) Power coefficient **(b)** Induction factor

Figure 5.11: Influence of porous roughness height on the GenIHS turbine using different reference velocities

The results for the two further characteristic values describing diffuser augmented turbines, the mass flow ratio and the thrust ratio, are listed in Table 5.1. It can be seen that both values are not very sensitive to the problem. The mass flow ratio is minimally affected by the change of the induction factor for the optimum operation point. Also the influence on the thrust ratio is very small. The flow fields for the different roughness scenarios in channel D2 around the optimum operation point of the GenIHS turbine are presented in Figure 5.12.

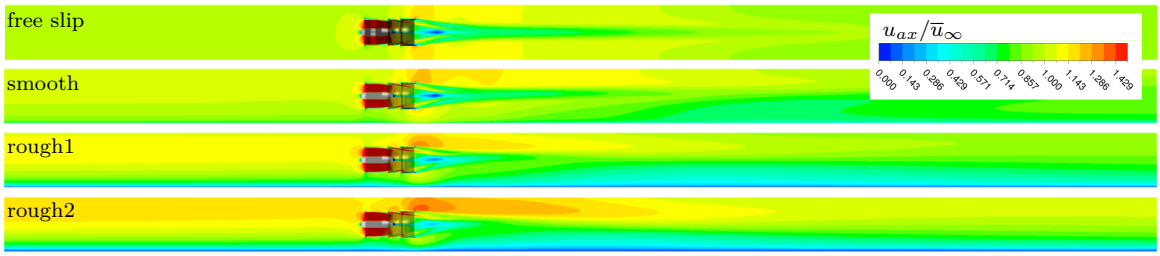

Figure 5.12: Resulting flow fields for GenIHS in channel D2 with varying roughness

5.3 Conclusion

In summary, the results of the investigations in this section show a systematic influence on the performance for channel cross sections with different aspect ratios and blockage ratios. For the single rotor turbines, the laminar simulations correspond well with the theory provided by Garrett and Cummins. For RANS-simulations the influence of the channel aspect ratio on the results increases significantly. Consequently, a high dependence on turbulent phenomena can be concluded for this effect. Also for the influence of the sheared flow turbulence seems to play a major role, as the increase in power coefficient cannot fully be eliminated using an alternative reference velocity.

For diffuser augmented turbines, the results of the investigations of the blockage effects are strongly varying with the detailed diffuser geometries. Therefore, it is difficult to exactly describe the problem mathematically in general terms. This means that the relationship cannot be transferred from one diffuser geometry to another and must therefore be determined separately for each geometry through several extensive 3d simulations in order to identify suitable functions. Also for the sheared flow the results for the diffuser augmented turbine GenIHS differ from the ones observed for a single rotor. The results also suggest that the correlation observed for GenIHS is not necessarily transferable to other diffuser augmented turbines due to the influence of the very extensive vents and the large diffuser aspect ratio.

The findings on the sheared flow effect are only valid for the specific positioning in the middle of the channel. Furthermore, it has to be mentioned that for the simulations the actuator disk model is used. Therefore, the rotor geometry is not resolved and consequently flow components like swirl and rotor induced turbulence are neglected. In addition, the applied SST-k-ω-model is a not very high quality turbulence model especially since turbulence seems to play a major role with regard to site effects. In addition, a possible change of the water level was neglected in all investigations. These simplifications are necessary to carry out the extensive number of simulations with reasonable effort. However, the used approaches are sufficient to obtain a basic overview of the various relevant effects.

6 Development of an Advanced Turbine Model for Shallow Water Solvers

The results of the previous investigations show that various site factors have a great influence on the performance of kinetic turbines. Especially for a low flow depth and sheared flow conditions, the existing turbine models cannot be used directly. Also the correct representation of diffuser augmented turbines requires adaptations. In the following, a flexible turbine model is developed which considers the special site effects for single rotor turbines and for the diffuser augmented turbine GenIHS. In addition to the detailed description in the following, the turbine model is summarized schematically in Figure 6.1.

6.1 Advanced Single Rotor Model

Similar to the existing turbine model presented in Section 3.4 the advanced Single Rotor Actuator Disk Model is based on the assumption that the 2d thrust in the turbine cell has to be equal to the actual thrust of the modeled turbine. The bottom roughness drag coefficient in the turbine cell is increased by that value.

For the advanced turbine model the site effects investigated in Chapter 5 are considered by manipulating the power coefficient and induction factor. For this purpose the original determination of the 2d turbine drag coefficient $c_{D,t}$ (Equation 3.8) must be rearranged as follows:

$$c_{D,t} = \frac{A_r c_P \, \overline{u}_{t,\infty}{}^2}{(1-a)\, 2 A_{cell} \overline{u}_{cell}{}^2} \tag{6.1}$$

In order to model the site effects correctly, a precise mathematical description of these problems is necessary. The determination of suitable modeling approaches is discussed in the following.

6.1.1 Consideration of Blockage Effects

The correlation between the blockage ratio and the flow quantities at a single rotor actuator disk can theoretically be described by the equations provided by Garrett and Cummins [34] (see Section 2.3). However, the results observed in Section 5.1.2 are deviating from this theory especially for high channel aspect ratios.

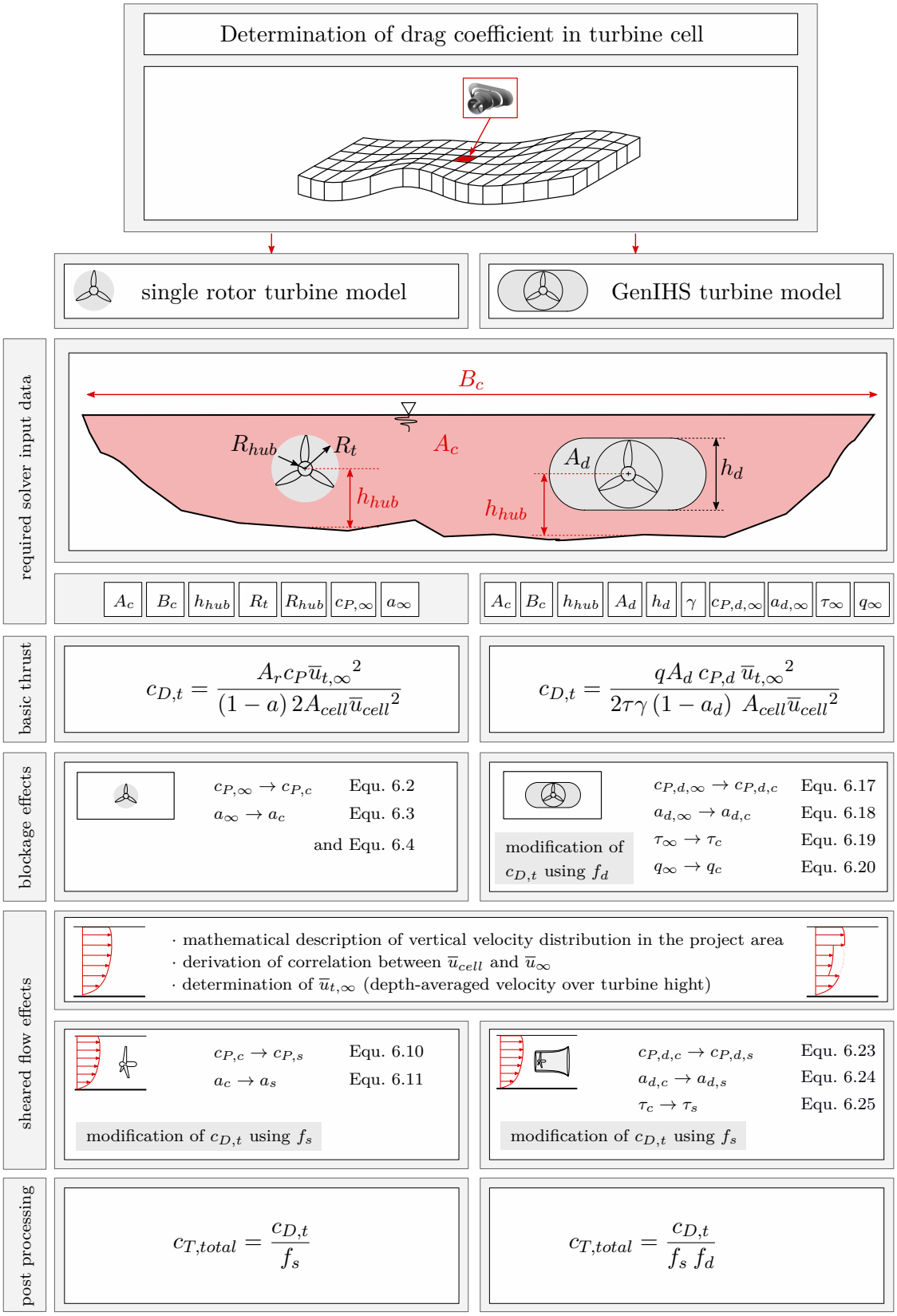

Figure 6.1: Schematic illustration of the turbine models

In order to correctly model the influence of the aspect ratio, the Garrett-Cummins-Theroy is extended through an additional term which is empirically determined. The equation for the maximum power coefficient is now:

$$c_{P,c} = \frac{c_{P,\infty}}{(1-\epsilon)^2} + x \tag{6.2}$$

And the induction factor for the optimum operation point is defined as follows:

$$(1-a_c) = \frac{(1-a_\infty)}{(1+\epsilon)} + x \tag{6.3}$$

The correction term x is expressed by the following empirical equation, which is determined by curve fitting:

$$x = (x_1 \epsilon^{x_2} + x_3) \frac{(\alpha - x_4)\,0.05}{\sqrt{1 + ((\alpha - x_4)\,0.05)^2}} \tag{6.4}$$

For the variables x_1, x_2, x_3 and x_4, different constants are introduced for c_P and a respectively. Those values are given in Table 6.1.

Table 6.1: Empirical constants for correction of the blockage effect considering the channel aspect ratio

	x_1	x_2	x_3	x_4
for c_P	0.22	0.43	-0.0015	10
for $(1-a)$	-0.75	0.75	0.0	7

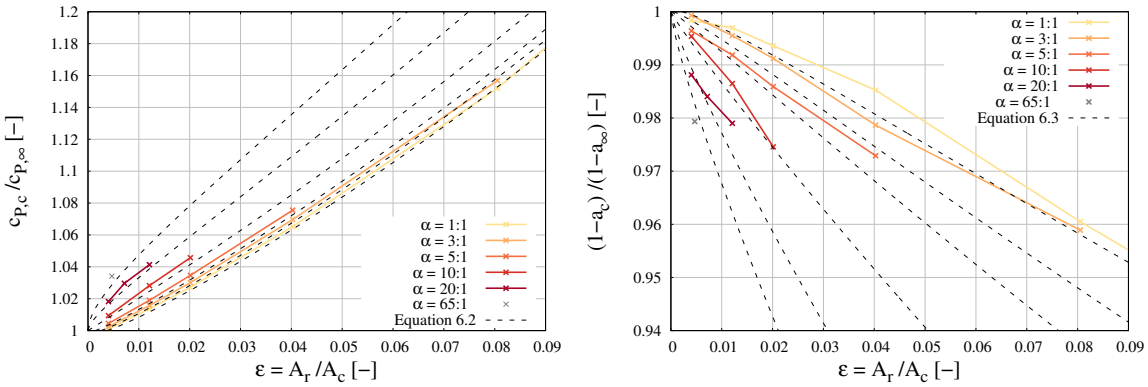

(a) Power coefficient **(b)** Induction factor

Figure 6.2: Modeling of influence of channel blockage on single rotor actuator disk

The plots of those equations for various channel cross sections are illustrated in Figure 6.2 (grey) in direct comparison with the numerical results from Section 5.1.2

(color). Generally, it can be observed that this model is able to represent the blockage effect in channels with varying area and aspect ratios quite good. Especially for large aspect ratios, which are characteristic for many rivers, the influence is predicted quite well as can be observed for example for the "Montreal" cross section ($\alpha = 65$). For very small blockage and aspect ratios the channel power coefficient is smaller than the infinit power coefficient and therefore the model provides wrong results. For those conditions the basic turbine model is valid and the correction model can be turned off.

The blockage correction model can be applied for different velocity distributions. However, for a first evaluation a block profile with constant velocity over the flow depth is applied. This ensures to test the model isolated from other effects. The relation between the mean velocity in the turbine cell $\overline{u}_{cell}$ (disturbed) and the upstream velocity u_∞ (undisturbed) is determined by integrating the velocity profile disturbed by the rotor (corresponding to Equation 3.9):

$$\overline{u}_{cell} = \frac{h - 2R_t}{h}\overline{u}_\infty + \frac{2R_t}{h}(1-a)\,\overline{u}_\infty = \overline{u}_\infty\left(1 - \frac{2R_t}{h}a\right) \tag{6.5}$$

Analogous to the procedure in the basic turbine model (see Section 3.4), this correlation is used by the solver to calculate the reference velocity u_∞ which is required to determine turbine thrust, turbine power and wake velocity. This is necessary, as the velocity in the turbine cell is influenced by the turbine model and consequently somewhat lower than the actual undisturbed upstream velocity. Hence, the upstream undisturbed velocity u_∞ calculated by the turbine model is a fictitious value.

The model is evaluated by applying it to the different channel geometries already investigated in Section 5.1.2. The 2d simulations are performed using four meshes with different turbine cell size. The investigated cell dimensions are listed in Table 6.2:

Table 6.2: Investigated dimensions of the turbine cell

turbine cell name	**width [m]**	**axial length [m]**
rotor size	4.9	1.0
long	4.9	8.0
wide	12.0	1.0
large	12.0	8.0

The solver input data for the single rotor turbine are documented in the appended Table B.1. Two values are considered for the evaluation: The undisturbed upstream velocity calculated by the solver from the data in the turbine cell $u_{\infty,calc}$ is compared to the velocity specified at the inlet boundary condition $u_{\infty,BC}$. As the channel geometry is very simple those values ought to be equal. Furthermore, the turbine power determined by the turbine model is compared to the results from the 3D simulations.

Figure 6.3a shows the ratio between the calculated and the actual upstream velocity for the different channels and different meshes. It can be seen, that the accuracy of

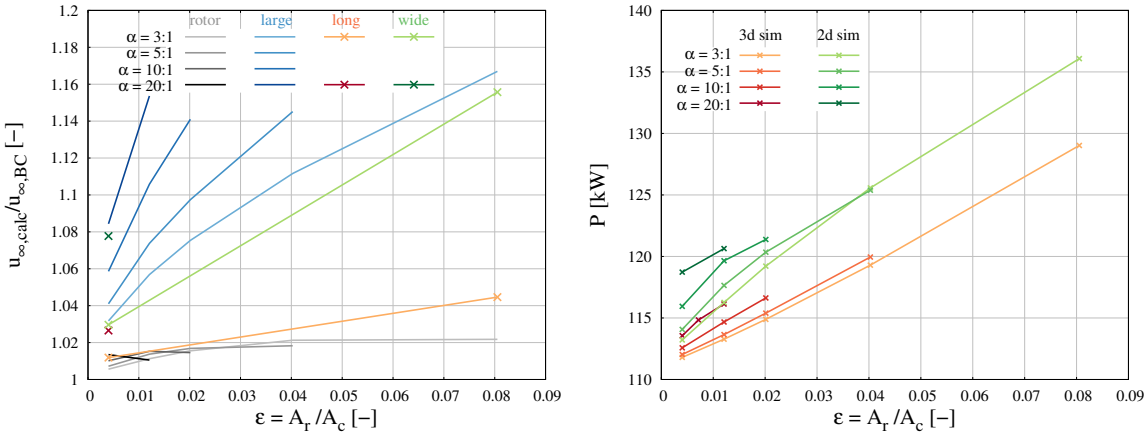

(a) Fraction of calculated and defined u_∞ for different turbine cell sizes

(b) Turbine power resulting from 2d (rotor size turbine cell) and 3d simulations for $u_\infty = 2.69$ m/s

Figure 6.3: Evaluation of single rotor turbine model considering channel blockage in test channels

the prediction of the upstream undisturbed velocity is around 2% for the rotor size turbine cell. The result is nearly independent from the channel dimensions in this case. If the length of the turbine cell in flow direction is changed the determination is slightly more unprecise. In case that the turbine cell is significantly wider than the dimension of the modeled rotor, the upstream velocity is clearly overestimated for all channel dimensions. If this cell is additionally stretched in axial direction the results are only slightly changing.

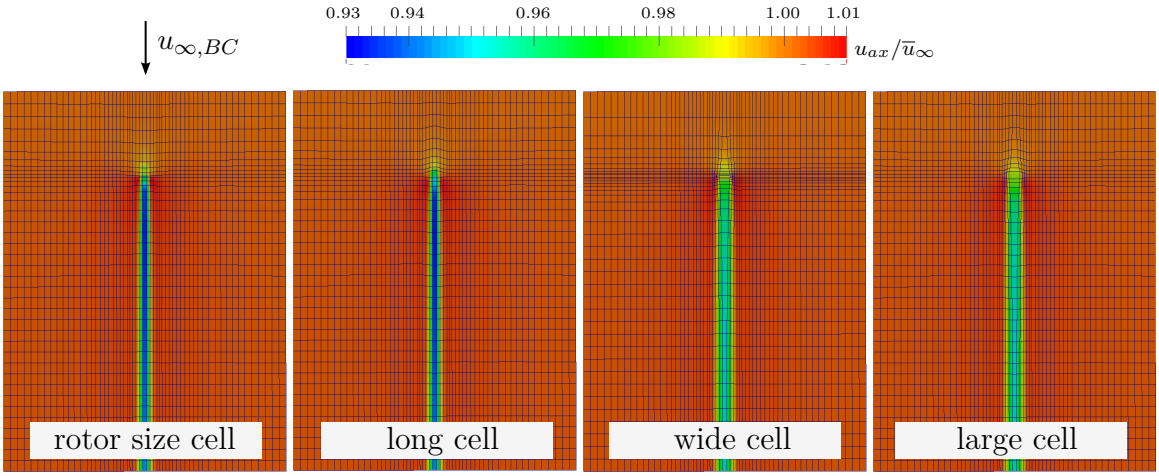

Figure 6.4: Topview on resulting velocity fields for single rotor turbines in channel D1 with different turbine cell size - flow direction top to bottom

The problem can also be seen in the resulting depth-averaged velocity fields of the 2d simulations for the different meshes in Figure 6.4. For the wide turbine cells the velocity in the turbine cell is not decelerated sufficiently. The reason for this is probably the 2d blockage effect: In an additional study where the drag coefficient in the turbine cell $c_{D,t}$ is defined as fixed value, it could be observed that the velocity in the turbine cell is highly dependent on the channel geometry also for a fixed drag coefficient. This effect increases for increasing drag coefficients (see Figure B.1 in Appendix B).

Comparing the absolute turbine power determined when using the 2d turbine model with the results of the 3d simulation in Figure 6.3b, it can be seen that the model can qualitatively represent the behavior in different channel geometries well. In absolute terms, however, the power is always overestimated by the model. This deviation is caused by the over-predicted upstream undisturbed velocity, which is considered cubical in the power.

6.1.2 Consideration of the Sheared Flow Effect

In the previous chapter, it is proven that there is a clear influence of sheared flow conditions on the turbine performance. Therefore, the turbine model must also be extended in terms of this aspect. For this purpose, the velocity profile at the site must be described mathematically. Regarding the profiles measured in the project area in Figure 6.5a it is obvious that the 1/7-power law is not providing a sufficient approach for this. A more appropriate description is reached using the following formula presented by Ferro, which was developed for describing velocity profiles in gravel-bed rivers [29]:

$$u_* = b_0 + b_1 \ln(z_*) + b_2 {z_*}^2 (1 - z_*) + b_3 {z_*}^2 (3 - 2z_*) \tag{6.6}$$

with $u_* = u(z)/\overline{u}$ and $z_* = z/h$. For the velocity profile measured in the project area the constants are determined as follows:

Table 6.3: Empirical constants for the description of the velocity profile

b_0	b_1	b_2	b_3
1.2	0.125	0.4	0.0

Integrating Equation 6.6 over the flow depth provides the following expression:

$$\int u_* (z_*)\, dz_* = -0.1 {z_*}^4 + 0.13333 {z_*}^3 + 0.985 z_* + 0.215 z_* \ln(z_*) \tag{6.7}$$

Applying the integral over the total flow depth by setting the integration limits from $z_* = 0$ to $z_* = 1$ provides a value of 1.018. Ideally this value should be 1. However, the deviation is accepted as it is very small.

Analogous to the procedure described in Section 3.4, the velocity profile disturbed by the rotor is used to determine the fictitious upstream undisturbed velocity. Over the height of the turbine the velocity is reduced using the induction factor in order to model the deceleration of the flow by the rotor. This is illustrated in Figure 6.5b. The corresponding formulation for the disturbed velocity profile is:

$$\overline{u}_{cell} = \left(\int_0^{\frac{(h_{hub}-R_t)}{h}} u_*\left(z_*\right)\, dz_* + \int_{\frac{(h_{hub}-R_t)}{h}}^{\frac{(h_{hub}+R_t)}{h}} u_*\left(z_*\right)\, dz_*\,(1-a) + \int_{\frac{(h_{hub}+R_t)}{h}}^{1} u_*\left(z_*\right)\, dz_* \right) \overline{u}_\infty \tag{6.8}$$

Inserting Equation 6.7 to this equation the correlation between the velocity in the turbine cell $\overline{u}_{cell}$ and the calculated upstream depth-averaged undisturbed velocity $\overline{u}_\infty$ is derived. This formula is quite extensive. Therefore, the source code can be found in Listing B.1 in Appendix B.

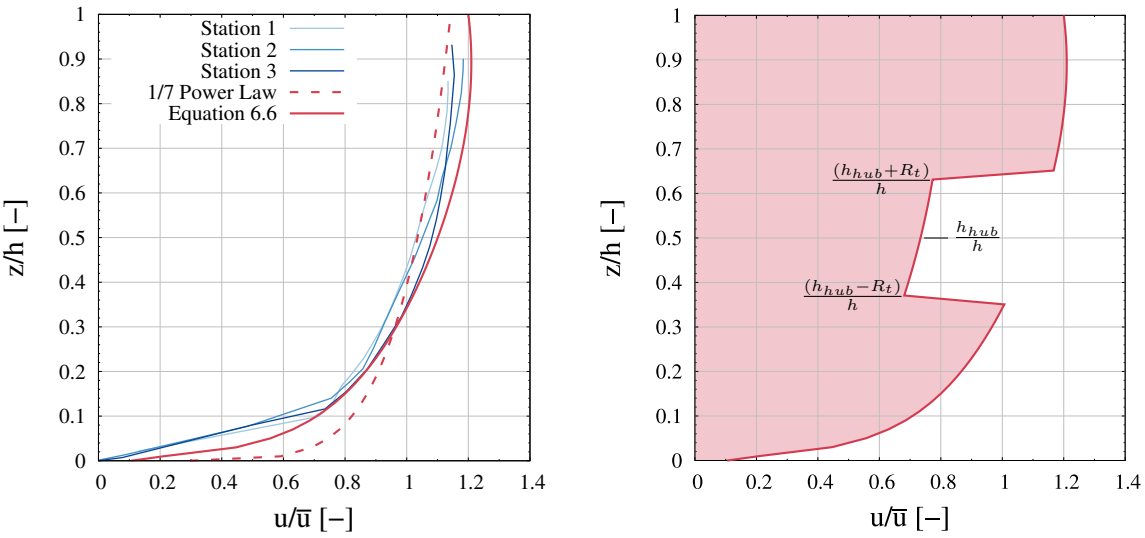

(a) Undisturbed velocity profiles **(b)** Velocity profile disturbed by the turbine

Figure 6.5: Derivation of the model for sheared flow conditions

In Section 5.2.2 it was observed that using the depth-averaged velocity over the turbine height u_d as characteristic velocity is most suitable for reducing sheared flow effects. Therefore, this approach is chosen to determine the relevant upstream undisturbed velocity for the turbine $\overline{u}_{t,\infty}$ which is used to calculate the rotor thrust and turbine power in the model:

$$\overline{u}_{t,\infty} = \overline{u}_\infty \int_{\frac{(h_{hub}-R_t)}{h}}^{\frac{(h_{hub}+R_t)}{h}} u_*\left(z_*\right)\, dz_* \frac{h}{2R_t} \tag{6.9}$$

In that section it was noted that the influence of the shear flow on turbine performance and operation point could not fully be eliminated by an adept choice of the reference velocity. The channel power coefficient and the optimum operation point are therefore adapted according to the following functions for the regression lines derived from the observations made in Section 5.2.2:

$$c_{P,s} = (1.408 u_{dev} - 0.347)\, c_{P,c} \tag{6.10}$$

$$a_s = (0.7646 u_{dev} + 0.2638)\, a_c \tag{6.11}$$

This correlation is only valid if the turbine is placed at half of the flow depth. The accuracy of this approach is illustrated in Figure 6.6a. The sheared flow characteristic values are a function of the deviation of the velocity at half of the flow depth and the depth-averaged velocity, which is calculated from Equation 6.6. The sheared flow power coefficient and induction factor are used to determine the 2d drag coefficient (Equation 6.1) for the sheared flow turbine model.

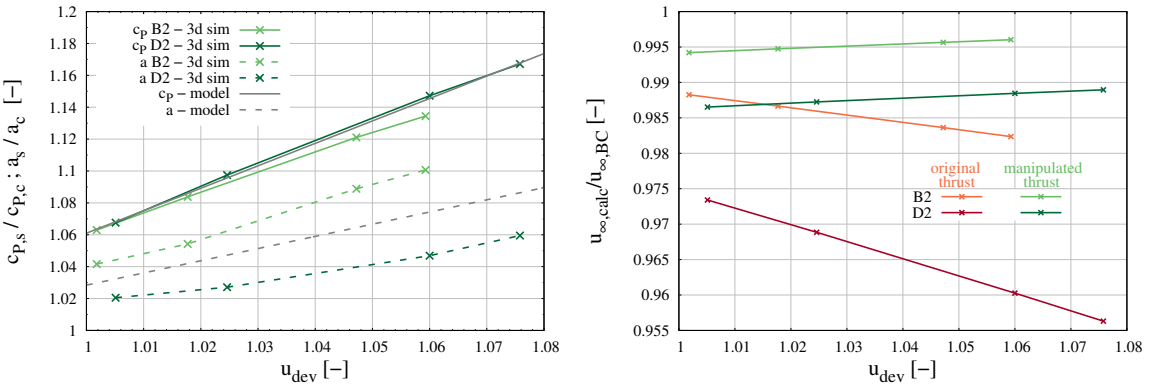

(a) Modeling of power coefficient and induction factor compared to the 3d simulation results

(b) Fraction of calculated and defined u_∞ without and with correction of turbine thrust

Figure 6.6: Modeling of single rotor turbines in sheared flow conditions

However, using the approach to increase the 2d drag in the turbine cell leads to a change of the cell velocity $\overline{u}_{cell}$ and consequently to a more or less strong deviation of the calculated $\overline{u}_\infty$. This can be seen from the red curves in Figure 6.6b showing the ratio of the velocity calculated by the solver to the actual upstream undisturbed velocity defined at the inlet. For both channel geometries and both velocity profiles a major deviation can be observed between those values, which actually should be equal. The deviation is higher for large blockage or aspect ratios. The observed effect is most probably similar to the 2d blockage effect (see Figure B.1), which also causes the model's sensitivity concerning the dimensioning of the turbine cell.

In this case a solution to the problem is to manipulate the thrust in the turbine cell by ignoring the influence of the sheared flow effect on the power coefficient. The resulting factor for the manipulation f_s is:

$$f_s = \frac{c_{P,c}}{c_{P,s}} \tag{6.12}$$

Multiplying the turbine drag coefficient $c_{D,t}$ with this manipulation factor a significant improvement in the determination of $\overline{u}_\infty$ can be seen from the green curves in Figure 6.6b.

This approach violates the conservation of momentum between the 2d and the 3d turbine. For an investigation of a few machines at a site, where the macroscopic energy balance is not the primary concern, it makes sense to accept a slightly incorrect representation of thrust in the turbine cell and therefore obtain a relatively precise prediction of the reference velocity in return, since this value is considered cubical when determining the turbine power. The manipulated thrust is corrected in post processing by dividing the drag coefficient through the manipulation factor in order to obtain the correct power output.

The sheared flow turbine model is implemented for the roughness conditions at the potential turbine site. This corresponds to the *rough2* 3d simulations presented in Section 5.2.2. The final evaluation of the turbine model is performed comparing those 3d simulation results to the corresponding 2d results in Table 6.4:

Table 6.4: Results for simulations with the final single rotor turbine model (rough2)

Case		$\boldsymbol{P}$ **[kW]**	$\boldsymbol{T_r}$ **[kN]**	$\boldsymbol{T_{cell}}$[1] **[kN]**	$\boldsymbol{\overline{u}_\infty}$ $[\frac{\mathbf{m}}{\mathbf{s}}]$
B2	2d	165.8	90.8	80.5	2.678
	3d	169.0	93.3	-	2.690
D2	2d	164.5	95.2	83.1	2.659
	3d	172.4	95.1	-	2.690

[1] manipulated thrust in turbine cell

It can be seen that the performance of the turbine in channel B2 is predicted quite well. For channel D2, a higher deviation can be observed. It results almost exclusively from the small error in the prediction of the reference velocity $\overline{u}_{t,\infty}$ which cannot be avoided.

6.2 Turbine Model for Diffuser Augmented Turbine GenIHS

As already discussed in the course of this work, the behavior of diffuser augmented hydrokinetic turbines does not strictly follow the linear momentum actuator disk theory. Through the diffuser a component is added to the system which cannot be described properly by an analytical model. Therefore, the turbine model for the GenIHS diffuser augmented turbine is developed based on the definitions presented

in Section 2.2.1. For this model the transport velocity in the rotor plane u_r may be calculated applying the continuity equation:

$$u_r = \frac{u_d A_d}{q A_r} = \frac{(1 - a_d)\gamma u_\infty}{q} \tag{6.13}$$

Using this equation the rotor thrust is determined from the power gained by the turbine:

$$T_r = \frac{P_r}{u_r} = \frac{\rho q}{2\gamma\,(1 - a_d)}\, A_d\, c_{P,d}\, {u_\infty}^2 \tag{6.14}$$

The total turbine thrust may be expressed using the thrust ratio:

$$T_{Total} = \frac{T_r}{\tau} = \frac{\rho q}{2\tau\gamma\,(1 - a_d)}\, A_d\, c_{P,d}\, {u_\infty}^2 \tag{6.15}$$

Similar to the single rotor model, this 3d total machine thrust is assumed to be equal to the 2d thrust in the turbine cell to achieve the correct deceleration of the flow in the 2d shallow water model. Based on this assumption the 2d drag coefficient $c_{D,t}$ for the turbine cell is derived:

$$c_{D,t} = \frac{q A_d\, c_{P,d}\, {u_\infty}^2}{2\tau\gamma\,(1 - a_d)\;\; {A_{cell}\overline{u}_{cell}}^2} \tag{6.16}$$

This model is valid for a diffuser augmented turbine in an infinitely large flow field. The required initial parameters $c_{P,d}$, a_d, τ and q have to be determined from 3d flow simulations of the full turbine geometry in an infinite flow field.

6.2.1 Consideration of the Blockage Effect

Similar to the single rotor actuator disk model, also for diffuser augmented turbines the channel blockage effect has to be considered. The GenIHS diffuser is observed to behave very different to the theory presented by Garrett and Cummins [34]. Therefore, the following fully empirical equations are derived to approach the correlations between blockage ratio, aspect ratio, power coefficient and induction factor identified in Section 5.1.3:

$$c_{P,d,c} = \Big(\Big(-0.0014\alpha^2 + 0.224\alpha + 1.3\Big)\,\epsilon + 1\Big)\, c_{P,d,\infty} \tag{6.17}$$

$$(1 - a_{d,c}) = \Big(-\Big(0.05\alpha^2 - 0.34\alpha + 1.7\Big)\,\epsilon^2 + (0.063\alpha + 0.23)\,\epsilon + 1\Big)\,(1 - a_{d,\infty}) \tag{6.18}$$

The functions are plotted in Figure 6.7 in direct comparison with the corresponding 3d numerical results.

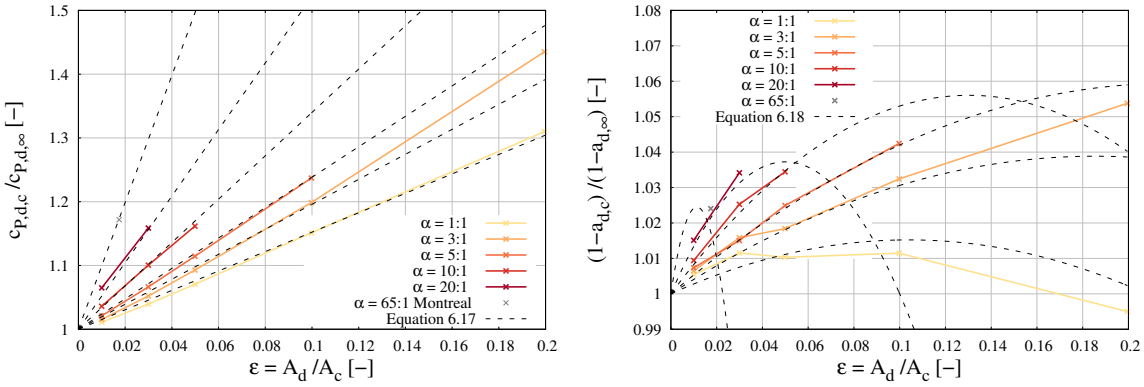

(a) Power coefficient **(b)** Induction factor

Figure 6.7: Modeling of the influence of the channel blockage on GenIHS turbine

The influence on the DAT-specific quantities τ and q are observed to be significantly influenced by the blockage ratio but not by the channel aspect ratio (see Section 5.1.3). Therefore, the functions describing those correlations are only depending on the blockage ratio:

$$\tau_c = \left(2.83144\epsilon^2 + 0.3193\epsilon + 1\right) \tau_\infty \tag{6.19}$$

$$q_c = \left(0.8779\epsilon^2 + 0.1062\epsilon + 1\right) q_\infty \tag{6.20}$$

The change in all four characteristic values for the GenIHS turbine in a limited channel cross section is considered in Equation 6.16. Furthermore, compared to the single rotor model, additional information on the turbine geometry like the diffuser exit area, the diffuser area ratio and the maximum height of the diffuser are required by the solver. At this stage the GenIHS turbine model is evaluated applying it to the academic channel cross sections. For those test cases a constant velocity distribution over the flow depth (Equation 6.5 with $2R_t = h_d$) is assumed. According to the results from Section 6.1.1 the turbine cell size is chosen in the dimensions of the machine size (12 m × 8 m). The solver input data for the GenIHS turbine are listed in Table B.2 in the Appendix.

From the red curves in Figure 6.8a it can be seen that using Equation 6.16 for the determination of the 2d turbine drag the model is not capable of calculating the upstream undisturbed velocity correctly. The deviation increases with increasing blockage and area ratio. This is similar to the observations made for the sheared flow single rotor model. In both cases the drag coefficient in the turbine cell $c_{D,t}$ is increased without changing the approach for the determination of $\overline{u}_\infty$. Also in this case the drag coefficient is manipulated by multiplying it with the following factor in order to reduce the 2d drag coefficient:

$$f_d = \frac{\gamma\, \tau_s}{q} \tag{6.21}$$

This manipulation leads to a drag coefficient which would be achieved by a single rotor of the size of the diffuser exit area:

$$c_{D,t} = \frac{A_d c_{P,d} {u_\infty}^2}{(1 - a_d)\, 2 A_{cell} {\overline{u}_{cell}}^2} \tag{6.22}$$

The 2d simulation results using this approach are represented in Figure 6.8a by the green curves. It can be seen that the thrust manipulation clearly improves the situation and the upstream velocity is precisely determined by the model. In order to obtain the correct turbine power output from the model, the manipulated thrust is corrected in post processing by dividing the drag coefficient through the manipulation factor. The turbine power determined by the 2d simulations is plotted in green in Figure 6.8b in direct comparison with the 3d simulation results from Section 5.1.3. A good agreement can be observed.

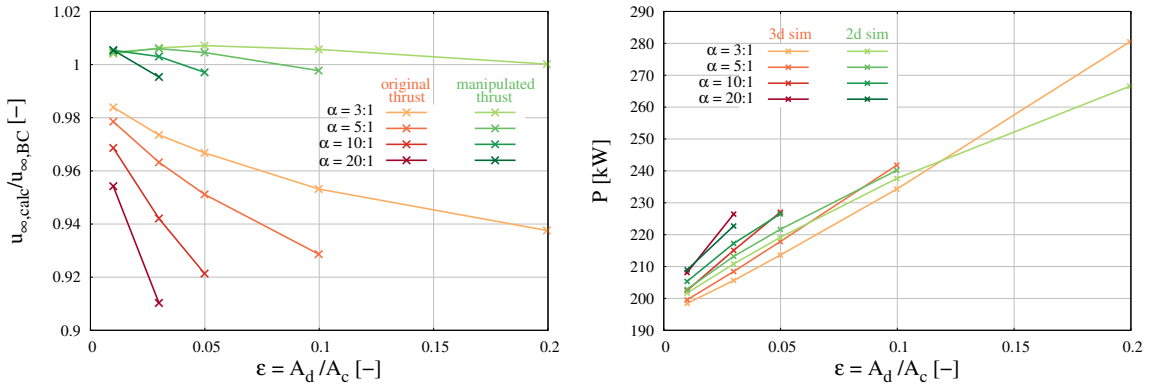

(a) Fraction of calculated and defined u_∞ without and with correction of the turbine thrust

(b) Turbine power resulting from 2d and 3d simulations for $u_\infty = 2.69$ m/s

Figure 6.8: Evaluation of GenIHS turbine model considering the channel blockage in test channels

6.2.2 Consideration of Sheared Flow Effect

Also for the diffuser augmented turbine GenIHS the sheared flow conditions have to be considered. The results from Section 5.2.3 suggest to use the depth-averaged velocity over the height of the diffuser u_d as reference velocity. This velocity is determined through Equation 6.9 similar to the approach for the single rotor in sheared flow, when $2R_t$ is replaced by the diffuser height h_d.

In Section 5.2.3 it was furthermore observed that also for the GenIHS turbine the sheared flow effects are not fully eliminated by the choice of the reference velocity.

For the consideration of the remaining deviations the following correlations are derived by empirically approaching to the results in Section 5.2.3:

- Diffuser power coefficient:

$$c_{P,d,s} = (-1.538 u_{dev} + 2.551)\, c_{P,c} \tag{6.23}$$

- Diffuser induction factor:

$$a_{d,s} = (6.713 u_{dev} - 5.824)\, a_c \tag{6.24}$$

- Thrust ratio:

$$\tau_s = 0.87 \tau_c \tag{6.25}$$

The mass flow ratio is observed to be not significantly affected by the sheared flow conditions (see Section 5.2.3). Similar to the previous models also in this case the thrust is artificially increased compared to the actuator disk theory. Again, this must be considered using the manipulation factor f_s (Equation 6.12) in order to correctly determine the upstream undisturbed velocity. This factor is used in addition to the diffuser thrust manipulation factor f_d here. The manipulation of the turbine cell drag during the simulation is again compensated in the post processing with a division by both manipulation factors in order to predict the correct turbine power.

Table 6.5: Results for simulations with the final GenIHS turbine model

Case		$\boldsymbol{P}$ **[kW]**	$\boldsymbol{T_r}$ **[kN]**	$\boldsymbol{T_{total}}$ **[kN]**	$\boldsymbol{T_{cell}}$[1] **[kN]**	$\boldsymbol{\overline{u}_\infty}$ $[\frac{\mathbf{m}}{\mathbf{s}}]$
B2	2d	254.3	57.7	292.4	126.8	2.679
	3d	260.0	56.1	273.8	-	2.690
D2	2d	263.1	59.4	301.4	131.3	2.668
	3d	271.9	61.2	294.8	-	2.690

[1] manipulated thrust in turbine cell

The final GenIHS turbine model is evaluated by applying it to the test channels B2 and D2 assuming the *rough2*-conditions as bed roughness. The results are presented in Table 6.5. It can be observed that the turbine power is slightly underestimated in both scenarios. It is also visible that in this case the actual and the manipulated thrust in the turbine cell are significantly deviating. So for a macroscopic energy balance the results of the simulation are not very representative. Still, this approach is the only possibility to correctly determine the upstream undisturbed velocity.

6.3 Conclusion

Figure 6.1 gives a summarizing overview over the turbine model and its modules developed in this work. In addition, the following key findings are summarized. It could be observed that the turbine cell has to be in the dimensions of the actual turbine geometry when considering site effects. The size of the turbine cell normal to the flow direction is more sensitive than in flow direction. For situations which cannot be directly derived from the LMADT, like the modeling of diffuser augmented turbines or sheared flow conditions, it is necessary to choose between a correct representation of the total turbine thrust and a correct determination of the upstream undisturbed velocity. In this work a manipulation of the turbine cell drag is applied to solve the problem. Only when modeling a single rotor turbine at constant upstream velocity conditions or the GenIHS turbine in an infinitely large flow field, no correction of the turbine cell drag is required.

The described model is very complex and tailored precisely to the problems and conditions treated in this work, but it can be easily simplified and is therefore variable in application (e.g. without turbulence correction for sheared flow or consideration of aspect ratio). In future, an automatic determination of channel cross section and aspect ratio by the solver would be desirable.

7 Site Evaluation Montreal

In the following, the advanced turbine model and its modules are tested under realistic conditions. For this purpose, a large-scale 2d shallow water model and a detailed 3d model of the potential project area in Montreal is built up. In the 2d simulations the turbine model is applied, whereas the 3d simulations resolve the diffuser geometry. Finally, the GenIHS turbine model is applied to predict the performance of an arrangement of five turbines.

7.1 Project Site

As already mentioned in Section 1.2 the project area for a future application of the GenIHS turbine is located at the St. Lawrence Stream in the urban area of Montreal, Canada. At this site a kinetic turbine developed in a previous project is operated since 2010. An overview over the region is given in Figure 7.1a. Several site data, such as bathymetry, annual run-off duration curve, water levels, depth-averaged velocities and vertical velocity profiles are available from the previous project.

The shoreline and bathymetric data were gained from ADCP measurements in the area of the installed turbine in the lower course and from maps of Fishery and Oceans Canada in the upper course (see Figure 7.1b). The annual duration curve provides the run-off data for the main course of the river (see Figure C.2). Also the downstream stage-discharge relation is known from the previous project. Those data are essential to built up an adequate site model.

Besides those basic data, a set of different stage and velocity measurement data in the immediate vicinity of the current turbine site are available. They were recorded during an extensive measurement campaign in 2008 via ADCP. During those measurements, a run-off of around $10,000$ m^3/s was determined. A cross sectional velocity distribution was determined in 14 river cross sections (locations marked red in Figure 7.1c). In addition, the water level in three longitudinal sections was measured (locations marked blue in Figure 7.1c). For three stations in this region also time resolved velocity profiles were recorded (locations marked green in Figure 7.1c). The resulting velocity profiles are also used in Section 5.2.1 for the sheared flow investigations. The gathered data are suitable to calibrate the bottom roughness and to verify the 2d and the 3d model. The measurement data are presented in Figure 7.1d and in Appendix C. For the evaluation of the turbine model, the site of the currently operated kinetic turbine marked in Figure 7.1a is assumed as turbine location (UTM-coordinates: 18T 613858, 5040469). At this location, flow depth and flow velocity are sufficiently large for a feasible operation.

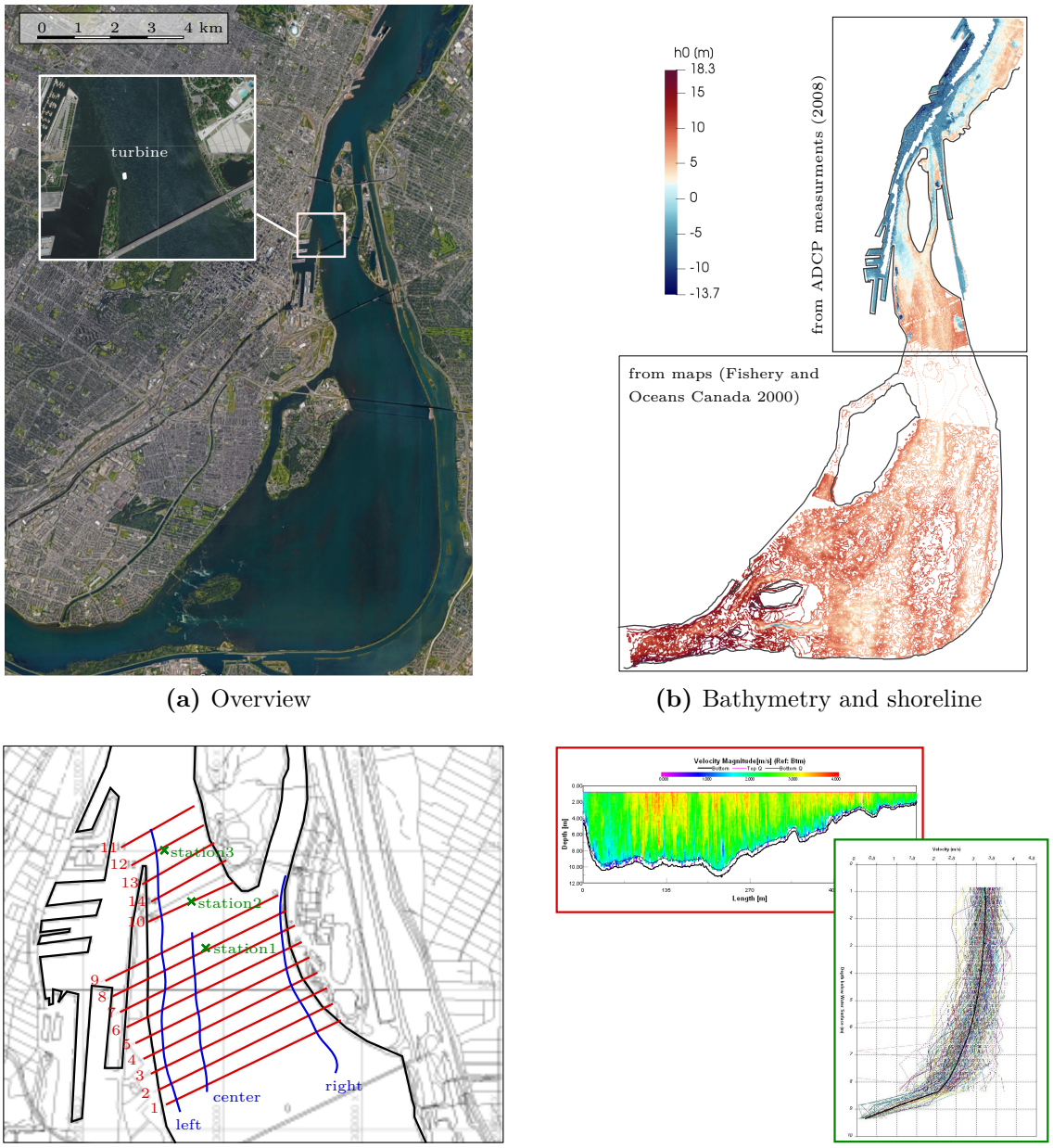

(a) Overview

(b) Bathymetry and shoreline

(c) Measurement locations

(d) Exemplary measurement results

Figure 7.1: Available data for the project area in Montreal

7.2 2d Simulation Setup

For the 2d shallow water simulations the bathymetry data are mapped to the 2d mesh such that each cell is assigned to a constant bed elevation value h_0. At the domain inlet, a constant specific discharge hU with flow direction normal to the boundary is defined. This constant distribution is actually not realistic. However, the velocity field develops with increasing distance to the inlet boundary. Due to the very large extension of the solution domain, the horizontal velocity distribution in the region

of the turbine site is assumed to be independent from the inlet condition. At the domain outlet a fixed water level is defined. According to the stage-discharge relation the water level at the outlet is 6.25 m (AMSL) for the 50% probability discharge of $Q = 8,500$ m^3/s and 7.08 m (AMSL) for $Q = 10,000$ m^3/s which was the discharge during the ADCP measurements. The side walls of the investigated river section are defined as slip walls. The boundary conditions for the 2d model are summarized in Figure 7.4a. For turbulence modeling the depth-averaged Smagorinsky model is applied.

The site information required by the turbine model is extracted from the solution domain ($A_c = 3115.3$ m^2, $B_c = 526.1$ m). Both the cross sectional area and the channel width are determined in planes normal to the flow direction. Furthermore, both the single rotor and the GenIHS turbine are placed in the middle of the channel flow depth which leads to a hub height of 4.06 m. The turbine related solver input data can be found in Table B.1 and B.2 in the Appendix.

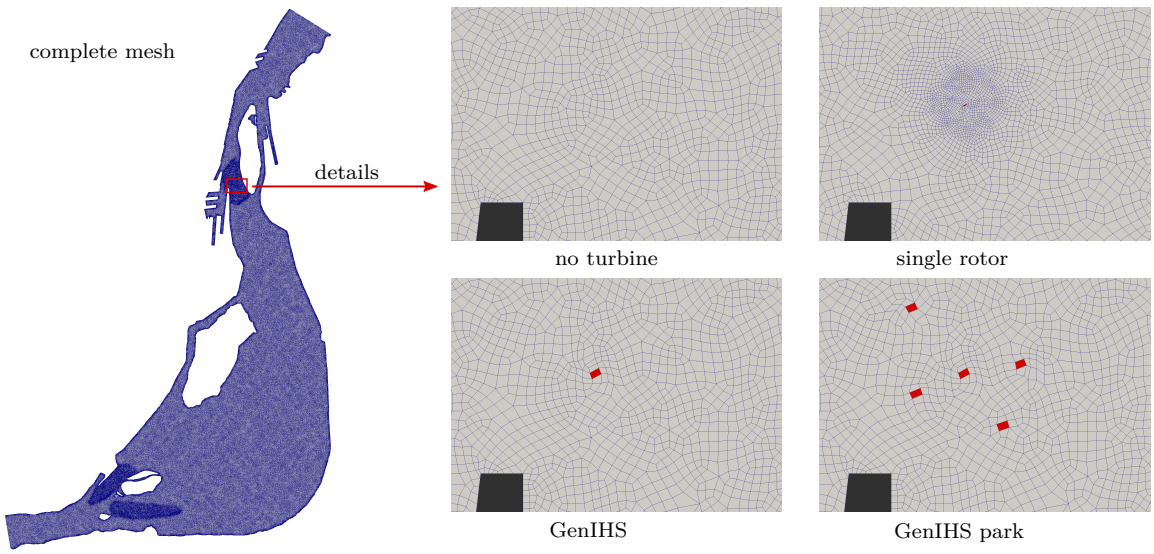

Figure 7.2: Unstructured hexahedral mesh for 2d simulations

The 2d solution domain is discretized into around 200,000 cells using an unstructured hexahedral mesh (see Figure 7.2). In the upper course of the project area some refinements are required for stability reasons, as in those regions large gradients in bathymetry, a partly low flow depth and high flow velocities are prevalent. Also the immediate vicinity of the turbine site is resolved more detailed. As outlined in Chapter 6, the size of the turbine cell plays a major roll for the correct determination of the upstream undisturbed velocity and must roughly have the dimensions of the actual turbine. Four different scenarios are considered: the application of one single rotor turbine, the application of one GenIHS turbine, a park arrangement of five GenIHS turbines and a scenario without any turbine. Therefore, the mesh is adjusted at the turbine location(s) according to the investigated machine(s) as illustrated in Figure 7.2.

For the time discretisation a timestep of $\Delta t = 0.01$ s is applied. Due to the extensive dimensions of the modeled river section a time period of around $30,000$ s has to be simulated until steady state conditions are reached.

Calibration of Manning Roughness:

Water level measurements collected as part of the ADCP measurement series are used to calibrate the Manning roughness for the 2d shallow water model. The measurement locations are shown in Figure 7.3a. They consist of three longitudinal sections close to the old harbor of Montreal. For the calibration simulations the hydraulic conditions during the measurements - a run-off of $Q = 10,000$ m^3/s and a downstream water level of $h_{ds} = 7.08$ m - are specified.

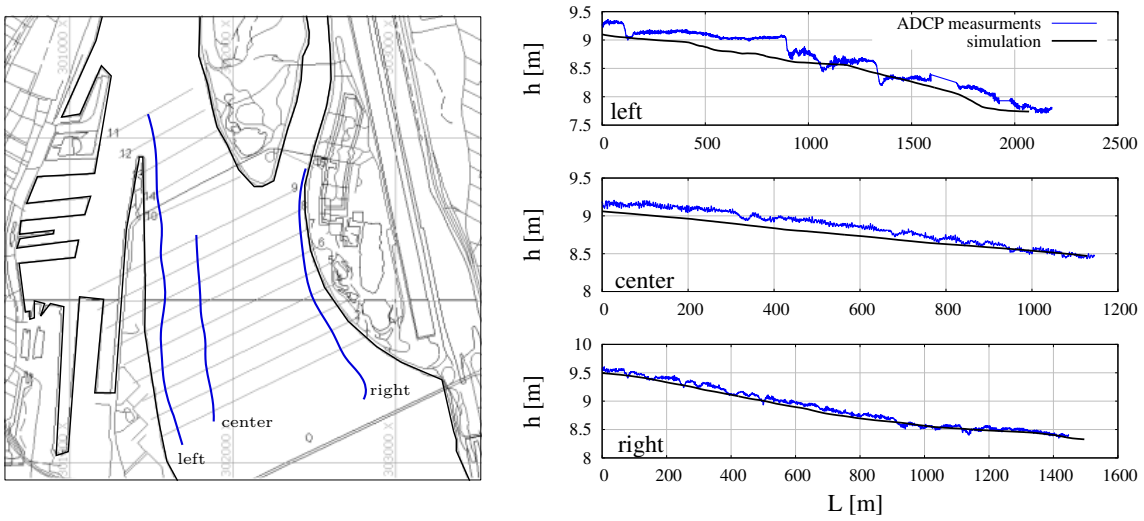

(a) Location of measurement sections **(b)** Water level along longitudinal sections

Figure 7.3: Calibration of the model through ADCP measurements

The 2d model is simulated for several bed roughness conditions defined through the Manning roughness which is assumed to be constant for the entire solution domain. The best agreement between measurement and simulation in all three sections is achieved for a Manning roughness of $n = 0.04$. The respective resulting water levels are shown in Figure 7.3b. The determined Manning roughness is comparatively high, but fits the vertical velocity distributions measured in the project area, which also indicate a high bottom roughness.

7.3 3d Simulation Setup

For the 3d simulation only the closer vicinity of the turbine site is considered, since the required number of cells would be far too large when modeling the entire river section. The selected dimension and location of the 3d solution domain is shown in Figure 7.4. The entry to a part of the old port is closed by a solid wall as the stagnant

water around the docks is assumed to play a minor roll for the flow situation in the main channel.

The domain bottom geometry representing the river bed is derived from the bathymetric data. The water surface is not modeled (e.g. through a 2-phase approach) but represented by a solid boundary condition. Its local position is extracted from the corresponding 2d shallow water simulation (without turbine). As the water level is influenced by the river run-off, the top boundary is adapted according to the modeled scenario. Using this approach, the influence of the kinetic turbine on the water surface is not considered.

Similar to the investigations of sheared flow conditions in Section 5.2 the high bottom roughness is modeled through a porous zone of 0.25 m thickness above the smooth wall bottom boundary. The isotropic loss coefficient is defined using Equation 3.2 with $b = 0.025$ m. Also the deceleration of the flow at the water surface is considered through a porous zone of 0.20 m thickness assuming a loss coefficient of 0.015 m^{-1} in both horizontal directions. The top boundary above this layer is defined as free slip wall.

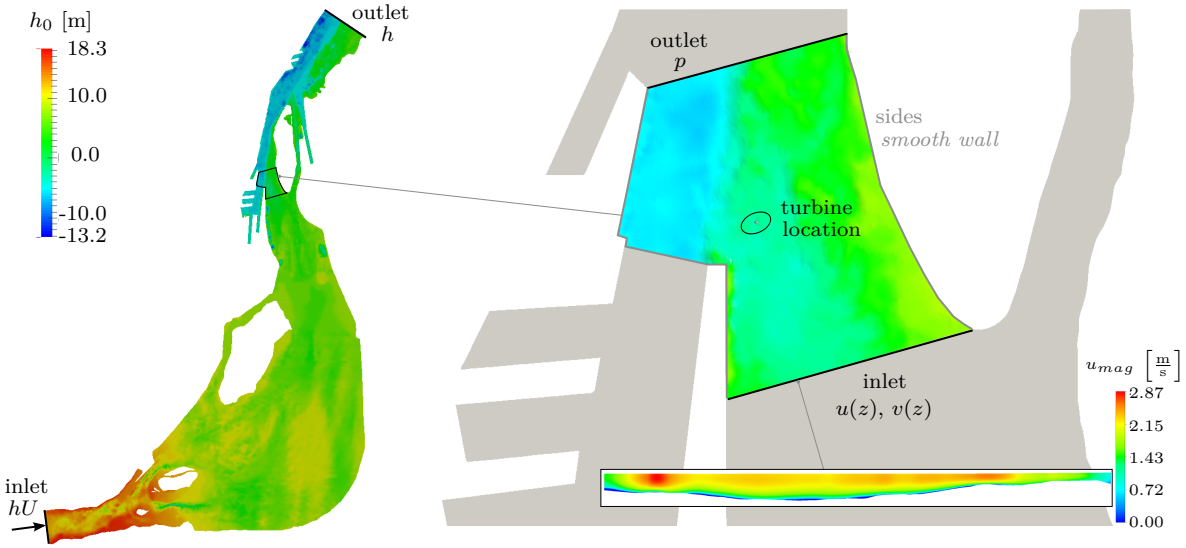

(a) 2D model **(b)** 3D model

Figure 7.4: Overview of the 2d and 3d setup and boundary conditions

Since the solution domain is tightly dimensioned, the distance from the inlet to the turbine location is not large enough for the flow to fully develop. Therefore, an appropriate velocity field must be specified at the inlet. For this purpose, the velocities in the respective cross section are extracted from the results of the 2d shallow water simulations. As those values are depth-averaged a realistic vertical velocity distribution is generated using Equation 6.6. The resulting velocity field at the inlet is shown in Figure 7.4b. At the outlet, a constant static pressure is defined. All channel side walls are defined as smooth wall. Furthermore, the turbulence is modeled through the SST-k-ω-model and steady state conditions are assumed.

A single rotor turbine and the GenIHS diffuser augmented turbine are investigated under those conditions. They are each arranged in a way that the rotor plane is normal to the flow direction, which is determined from an empty river simulation. The turbine is placed in the middle of the flow depth. Consequently, the axis of rotation is located in a height of 4.06 m above the river bed. The single rotor turbine is modeled using the actuator disk model (see Section 3.1). Also for the GenIHS turbine the rotor is modeled in this way, whereas the diffuser is geometrically resolved. The optimum operation point is determined simulating five operation points by varying the disk load.

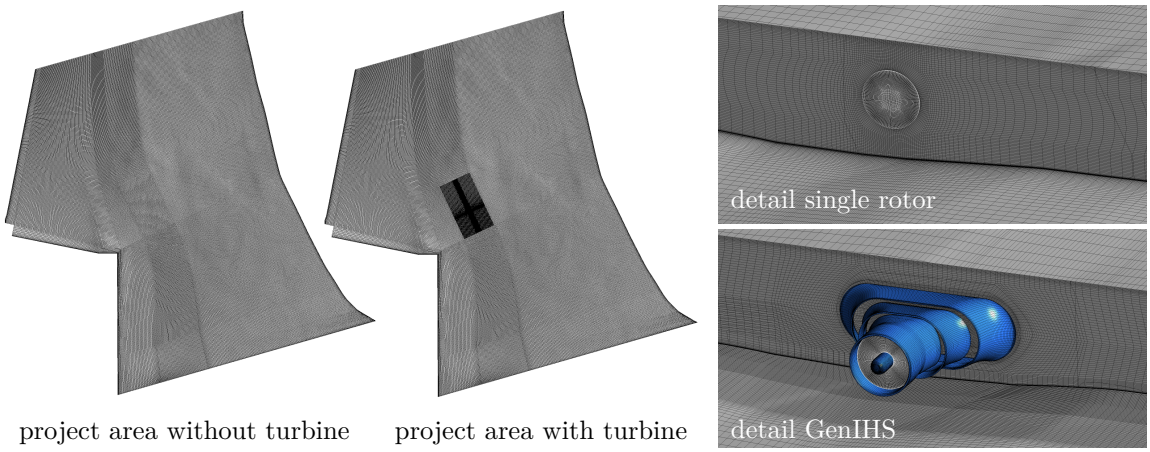

Figure 7.5: Block-structured hexahedral mesh for 3d simulations

The solution domain is discretized by a block-structured hexahedral mesh. For the empty channel simulations the meshes consist of 5.1 M cells. For the turbine simulations the vicinity of the turbines is highly resolved by a separate mesh and coupled to the main domain through GGI interfaces. This leads to a cell number of 8.2 M for the single rotor actuator disk simulations and 9.9 M for the GenIHS simulations. An impression on the different meshes is given in Figure 7.5.

7.4 Verification and Comparison of Numerical Models

The 2d shallow water model and the 3d model are verified through the ADCP velocity measurements. Consequently, for the 2d simulations a discharge of $Q = 10,000$ m^3/s is defined at the domain inlet. The inlet discharge in the 3d simulations resulting from the mapped velocity distribution is a bit lower ($Q = 8,947$ m^3/s) as the inlet cross section is located downstream of a junction where a part of the flow bypasses the main channel. This can be seen in Figure 7.4. The river section is modeled without considering a kinetic turbine in both the 2d and the 3d model.

Table 7.1: Comparison between simulation and measurement results for $Q = 10,000$ m^3/s

Station		h [m]	$\overline{u}_{mag}$ [m/s]	hU_{mag} [m^2/s]
1	**ADCP**	5.9	2.3	13.57
	2d Sim	6.4	1.49	9.54
2	**ADCP**	7.9	2.5	19.75
	2d Sim	6.9	2.13	14.70
	3d Sim	7.7	2.17	16.71
3	**ADCP**	9.2	2.8	25.76
	2d Sim	8.58	2.98	25.57
	3d Sim	8.26	3.12	25.77

The measurements of the velocity profiles in the three measurement stations are used as reference, whereby Station 1 is located outside the solution domain of the 3d model. In Table 7.1 significant deviations between the measurements and simulations for both the flow depth and the magnitude of the depth-averaged velocity can be observed. Also the agreement between those values in the 2d and the 3d model is insufficient in some cases.

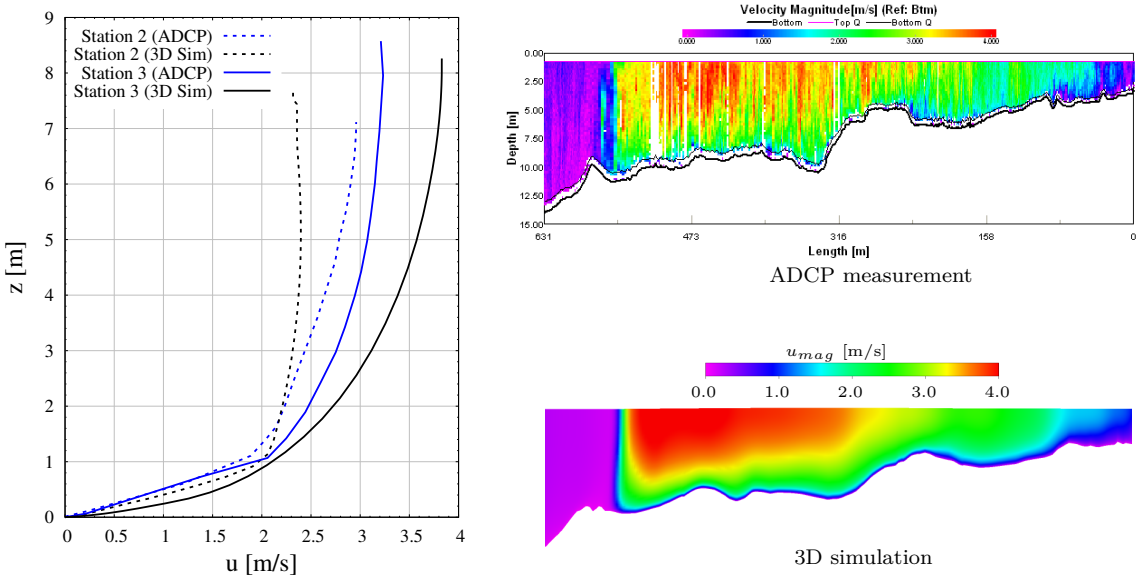

(a) Velocity profile at station 2 and 3

(b) Velocity distribution in section 12

Figure 7.6: Comparison of site measurements and 3d simulations for $Q = 10,000$ m^3/s

The deviations are probably caused by the fact that the exact locations of the stations are reconstructed from image maps which is relatively inaccurate (several meters). Due to the high gradients in river bed, even small deviations from the actual location can lead to significant deviations in flow depth and consequently velocity. Another source

of error is the different interpolation between the points of the bathymetry data in the 2d and the 3d model caused by different calculation meshes and mapping tools.

This explanation is supported by the fact that the specific discharge hU at least for station 2 and 3 is consistent. This can be seen from Table 7.1 and Figure 7.6a. The later shows that the vertical velocity distributions measured at the stations do not exactly match those determined in the 3d simulation. The 3d model overestimates the velocity at Station 3 whereas the flow depth is underestimated. For Station 2, the velocity is underestimated and the flow depth is only slightly underestimated.

Also a qualitative evaluation of the velocity distribution in several river cross-sections confirmed that both the 2d and the 3d models are generally capable of modeling the flow situation in the river. Figure 7.6b exemplary shows this for Section 12, which is closest to the turbine site. The resulting distributions in several further river sections can be found in the Appendix (Figure C.3).

7.5 Final Site Evaluation Montreal

With the verified models the 50% probability flow situation with a total river run-off of $Q = 8,500$ m^3/s is investigated. This leads to a discharge of $Q = 7,032$ m^3/s at the inlet for the 3d simulations. Three scenarios are simulated with both the 2d and the 3d model: the empty river without a turbine, one single rotor turbine and one GenIHS turbine with the same rotor diameter of 4 m each placed at the current turbine location. The latter simulations allow an evaluation of the turbine models under realistic conditions. Finally, the 2d model is applied to find a convenient arrangement for five GenIHS turbines at the Montreal project area and to determine the power output of this turbine park.

7.5.1 Empty River Simulations

For the empty river simulation no turbine is considered similar to the verification simulations presented in previous section. The resulting flow field for the entire solution domain is presented in Figure 7.7 showing the magnitude of the depth-averaged velocity and the local flow depth. It can be observed that the current turbine location is a good choice as high flow velocities occur in this region. The only other region in the investigated area where similar velocities occur over a large area is further upstream close to the domain inlet. However, project planning is not possible there for legal reasons.

A more detailed impression of the 2d simulation results in the direct vicinity of the turbine site is given in Figure 7.8a. Figure 7.9a shows the results from the corresponding 3d simulations. The flow fields of the 2d and the 3d simulations cannot be directly compared as the 2d results show the magnitude of the depth-averaged velocity whereas the 3d results show the magnitude of the local velocity in a horizontal plane at the elevation of the turbine rotor axis.

Table 7.2: Comparison between 2d and 3d empty river simulation at current turbine site

	h [m]	$\overline{u}_{mag}$ [m/s]	β [°]
2d	8.13	3.021	21.74
3d	8.13	2.945	25.45

In Table 7.2 the results of the 2d and the 3d simulations at the current turbine site are compared. It can be seen that the flow depth totally agrees, which was to be expected, since the domain height in the 3d simulation is a result of the 2d simulation. Also the resulting magnitude of the depth-averaged flow velocity corresponds very well. Only the direction of the flow provided as flow angle shows larger deviations. They are probably a result of 3d flow effects caused by strong gradients in the river bed which cannot be resolved by the 2d simulations.

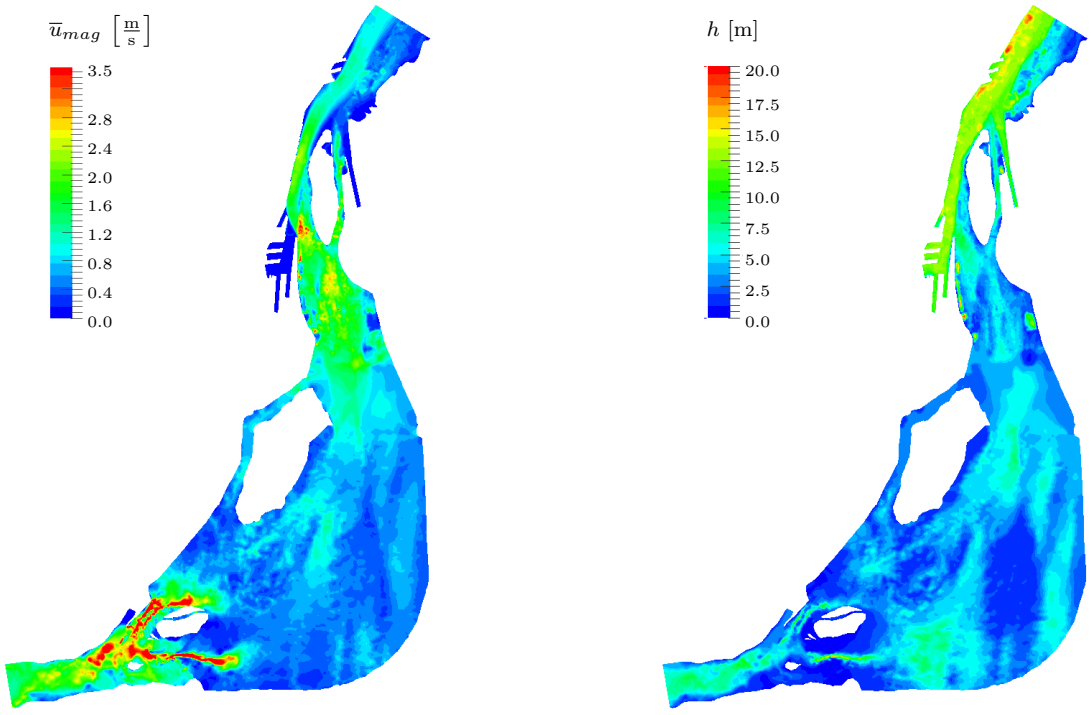

(a) Depth-averaged flow velocity **(b)** Local flow depth

Figure 7.7: Results for 2d simulations at $Q = 8,500$ m^3/s

7.5.2 Single Rotor Turbine at the Current Turbine Site

The results of the investigations of a single rotor turbine at the current turbine site are provided in Table 7.3. It can be noted that the power and thrust predicted by the turbine model in the 2d simulation correspond quite well with the results of the 3d simulation. Both values are only slightly overestimated by the turbine model.

The turbine model also provides a very accurate prediction of the upstream undisturbed velocity (u_∞ = 2.96 m/s). For the dramatic reduction of the effort in model setup and computational time, the observed deviation of around 6% in performance data is acceptable.

Table 7.3: Comparison of 2d and 3d simulation of a single rotor turbine at the current site

	P [kW]	T_R [kN]
2d	150.20	76.82
3d	141.73	72.16

Comparing the resulting flow fields of the 2d and the 3d simulation in Figure 7.8b and 7.9b it can be observed that the turbine wake flow seems to be more developed in the 3d simulations. The main reason for this obvious deviation is that the resulting 2d flow field is depth-averaged whereas the 3d results are provided as local velocity at the elevation of the turbine hub and therefore fully resolve the turbine wake flow. However, a detailed analysis shows that the turbine wake flow is indeed more developed in the 3d model: The ratio of the local wake velocity to the velocity from the empty river simulations at the same location (around 50 m downstream of the turbine) is 0.85 for the 3d simulation whereas for the 2d a value of 0.93 is determined. Besides the neglected turbulent and 3d effects this underestimation of the turbine wake can also be caused by the very coarse mesh resolution used for the 2d simulations which has a diffusive effect on the flow. Consequently, for investigating an arrangement of multiple kinetic turbines in series where the wake flow has a relevant impact on the performance, the present model may provide significantly inaccurate results. Both, the general underestimation of the wake flow and the smearing of the downstream stream tube through the depth-averaging, results in the turbine facing an incorrect velocity. In general, however, the results of the 2d simulation are very satisfactory.

7.5.3 GenIHS Turbine at the Current Turbine Site

Also for the investigation of the GenIHS diffuser augmented turbine at the current turbine site, it can be observed that the power and the rotor and diffuser thrust are overestimated in the 2d simulation in comparison to the 3d simulation (see Table 7.4). In this case the overestimation of the upstream undisturbed velocity is partly responsible for this: The depth-averaged velocity predicted by the turbine model is u_∞ = 3.00 m/s whereas the empty river 3d simulation provides a value of 2.95 m/s. This explains a deviation in power of around 5%.

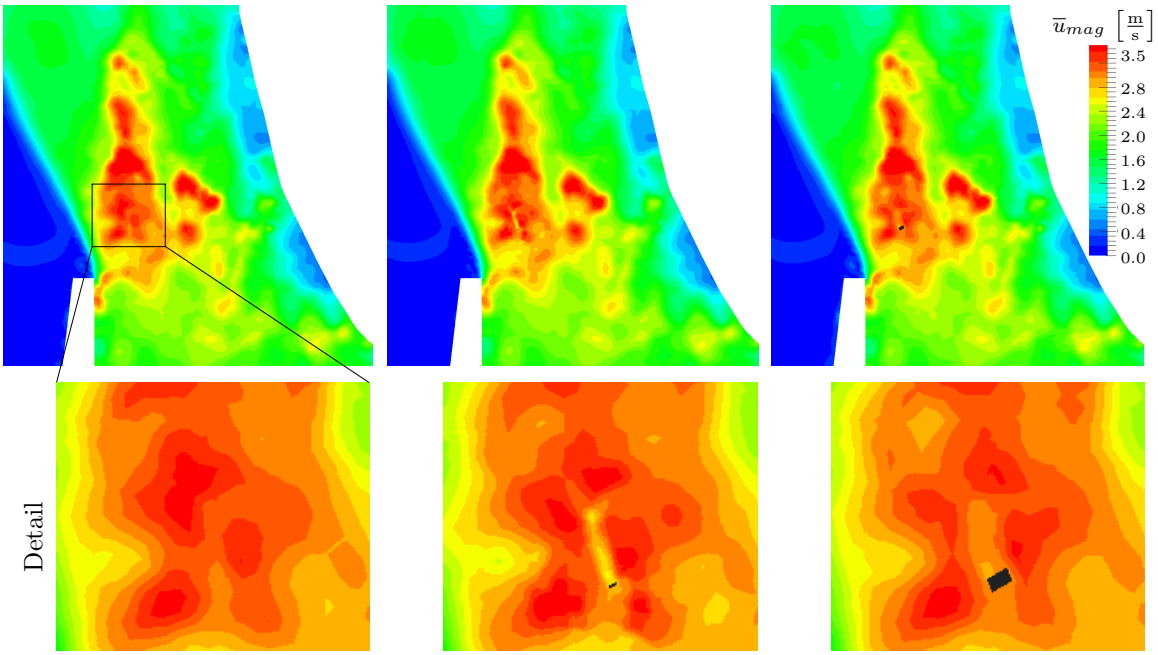

(a) empty channel (b) single rotor turbine (c) GenIHS turbine

Figure 7.8: Depth-averaged flow field resulting from 2d simulations

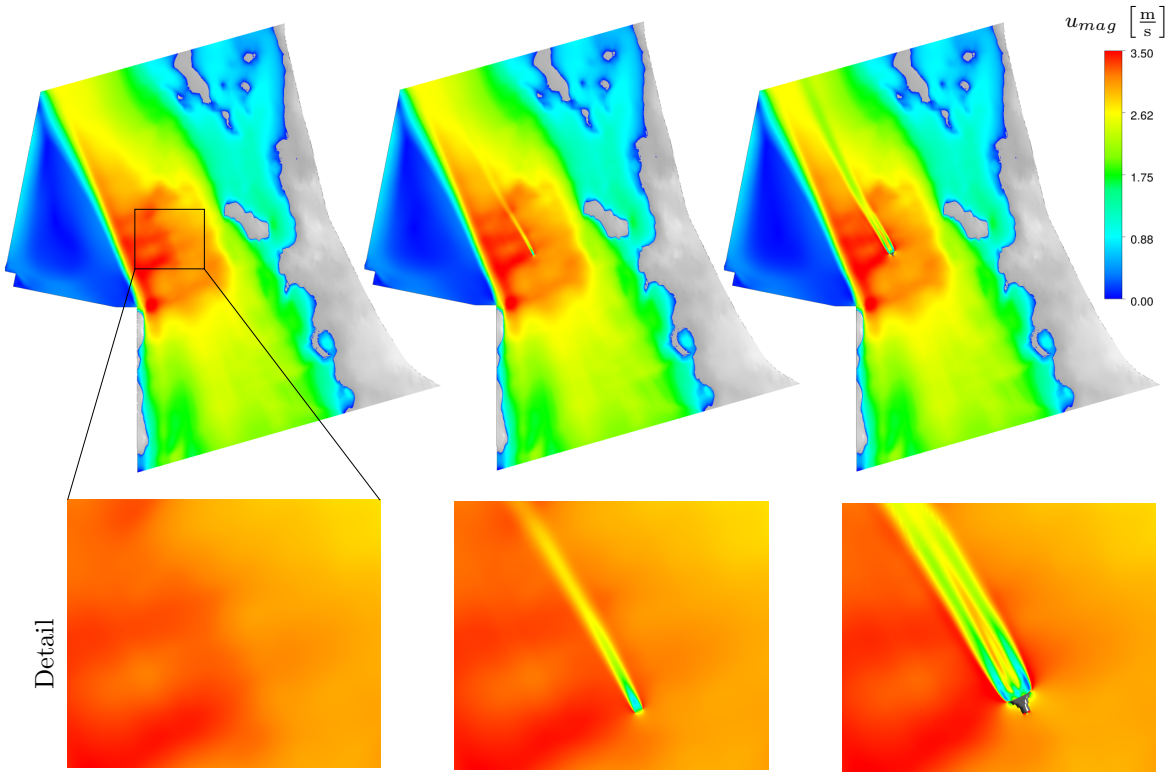

(a) empty channel (b) single rotor turbine (c) GenIHS turbine

Figure 7.9: Flow field in horizontal plane in turbine hub height resulting from 3d simulation

Regarding the resulting flow field from the 3d simulations in Figure 7.9c it is obvious at first glance that the wake flow of the GenIHS turbine is much more developed and also much longer compared to the wake flow of the single rotor turbine. This results from the increased energy extraction and is an important observation with regard to turbine park arrangements. The considerations on the turbine wake flow in the 2d simulations described in the previous section are also valid for the GenIHS turbine model.

Table 7.4: Comparison between 2d and 3d simulation of a GenIHS turbine at the current site

	P [kW]	T_R [kN]	T_{total} [kN]
2d	371.93	75.74	386.53
3d	337.40	70.18	336.70

A comparison of the energy yield of the GenIHS machine with that of a single rotor turbine of the same height shows that the GenIHS machine can generate about 2.4 times more power. However, the power is provided by the solver as hydraulic power in both turbine models. For a final evaluation, the blade and generator efficiency would each have to be considered. In the end, it is a matter of economic considerations whether to use one GenIHS turbine or two to three single rotor turbines to yield the same amount of energy at this site.

7.5.4 Investigation of a Park Arrangement of GenIHS Turbines

The GenIHS turbine model is now applied to estimate the power output of a turbine park consisting of five machines in the project area of Montreal. A minimum flow depth of 7.5 m is specified as condition for a potential turbine location.

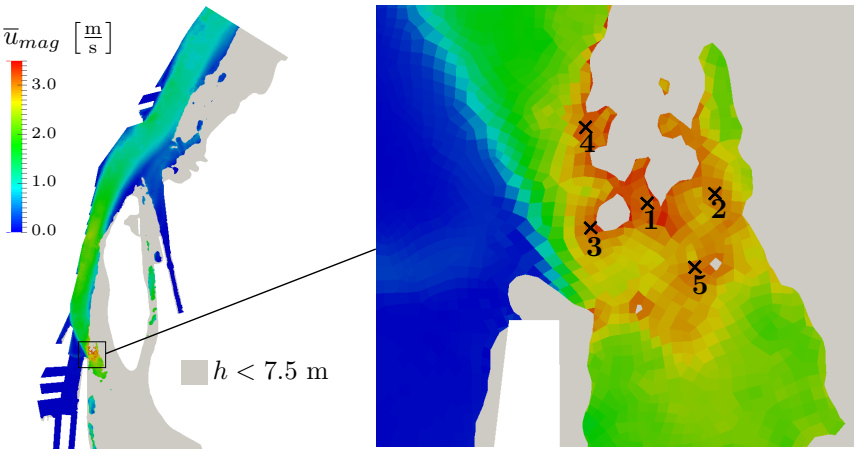

(a) Eligible locations (b) Selected sites for five turbines

Figure 7.10: Selection of sites for a turbine park

For a machine height of around 4.0 m a sufficient distance to the water surface (surface waves, fluctuations in water level) but also to the bottom (sediment transport, low velocity) is ensured when placing the machine in the middle of the channel height.

Table 7.5: Results of the turbine park simulation in the Montreal project area

turbine	P [kW]	T_R [kN]	T_{total} [kN]	$\overline{u}_\infty$ [$\frac{m}{s}$]	UTM-coordinates
1	356.10	73.57	375.46	2.99	613858, 5040469
2	367.89	75.48	385.25	2.96	613924, 5040479
3	394.16	78.87	402.53	3.06	613802, 5040445
4	378.60	76.17	389.14	3.00	613797, 5040545
5	333.40	70.98	361.96	2.90	613904, 5040407

Figure 7.10a shows the flow velocity at locations satisfying this condition resulting from the empty river simulations (Section 7.5.1). It is obvious that the region around the current turbine site is an ideal location as high flow velocities occur at a sufficient flow depth. Therefore, the current turbine location is further maintained for the turbine park (turbine 1). In addition, four further positions are identified considering the highest occurring flow velocities. The resulting sites are marked in Figure 7.10b and the corresponding coordinates are provided in Table 7.5. For each of the turbines a hub height of 4.0 m is assumed.

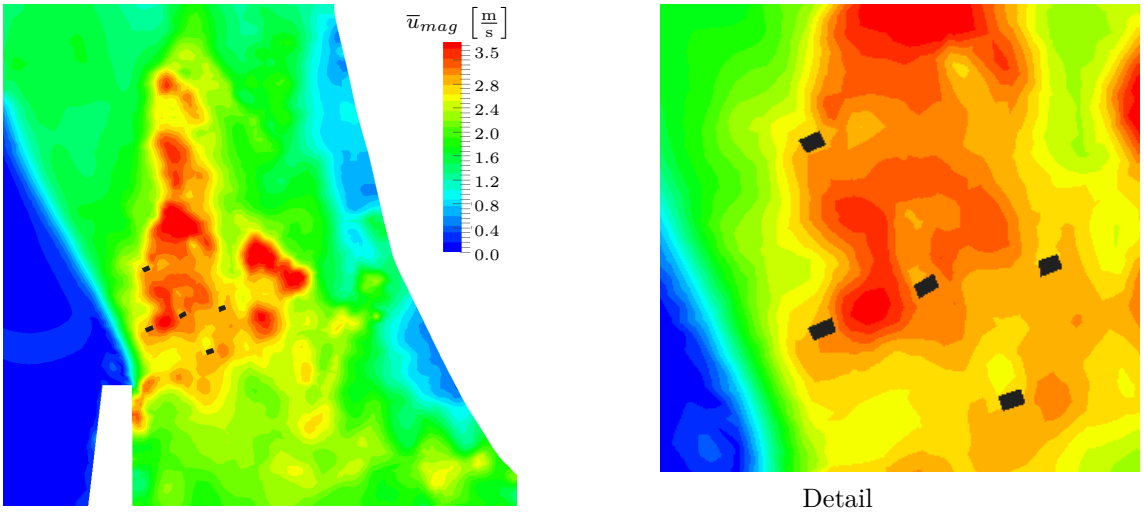

Figure 7.11: Resulting flow field for the turbine park arrangement

The results of the 2d simulations are presented in Table 7.5 and Figure 7.11. It can be observed that turbine 1 is partly in the wake flow of turbine 5. This explains the reduction in power for turbine 1 compared to the simulation of a single GenIHS turbine at the current site. In sum the five diffuser augmented turbines gain a hydraulic power of around 1.83 MW in this arrangement. This value is determined for the

50% probability discharge, but due to the extensive channel dimensions local flow velocities were observed to be nearly independent from the discharge. This suggests that throughout an entire year the energy production is expected to remain relatively constant at this level. Assuming an uncertainty of the 2d model of 10% and considering the blade efficiency which is determined to 0.9 in Section 4.2.2, the resulting power is still 1.48 MW. This could supply around 635 Canadian households[1] with electricity.

[1] Assuming a annual electricity consumption of 20.4 MWh per household in Quebec published by *Statistics Canada Table 25-10-0060-01 Household energy consumption, Canada and provinces*

8 Discussion

The presented work provides a fundamental overview of various aspects of diffuser augmented turbines and their application in rivers. However, there are some approaches and results which need to be critically reflected. This includes substantial simplifications made in the numerical modeling, as well as the applicability and transferability of the developed turbine model. Furthermore, the general sense of purpose for an application of diffusers around kinetic turbines is discussed.

8.1 Limitations of Numerical Models

All investigations in this work are based exclusively on numerical simulations which are a mathematical description of reality and therefore a potential subject to errors. For the complex and extensive flow situations, several simplifications in both the geometrical and the physical modeling are necessary in order to keep the computational effort reasonable.

For example, the actuator disk model is used for many of the investigations to simulate the pressure drop over the rotor. The blade geometry is not resolved and thus effects such as flow separation at the blades, downstream swirl and tip vortices are neglected. This simplification are especially relevant for the investigation of single rotor turbines, where the rotor is not shrouded. For the diffuser augmented turbine GenIHS, this error is observed to be rather small. It is shown that the assumption of steady state flow conditions has a larger impact on the result.

Another uncertainty is the treatment of turbulence. Although the two-equation model applied in this work is state of the art in numerical flow simulation, it is possibly not ideal to correctly resolve the turbine wake flow. Therefore, especially with regard to the investigation of site influences where turbulent effects are observed to play a major role, the quality of the results may be limited. However, hybrid RANS/LES-methode based simulations, which are increasingly being used to investigate wake flows in wind power, would be too extensive for the number of investigations performed in this work due to high Reynolds-numbers.

For the same reason, also the consideration of the free water surface e.g. using the VoF-method is neglected in the 3d site simulation. Therefore, local deformations of the water surface caused by the kinetic turbines are not resolved. However, a part of the effect is considered by the pressure difference upstream and downstream of the turbine, which is developing for a non-realistic solid water surface in the 3d model.

Regarding especially the results from the investigation of diffuser attributes, it can be observed that the applied numerical models are valid, since the results agree

well with the various data from the literature. Also the consistency of numerical results and theoretical approach for the investigation of the blockage effect indicates a fundamental validity of the numerical 3d investigations.

Due to the reduction of model dimensions, even more simplifications are necessary for the 2d shallow water simulations. Especially the neglection of the vertical velocity components causes a deviation for large gradients in the river bed elevation. Also the available data (e.g. exact location and bathymetric data) are rather imprecise and poorly resolved in some cases. However, the great advantage for these investigations is that measurement data for calibration and validation are available. This means that the reliability of the model is evaluated and in this case is generally confirmed.

In general, solid numerical models are applied in this work which are capable of identifying the most important effects and phenomena related to kinetic turbines and their application in rivers with reasonable effort.

8.2 Considerations on Diffuser Augmentation

In this work, the hydraulic properties of numerous different diffusers are investigated. It is shown that they often have a lower power coefficient than a single rotor turbine of the same projected machine area. However, some well designed geometries achieve efficiencies beyond the Betz limit. Therefore, the general suitability of diffusers for kinetic turbines besides the known advantages and disadvantages has to be evaluated.

From the investigations of attributes of diffuser augmented turbines it can be observed that they are very sensitive to flow separations. This means that for a poor design or minor errors or uncertainties in the design process the resulting diffuser geometry is not working properly and major stagnation zones in the diffuser occur. This leads to a dramatically low diffuser power coefficient. Especially diffusers with large area ratio and no BLC concept are potentially affected. Therefore, from a sole hydraulic point of view and for a very large flow field, it may be more appropriate to increase the rotor diameter and give up the concept of diffuser augmentation to generate the same or even more power output (in this considerations the suppression of the tip vortex by the diffuser is neglected). Only very compact concepts with small area ratio like the wind-lens presented by Ohya and Karasudani [70] where the entire diffuser acts basically as spoiler and the single stage diffuser V3 developed in this work or well designed multi-stage concepts like the one presented by Ruprecht and Reinhardt [85] provide reliably stable flow conditions.

Another argument against the use of extensive diffusers is that, depending on the area ratio and detailed shape, the diffusers induce a large drag, which leads to high requirements in terms of stability and mounting. This again results in high costs. Also for multi-stage diffusers high costs caused by the complex design have to be considered when evaluating a possible application.

The situation is different for sites with limited flow depth, such as rivers or some shallow tidal channels, where the rotor diameter cannot arbitrarily be increased. At

such sites, non-circular diffusers offer the possibility to increase the projected machine area to the side and thus increase the power. The implementation of a large area ratio can also be useful if a multi-stage concept is applied. However, it must always be taken into account that only somewhat lower diffuser power coefficients are achieved for non-circular diffusers compared to rotationally symmetric geometries or single rotor turbines. The diffuser has a further advantage when located in rivers: it protects the rotor from damage by larger debris.

Finally, also for river sites it is an economic decision whether to install one diffuser augmented turbine or multiple single rotor turbines in parallel at the chosen site. It must be weighted between the manufacturing, transport and installation costs of a large diffuser and the costs for additional turbines including generators, bearings, and so forth.

It can be concluded that a fundamental decision for or against a diffuser augmentation of kinetic turbines cannot be made in general as it significantly depends on parameters such as the turbine location, design specifications and the costs for individual components.

8.3 Considerations on the Advanced Turbine Model

The advanced turbine model developed in this work consists of the single rotor model and the GenIHS DAT model. The verifications show a comparatively high accuracy for the single rotor model. It is universally applicable without further investigations and can be used to estimate the power of different single rotor turbines independent from their detailed turbine geometry at various sites. Only the vertical velocity profile occurring in the project area has to be described mathematically. The turbine specific blade efficiency can be considered in post processing to calculate the net power output. The site effects considered in the model are determined in extensive 3d simulations and turned out to be quite complex. Accepting a lower accuracy, the model can also be simplified significantly, e.g. by describing the blockage effect only through the theory provided by Garrett and Cummins and neglecting the influence of the channel aspect ratio. Also the influence of sheared flow conditions besides the choice of the correct reference velocity can be neglected.

For the GenIHS model, basically the same applies. However, it is only valid for the GenIHS turbine and cannot be transferred to other diffuser geometries. This is a problem, because the studies which are necessary to create such a model are very extensive. In order to describe other diffuser augmented turbines the whole process described in this work has to be repeated. At first, the characteristic diffuser attributes at the optimum operation point have to be predicted in an infinitely large flow field. Then the influence of the site effects on the machine must be investigated, since they cannot be described by the correlations determined for the GenIHS turbine. To reduce

the effort, it would be possible also in this case, to neglect the influence of the channel aspect ratio and the sheared flow effects.

The effort is only justified if a large number of the same turbine type has to be arranged and evaluated. This can be the case for a park arrangement or individual machines at many different locations. For an investigation of only a few diffuser augmented turbines it is preferable to directly use a 3d numerical model. For this problem, also a 2d-3d coupling between the macroscopic surrounding river and the turbine resolved in detail could be an interesting approach.

In addition to the model construction, there are other aspects of the advanced turbine model that need to be discussed. The model is very sensitive regarding the dimensions of the turbine cell which has to be roughly the size of the modeled machine. This is most likely caused by 2d blockage effects in limited cross sections. Furthermore, in case that the modeled situation cannot be described with the LMADT, the upstream undisturbed velocity cannot be correctly determined using the assumption that the machine thrust in the 3d model is equal to that in the 2d model. The problem occurs when modeling sheared flow conditions for single rotor turbines and limited channel cross sections or sheared conditions for diffuser augmented turbines.

The problem can only be solved by either adjusting the formula for the determination of the upstream undisturbed velocity or correcting the drag in the turbine cell accordingly. Due to the extremely complex correlations (e.g. the fact that the blockage effect strongly depends on the respective drag in the turbine cell) the first approach cannot be implemented in practice. In this work, the drag in the turbine cell is therefore adjusted in a way that the model can reliably determine the upstream undisturbed velocity, which is essential for predicting the turbine performance. However, it has to be kept in mind that this approach violates the global momentum and energy balance regarding the energy extraction by the turbine(s). This can influence the correct determination of the river water level. For the single rotor model the deviation is quite small, but for diffuser augmented turbines the total turbine thrust can be more than twice as large as the turbine thrust the solver is working with. In this case, the results for large turbine parks have to be interpreted with care. Also the underestimation of the turbine wake flow leads to a lower reliability of the model when turbines are placed in a row.

Despite the outlined limitations and problems, especially the single rotor turbine model can reliably predict the turbine performance. Also the GenIHS model can be applied for isolated machines or small parks.

9 Conclusion and Outlook

Hydrokinetic turbines are conventionally installed in tidal currents. This means that the environment is characterized by a very large flow field and single rotor turbines are applied. However, there is an unexploited potential for an application of hydrokinetic turbines in rivers. These sites are exceptional as in many cases a low flow depth and a highly sheared flow occur. Using diffuser augmented turbines the projected machine area can be increased by opening the diffuser to the sides. In this way, the power gained at a site can also be increased. Based on those considerations the multi-stage diffuser augmented turbine GenIHS was developed in a previous work.

The main objective of this work was to develop a turbine model which is able to represent the GenIHS turbine in 2d shallow water solvers. Furthermore, the influence of the specific site characteristics had to be considered in the model. An existing turbine model could be used as basis for this. It was originally developed for conventional tidal applications, which means that it is only valid for single rotor turbines in very large flow fields.

For the logical structure of the advanced turbine model a fundamental understanding of the basic working principle of diffuser augmented turbines is essential. A special approach in this work was to use the projected area of the entire machine as reference for the evaluation, not the commonly used rotor area. Based on this, a theoretical approach to the problem was derived analogues to the Linear Momentum Actuator Disk Theory identifying the thrust on the outer diffuser walls as main restriction for a fully analytical solution. However, a visualization of the derived equations shows a promising range where high diffuser power coefficients are theoretically possible. Furthermore, a clear dependency on the diffuser area ratio is visible.

To get a more practical idea of the working principle of diffuser augmented turbines, a number of different diffusers was investigated using numerical flow simulations. The numerical results were combined with reevaluated data from literature providing an extensive data base. The most significant result was that the maximum achievable diffuser power coefficient is decreasing with increasing area ratio between projected diffuser and rotor area. This is in accordance with the derived theory. Using the concept of boundary layer control the significance of the correlation was found to be decreasing. Furthermore, the simulations showed that for non-circular diffusers the limit for the maximum diffuser power coefficient seems to be lower. However, the flow situation at diffuser augmented turbines are too complex to derive a generally valid model only based on geometric data. Therefore, a semi-empirical approach based on several clearly defined input data like the diffuser power coefficient, the corresponding induction factor and the thrust ratio were chosen for a mathematical description in the

turbine model. Those values have to be determined in 3d numerical flow simulations of the entire machine in a very large flow field.

The most relevant site effects to be considered for hydrokinetic river turbines are the channel blockage effect and the sheared flow conditions caused by bed roughness effects. The theoretical approach describing the blockage effect predicts an increasing power coefficient for an increasing channel blockage. This could generally be confirmed by the respective numerical simulations of a single actuator disk in quadratic channel cross sections. However, the channel aspect ratio has an influence on this correlation. Furthermore, for diffuser augmented turbines in general but also among different diffuser geometries a deviating sensitivity to limited flow conditions could be observed. In the turbine model, different turbine types must therefore be treated separately. Regarding the sheared flow conditions, a large part of the vertical velocity distribution can be considered by the correct choice of reference velocity. It was found that for both, single rotor and GenIHS turbines, a depth-averaged velocity over the turbine height provides good results. Besides the velocity distribution, a further influence on the turbine performance was observed, which is probably caused by the increased turbulence in highly sheared flow.

The results of the investigated issues were used to develop the advanced turbine model by describing them mathematically and considering them for the determination of the drag coefficient in the turbine cell. It was observed that the model is strongly influenced by the 2d blockage effect. Therefore, it is very sensitive to the size of the turbine cell and the 2d thrust in the turbine cell must be manipulated for scenarios where the modeled problem is not based on LMADT to achieve the correct deceleration of the flow. This leads to a limited applicability of the model for large turbine parks. However, verifications through 3d simulations modeling a stand-alone single rotor and a GenIHS turbine in academic test channels but also at a realistic site provided good results. The final GenIHS model was applied for an evaluation of a park arrangement of five turbines at a potential project area. The simulation predicts a hydrokinetic power of 1.8 MW for a 50% probability discharge in the river. This example shows that there is indeed an usable potential for a comparatively uncomplicated and profitable utilization of hydropower. The developed turbine model can be applied to evaluate this potential for different project areas and identify the most promising sites and turbine arrangements.

Outlook

In large parts of this work, the very simple actuator disk model was used to represent the rotor. Furthermore, the applied turbulence model for the 3d simulations is very basic. For the investigated site effects, which turned out to be sensitive to turbulence and turbine wake flow, it would therefore be appropriate to at least randomly evaluate the accuracy of the results through simulations using a blade resolved rotor and a more advanced turbulence model. Moreover, the interactions between the kinetic turbine and the free water surface were neglected in the 3d simulations. This also offers potential for a systematic investigation.

With regard to the 2d site investigation, this work showed that the model developed for single rotor turbines and for the GenIHS machine can be directly applied for different sites. However, the model is not directly transferable to other diffuser augmented turbines. In order to integrate a further turbine into the existing model, many complex investigations are necessary. To solve the multiple scale problem and perform site evaluations with reasonable effort, it might be useful to implement a 2d-3d coupling. In this way the turbine geometry and its immediate environment could be fully resolved directly, while the wider surroundings could further be modeled by the 2d shallow water model.

Bibliography

[1] Amaral, S.; Jacobson, P.; Giza, D.: Survival and behavior of fish interacting with hydrokinetic turbines, 9^{th} ISE Vienna, 2012

[2] Anderer, P.; Dumont, U.; Heimerl, S.; Ruprecht, A.; Wolf-Schumann, U.: *Potenzialermittlung für den Ausbau der Wasserkraftnutzung in Deutschland als Grundlage für die Entwicklung einer geeigneten Ausbaustrategie*, Tech. Rep., Studie im Auftrag des Bundesministeriums für Umwelt, Naturschutz und Reaktorsicherheit, Berlin, 2010

[3] ANSYS CFX,: *Version 19.2, ANSYS CFX-solver theory guide*, Tech. Rep., ANSYS Inc., Canonsburg, PA, 2016

[4] Anyi, M.; Kirke, B.: Evaluation of small axial flow hydrokinetic turbines for remote communities, *Energy for Sustainable Development*, 14(2):110–116, 2010

[5] Aqua Libre Energieentwicklungs GmbH,: *Strom-Boje-3*, `http://www.aqualibre.at/DE/hauptmenue/strom-boje-3/strom-boje-3.html`, visited on 2021-07-27, 2021

[6] Aqua Libre GmbH,: *Die Strom-Boje*, `https://www.strom-boje.at`, visited on 2021-07-27, 2021

[7] Bahaj, A.; Molland, A.; Chaplin, J.; Batten, W.: Power and thrust measurements of marine current turbines under various hydrodynamic flow conditions in a cavitation tunnel and a towing tank, *Renewable energy*, 32(3):407–426, 2007

[8] Bartl, J.; Mühle, F.; Schottler, J.; Sætran, L.; Peinke, J.; Adaramola, M.; Hölling, M.: Wind tunnel experiments on wind turbine wakes in yaw: effects of inflow turbulence and shear, *Wind Energy Science*, 3(1):329–343, 2018

[9] Bedard, R.: *Prioritized research, development, deployment and demonstration (RDD&D) needs: marine and other hydrokinetic renewable energy*, Tech. Rep., Electric power research institute, Palo Alto, CA, 2008

[10] Belloni, C.: *Hydrodynamics of ducted and open-centre tidal turbines*, Ph.D. Thesis, University of Oxford, Oxford, UK, 2013

[11] Betz, A.: Die Windmühlen im Lichte neuerer Forschung, *Naturwissenschaften*, 15(46):905–914, 1927

[12] Blackmore, T.; Myers, L.E.; Bahaj, A.S.: Effects of turbulence on tidal turbines: Implications to performance, blade loads, and condition monitoring, *International Journal of Marine Energy*, 14:1–26, 2016

[13] Blocken, B.; Stathopoulos, T.; Carmeliet, J.: CFD simulation of the atmospheric boundary layer: wall function problems, *Atmospheric Environment*, 41(2):238 - 252, 2007

[14] Bomhof, J.: *Estimating Flow, Hydraulic Geometry, and Hydrokinetic Power at Ungauged Locations in Canada*, Ph.D. Thesis, University of Ottawa, 2014

[15] Bontempo, R.; Manna, M.: Effects of the duct thrust on the performance of ducted wind turbines, *Energy*, 99:274–287, 2016

[16] Burton, T.: *Wind Energy Handbook*, vol. 2. edition, Wiley, ISBN 978-0-470-69975-1, 2011

[17] Cada, G.F.; Bevelhimer, M.: *Attraction to and avoidance of instream hydrokinetic turbines by freshwater aquatic organisms*, Tech. Rep., Oak Ridge National Laboratory, Oak Ridge, Tennessee, 2011

[18] Cada, G.F.; Bevelhimer, M.S.; Riemer, K.P.; Turner, J.W.: *Effects on freshwater organisms of magnetic fields associated with hydrokinetic turbines*, Tech. Rep., Oak Ridge National Laboratory, Oak Ridge, Tennessee, 2011

[19] Coles, D.; Blunden, L.; Bahaj, A.: Experimental validation of the distributed drag method for simulating large marine current turbine arrays using porous fences, *International journal of marine energy*, 16:298–316, 2016

[20] Coles, D.; Blunden, L.; Bahaj, A.: Assessment of the energy extraction potential at tidal sites around the Channel Islands, *Energy*, 124:171–186, 2017

[21] Cresswell, N.; Ingram, G.; Dominy, R.: The impact of diffuser augmentation on a tidal stream turbine, *Ocean engineering*, 108:155–163, 2015

[22] De Vries, O.: *Fluid dynamic Aspects of Wind Energy Conversion*, Tech. Rep., Advisory Group for Aerospace Research and Development, Neuilly-Sur-Seine, France, 1979

[23] Del Rio, J.A.S.; Mancilla, C.C.C.; Zuluaga, D.A.H.; Arrieta, E.L.C.: A Numerical Simulation of Horizontal Axis Hydrokinetic Turbine with and without Augmented Diffuser, *International Journal of Renewable Energy Research*, 8(4):1833–1839, 2018

[24] Dighe, V.V.; Avallone, F.; Igra, O.; Bussel, G.v.: Multi-element ducts for ducted wind turbines: a numerical study, *Wind Energy Science*, 4(3):439–449, 2019

[25] Dighe, V.V.; Avallone, F.; Tang, J.; van Bussel, G.: Effects of gurney flaps on the performance of diffuser augmented wind turbine, in: 35^{th} *Wind Energy Symposium*, p. 1382, 2017

[26] Dighe, V.V.; de Oliveira, G.; Avallone, F.; van Bussel, G.J.: Characterization of aerodynamic performance of ducted wind turbines: A numerical study, *Wind Energy*, 22(12):1655–1666, 2019

[27] Dixon, D.; Bedard, R.: *Assessment of waterpower potential and development needs*, Tech. Rep., Electric power research institute, Palo Alto, CA, 2007

[28] Draper, S.; Houlsby, G.; Oldfield, M.; Borthwick, A.: Modelling tidal energy extraction in a depth-averaged coastal domain, *IET renewable power generation*, 4(6):545–554, 2010

[29] Ferro, V.; Baiamonte, G.: Flow velocity profiles in gravel-bed rivers, *Journal of Hydraulic Engineering*, 120(1):60–80, 1994

[30] Fleming, C.F.; McIntosh, S.C.; Willden, R.H.J.: Tidal turbine performance in sheared flow, in: 10^{th} *European Wave and Tidal Energy Conference*, 2014

[31] Foreman, K.M.; Gilbert, B.L.: *Further investigations of diffuser augmented wind turbines. Part I and II. Executive summary. Final report*, Tech. Rep., Grumman Aerospace Corp., Bethpage, NY (USA). Research Dept., July 1979

[32] Franca, M.J.; Ferreira, R.M.; Lemmin, U.: Parameterization of the logarithmic layer of double-averaged streamwise velocity profiles in gravel-bed river flows, *Advances in Water Resources*, 31(6):915–925, 2008

[33] Gaden, D.L.; Bibeau, E.L.: A numerical investigation into the effect of diffusers on the performance of hydro kinetic turbines using a validated momentum source turbine model, *Renewable Energy*, 35(6):1152–1158, 2010

[34] Garrett, C.; Cummins, P.: The efficiency of a turbine in a tidal channel, *Journal of Fluid Mechanics*, 588:243–251, 2007

[35] Gilbert, B.; Foreman, K.: Experiments with a diffuser-augmented model wind turbine, *Journal of Energy Resources Technology*, 105(47), 1983

[36] Gilbert, B.L.; Foreman, K.M.: Experimental demonstration of the diffuser-augmented wind turbine concept, *Journal of Energy*, 3(4):235–240, 1979

[37] Gilbert, B.L.; Oman, R.A.; Foreman, K.M.: Fluid dynamics of diffuser-augmented wind turbines, *Journal of Energy*, 2(6):368–374, 1978

[38] Göltenbott, U.; Ohya, Y.; Yoshida, S.; Jamieson, P.: Aerodynamic interaction of diffuser augmented wind turbines in multi-rotor systems, *Renewable Energy*, 112:25–34, 2017

[39] Government of Canada,: *St. Lawrence River: changes in the wetlands*, `https://www.canada.ca/en/environment-climate-change/services/st-lawrence-river/increase-decrease-wetlands.html`, visited on 2020-08-29, Nov 2017

[40] Grassmann, H.; Bet, F.; Ceschia, M.; Ganis, M.: On the physics of partially static turbines, *Renewable Energy*, 29(4):491–499, 2004

[41] Güney, M.; Kaygusuz, K.: Hydrokinetic energy conversion systems: A technology status review, *Renewable and Sustainable Energy Reviews*, 14(9):2996–3004, 2010

[42] Hansen, M.O.L.; Sørensen, N.N.; Flay, R.: Effect of placing a diffuser around a wind turbine, *Wind Energy: An International Journal for Progress and Applications in Wind Power Conversion Technology*, 3(4):207–213, 2000

[43] Hau, E.: Windmühlen und Windräder, in: *Windkraftanlagen*, pp. 1–22, Springer, 1996

[44] Hjort, S.; Larsen, H.: A multi-element diffuser augmented wind turbine, *Energies*, 7(5):3256–3281, 2014

[45] Houlsby, G.; Draper, S.; Oldfield, M.: Application of linear momentum actuator disc theory to open channel flow, January 2008

[46] Hydro-Energie Roth GmbH,: *Das bewegliche Wasserkraftwerk*, `https://hydroenergie.de/bewegliche-wka`, visited on 2020-08-05, 2009

[47] Igra, O.: Israeli Work on Aerogenerator Shrouds, in: *Wind Workshop*, vol. 2, pp. 149–55, 1975

[48] Igra, O.: Shrouds for aerogenerators, *AIAA Journal*, 14(10):1481–1483, 1976

[49] Igra, O.: Compact shrouds for wind turbines, *Energy conversion*, 16(4):149–157, 1977

[50] Johnson, J.B.; Pride, D.J.: *River, Tidal, and Ocean Current Hydrokinetic Energy Technologies: Status and Future Opportunities in Alaska*, Tech. Rep., Alaska Center for Energy and Power, 2010

[51] Joly, A.; Pham, C.T.; Andreewsky, M.; Saviot, S.; Fillot, L.: Using the DRAGFO subroutine to model Tidal Energy Converters in Telemac-2D, in: *Telemac User Club 2015*, 2015

[52] Karsten, R.; Swan, A.; Culina, J.: Assessment of arrays of in-stream tidal turbines in the Bay of Fundy, *Philosophical Transactions of the Royal Society A: Mathematical, Physical and Engineering Sciences*, 371(1985):20120189, 2013

[53] Karsten, R.H.; McMillan, J.; Lickley, M.; Haynes, R.: Assessment of tidal current energy in the Minas Passage, Bay of Fundy, *Proceedings of the Institution of Mechanical Engineers, Part A: Journal of Power and Energy*, 222(5):493–507, 2008

[54] Khan, M.; Bhuyan, G.; Iqbal, M.; Quaicoe, J.: Hydrokinetic energy conversion systems and assessment of horizontal and vertical axis turbines for river and tidal applications: A technology status review, *Applied Energy*, 86(10):1823–1835, 2009

[55] Kinsey, T.; Dumas, G.: Impact of channel blockage on the performance of axial and cross-flow hydrokinetic turbines, *Renewable energy*, 103:239–254, 2017

[56] Kolekar, N.; Banerjee, A.: Performance characterization and placement of a marine hydrokinetic turbine in a tidal channel under boundary proximity and blockage effects, *Applied Energy*, 148:121–133, 2015

[57] KSB AG,: *Flussturbinen am Netz*, `https://www.ksb.com/ksb-de/Presse_und_Aktuelles/Pressearchiv/2010-pressearchiv/flussturbinen-am-netz/117272/`, visited on 2020-09-09, 2010

[58] KSB AG,: *Kreiselpumpenlexikon-Flussturbine*, `https://www.ksb.com/kreiselpumpenlexikon/flussturbine/188278/`, visited on 2020-09-09, 2020

[59] Lalander, E.; Leijon, M.: In-stream energy converters in a river - Effects on upstream hydropower station, *Renewable energy*, 36(1):399–404, 2011

[60] Laws, N.D.; Epps, B.P.: Hydrokinetic energy conversion: Technology, research, and outlook, *Renewable and Sustainable Energy Reviews*, 57:1245–1259, 2016

[61] Lewis, R.; Williams, J.; Abdelghaffar, M.: A Theory and experimental Investigation of ducted Wind Turbines, *Wind Engineering*, 1(2):104–125, 1977

[62] Lilley, G.; Rainbird, W.: *A preliminary Report on the Design and Performance of Ducted Windmills*, Tech. Rep., College of Aeronautics Cranfield, 1956

[63] Loeffler Jr, A.; Steinhoff, J.: Computation of wind tunnel wall effects in ducted rotor experiments, *Journal of aircraft*, 22(3):188–192, 1985

[64] Mason-Jones, A.; O'Doherty, D.M.; Morris, C.E.; O'Doherty, T.; Byrne, C.; Prickett, P.W.; Grosvenor, R.I.; Owen, I.; Tedds, S.; Poole, R.: Non-dimensional scaling of tidal stream turbines, *Energy*, 44(1):820–829, 2012

[65] Mühle, F.; Rapp, C.; Mayer, O.: Experimentelle Untersuchungen an einem Wasserwirbel-Kraftwerk, *Wasserkraftprojekte Band II: Ausgewählte Beiträge aus der Fachzeitschrift WasserWirtschaft*, p. 172, 2014

[66] Münch-Alligné, C.; Richard, S.; Gaspoz, A.; Hasmatuchi, V.; Brunner, N.: New prototype of a kinetic turbine for artificial channels, in: *Advances in Hydroinformatics*, pp. 981–996, Springer, 2018

[67] Nishino, T.; Draper, S.: Local blockage effect for wind turbines, in: *Journal of Physics: Conference Series*, vol. 625, p. 012010, IOP Publishing, 2015

[68] Nishino, T.; Willden, R.H.: Effects of 3-D channel blockage and turbulent wake mixing on the limit of power extraction by tidal turbines, *International Journal of Heat and Fluid Flow*, 37:123–135, 2012

[69] Nishino, T.; Willden, R.H.: The efficiency of an array of tidal turbines partially blocking a wide channel, *Journal of Fluid Mechanics*, 708:596, 2012

[70] Ohya, Y.; Karasudani, T.: A shrouded wind turbine generating high output power with wind-lens technology, *Energies*, 3(4):634–649, 2010

[71] Ohya, Y.; Karasudani, T.; Sakurai, A.; Abe, K.i.; Inoue, M.: Development of a shrouded wind turbine with a flanged diffuser, *Journal of Wind Engineering and Industrial Aerodynamics*, 96(5):524–539, 2008

[72] Olsen, N.R.; Stokseth, S.: Three-dimensional numerical modelling of water flow in a river with large bed roughness, *Journal of Hydraulic Research*, 33(4):571–581, 1995

[73] Oman, R.; Foreman, K.; Gilbert, B.: *Investigation of diffuser-augmented wind turbines. Progress Report*, Tech. Rep., Grumman Aerospace Corp., Bethpage, NY (USA). Research Dept., 1975

[74] Oman, R.; Foreman, K.; Gilbert, B.: *Investigation of diffuser-augmented wind turbines. Part I and II. Executive summary*, Tech. Rep., Grumman Aerospace Corp., Bethpage, NY (USA). Research Dept., 1977

[75] Overhoff, G.; Keller, T.: Ökologische optimierte Wasserkraft-Innovationsvorhaben in Bayern, *Österreichische Wasser-und Abfallwirtschaft*, 67(7-8):292–298, 2015

[76] Pelz, P.; Metzler, M.: An analytic approach to optimize tidal turbine fields, in: *IOP Conference Series: Materials Science and Engineering*, vol. 52, p. 052019, IOP Publishing, 2013

[77] Phillips, D.; Flay, R.; Nash, T.: Aerodynamic analysis and monitoring of the Vortec 7 diffuser-augmented wind turbine, *Transactions of the Institution of Professional Engineers New Zealand: Electrical/Mechanical/Chemical Engineering Section*, 26(1):13, 1999

[78] Phillips, D.G.: *An Investigation on Diffuser Augmented Wind Turbine Design*, Ph.D. Thesis, ResearchSpace, Auckland, New Zealand, 2003

[79] Reinecke, J.: *Effect of an diffuser on the performance of an ocean current turbine*, Master's Thesis, Stellenbosch University, Matieland, South Africa, 2011

[80] Reinecke, J.; Von Backström, T.W.; Venter, G.: Effect of a Diffuser on the Performance of an Ocean Current Turbine, in: 9^{th} *European Wave and Tidal Energy Conference (EWTEC)*, 2011

[81] Riglin, J.; Carter III, F.; Oblas, N.; Schleicher, W.C.; Daskiran, C.; Oztekin, A.: Experimental and numerical characterization of a full-scale portable hydrokinetic turbine prototype for river applications, *Renewable Energy*, 99:772–783, 2016

[82] Ruopp, A.: *Optimierung von symmetrischen Gezeitenströmungsturbinen und deren Analyse in großräumigen Gezeitenströmungsgebieten*, Ph.d. Thesis, Institute of Fluid Mechanics and Hydraulic Machinery, University of Stuttgart, Oct 2016

[83] Ruopp, A.; Daus, P.; Biskup, F.; Riedelbauch, S.: Performance prediction of a tidal in-stream current energy converter and site assessment next to Jindo, South Korea, *Journal of Renewable and Sustainable Energy*, 7(6):061707, 2015

[84] Ruopp, A.; Ruprecht, A.; Riedelbauch, S.; Arnaud, G.; Hamad, I.: Development of a hydro kinetic river turbine with simulation and operational measurement results in comparison, in: *IOP Conference Series: Earth and Environmental Science*, vol. 22, p. 062002, IOP Publishing, 2014

[85] Ruprecht, A.; Reinhardt, H.: Development of a Maritime Current Turbine, in: *Proceedings of the ASME/JSME Joint Fluids Engineering Division Summer Meeting*, pp. 1871-1876, ASME, Hawaii,USA, July 2003

[86] Ruprecht, A.; Ruopp, A.: Entwicklung einer kinetischen Strömungsturbine, *WasserWirtschaft*, 101(10):34, 2011

[87] Rutschmann, P.; Sepp, A.; Geiger, F.; Barbier, J.: Das Schachtkraftwerk - ein Wasserkraftkonzept in vollständiger Unterwasseranordnung, in: *Wasserkraftprojekte*, pp. 286–291, Springer, 2013

[88] Schlichting, H.; Kestin, J.: *Boundary layer theory*, vol. 121, Springer, 1961

[89] Schluntz, J.; Willden, R.: The effect of blockage on tidal turbine rotor design and performance, *Renewable Energy*, 81:432–441, 2015

[90] Seidel, F.; Schultz, P.; Stadler, C.; Riedelbauch, S.; Nestmann, F.: Baden-Württembergisches Forschungsprojekt Wasserkraftschnecken und Fischabstieg, *WasserWirtschaft*, pp. 24–28, October 2017

[91] Seitz, A.C.; Moerlein, K.; Evans, M.D.; Rosenberger, A.E.: Ecology of fishes in a high-latitude, turbid river with implications for the impacts of hydrokinetic devices, *Reviews in Fish Biology and Fisheries*, 21(3):481–496, 2011

[92] Shives, M.; Crawford, C.: Developing an Empirical Model for Ducted Tidal Turbine Performance using numerical Simulation Results, in: *Proceedings of the Institution of Mechanical Engineers, Part A: Journal of Power and Energy*, vol. 226, pp. 112–125, SAGE Publications Sage UK: London, England, 2012

[93] Smagorinsky, J.: General circulation experiments with the primitive equations: I. The basic experiment, *Monthly weather review*, 91(3):99–164, 1963

[94] Smart Hydro Power GmbH,: *Smart Turbines*, `https://www.smart-hydro.de/renewable-energy-systems/hydrokinetic-turbines-river-canal/`, visited on 2021-07-27, 2021

[95] Sorensen, J.N.; Shen, W.Z.; Mikkelsen, R.: Wall correction model for wind tunnels with open test section, *AIAA Journal*, 44(8):1890–1894, 2006

[96] Stadler, C.; Wack, J.; Fraas, S.; Riedelbauch, S.: Development of an Adapted Turbine Model for Hydrokinetic Turbines in 2d Shallow Water Solvers, in: *IOP Conference Series: Earth and Environmental Science*, vol. 405, IOP Publishing, 2019

[97] Sutherland, G.; Foreman, M.; Garrett, C.: Tidal current energy assessment for Johnstone strait, Vancouver island, *Proceedings of the Institution of Mechanical Engineers, Part A: Journal of Power and Energy*, 221(2):147–157, 2007

[98] Tampier, G.; Troncoso, C.; Zilic de Arcos, F.: Numerical analysis of a diffuser-augmented hydrokinetic turbine, *Ocean engineering*, 145:138–147, 2017

[99] Tampier Brockhaus, G.; Zilic de Arcos, F.: Blade-resolved CFD analysis and validation of blockage correction methods for tidal turbines, in: *Advances in Renewable Energies Offshore: Proceedings of the 3rd International Conference on Renewable Energies Offshore (RENEW 2018), October 8-10, 2018, Lisbon, Portugal*, p. 137, CRC Press, 2018

[100] Ten Hoppen, P.: *An experimental and computational Investigation of a Diffuser Augmented Wind Turbine*, Master's Thesis, Delft University of Technology, Delft, The Netherlands, 2009

[101] Tismer, A.: *Entwicklung einer Softwareumgebung zur automatischen Auslegung von hydraulischen Maschinen mit Inselmodell*, Ph.d. Thesis, Institute of Fluid Mechanics and Hydraulic Machinery, University of Stuttgart, May 2020

[102] Van Bussel, G.J.: The science of making more torque from wind: Diffuser experiments and theory revisited., in: *Journal of Physics: Conference Series*, vol. 75, p. 012010, IOP Publishing, 2007

[103] Vennell, R.: Tuning turbines in a tidal channel, *Journal of fluid mechanics*, 663:253, 2010

[104] Vermaak, H.J.; Kusakana, K.; Koko, S.P.: Status of micro-hydrokinetic river technology in rural applications: A review of literature, *Renewable and Sustainable Energy Reviews*, 29:625–633, 2014

[105] Whelan, J.; Graham, J.; Peiro, J.: A free-surface and blockage correction for tidal turbines, *Journal of Fluid Mechanics*, 624:281–291, 2009

[106] Wu, Y.T.; Porté-Agel, F.: Atmospheric turbulence effects on wind-turbine wakes: An LES study, *energies*, 5(12):5340–5362, 2012

A Additional Information on Investigations of Site Effects

Table A.1 provides the detailed dimensions of the academic test channels used in Chapter 5 to evaulated the different site effects.

Table A.1: Dimensions of academic test channels

Channel	A_c [$\mathbf{m^2}$]	α [$-$]	B_c [m]	h_c [m]
Channel X1	4680.85	1	68.42	68.42
Channel X2	1560.28	1	39.50	39.50
Channel X3	936.17	1	30.60	30.60
Channel X4	468.08	1	21.64	21.64
Channel X5	234.03	1	15.30	15.30
Channel X6	114.68	1	10.71	10.71
Channel A1	4680.85	3	118.50	39.50
Channel A2	1560.28	3	68.42	22.81
Channel A3	936.17	3	53.00	17.67
Channel A4	468.08	3	37.47	12.49
Channel A5	234.04	3	26.50	8.83
Channel B1	4680.85	5	152.98	30.60
Channel B2	1560.28	5	88.33	17.67
Channel B3	936.17	5	68.42	13.68
Channel B4	468.08	5	48.38	9.68
Channel C1	4680.85	10	216.35	21.64
Channel C2	1560.28	10	124.91	12.49
Channel C3	936.17	10	96.76	9.68
Channel D1	4680.85	20	305.97	15.30
Channel D15	2632.98	20	229.48	11.47
Channel D2	1560.28	20	176.65	8.83

The following Figures A.1 to A.4 show the complete results of the investigation of the influence of the blockage effect on the diffuser augmented turbines V0, V3, NC1 and geometry presented by Ruprecht and Reinhardt [85]. As reference the theoretical correlations for single rotor kinetic turbines in rectangular channels derived by Garrett and Cummins [34] are included in all plots. Parts of the results are presented in Section 5.1.3 in a summarizing plot (Figure 5.4).

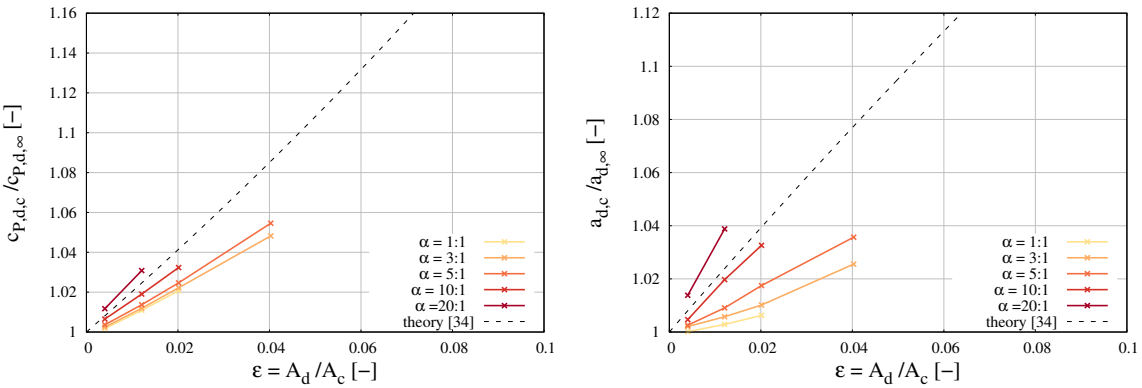

(a) power coefficient **(b)** induction factor

Figure A.1: Influence on V0 diffuser in different channel geometries

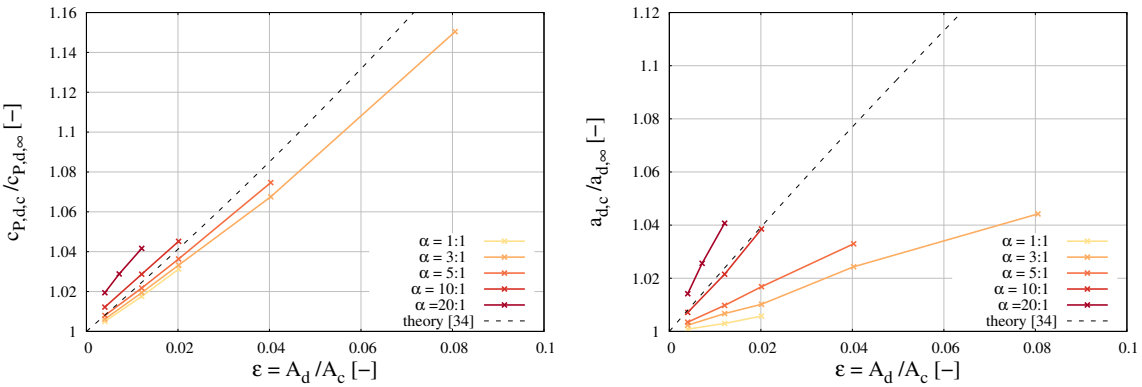

(a) power coefficient **(b)** induction factor

Figure A.2: Influence on V3 diffuser in different channel geometries

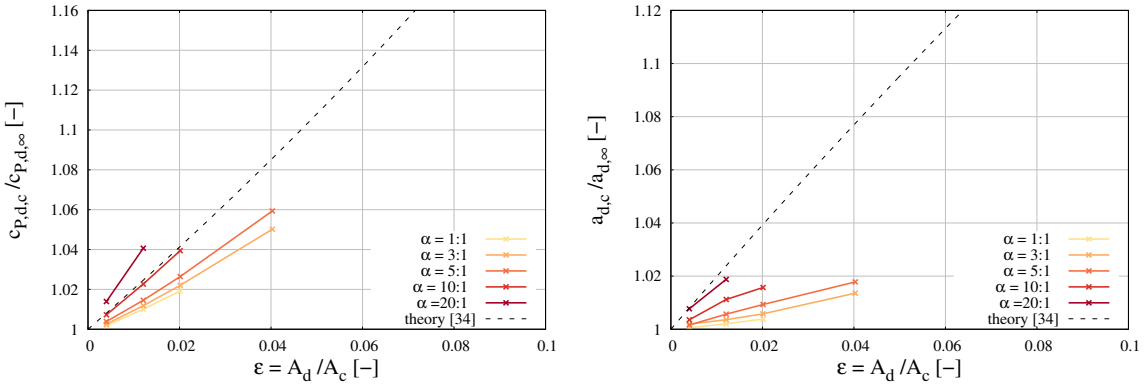

(a) power coefficient **(b)** induction factor

Figure A.3: Influence on NC1 diffuser in different channel geometries

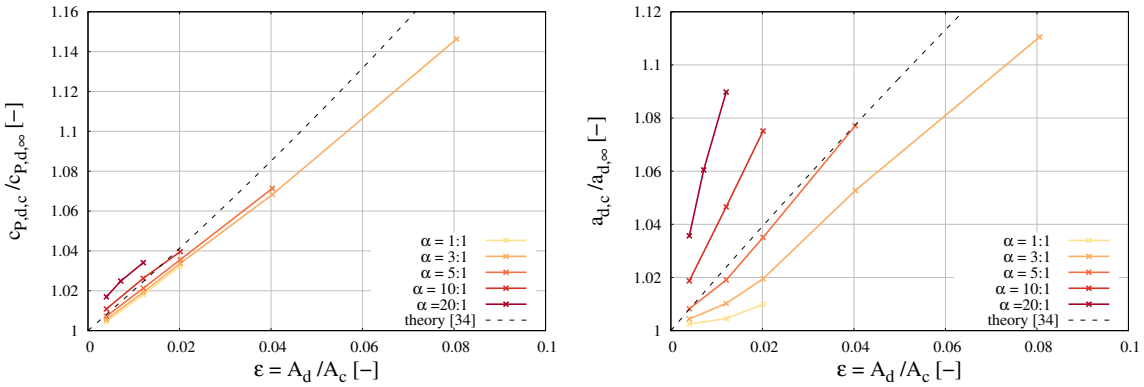

(a) power coefficient **(b)** induction factor

Figure A.4: Influence on Ruprecht's and Reinhardt's diffuser in different channel geometries

Table A.2 contains the constants h_{bed} and b applied for the generation of the different bed roughness scenarios in Section 5.2. Furthermore, the turbulence conditions for the fully developed profiles for different bed roughness conditions used as inlet boundary conditions are included. The turbulent inlet quantities are average values and are calculated from the nummerical simulations as follows:

Turbulence intensity I:

$$I = \frac{\left(\frac{2}{3}k\right)^{0.50}}{\overline{u}} \tag{A.1}$$

and turbulence length scale L:

$$L = \frac{k^{0.5}}{{C_\mu}^{0.25}\omega} \tag{A.2}$$

where k is the turbulent kinetic energy, ω is the turbulent eddy viscosity and $C_\mu = 0.09$ a constant defined in the turbulence model.

Table A.2: Roughness conditions and averaged turbulent inlet quantities for sheared flow channels

			Channel B2		**Channel D2**	
condition	$\boldsymbol{h_{bed}}$ **[m]**	$\boldsymbol{b}$ **[m]**	$\boldsymbol{I}$ **[%]**	$\boldsymbol{L}$ **[m]**	$\boldsymbol{I}$ **[%]**	$\boldsymbol{L}$ **[m]**
smooth	0.0	0.0	3.01	0.49	2.85	0.24
rough0	0.05	0.0005	6.51	0.62	6.76	0.32
rough1	0.16	0.005	8.00	0.71	8.95	0.40
rough2	0.5	0.05	10.97	0.92	13.16	0.54
rough3	0.7	0.1	12.24	1.00	14.87	0.59

Figure A.5 and A.6 show resulting flow fields for a single rotor turbine and the GenIHS turbine in channel B2 with varios bed roughness conditions. The corresponding results for channel D2 can be found in Figure 5.10 and 5.12.

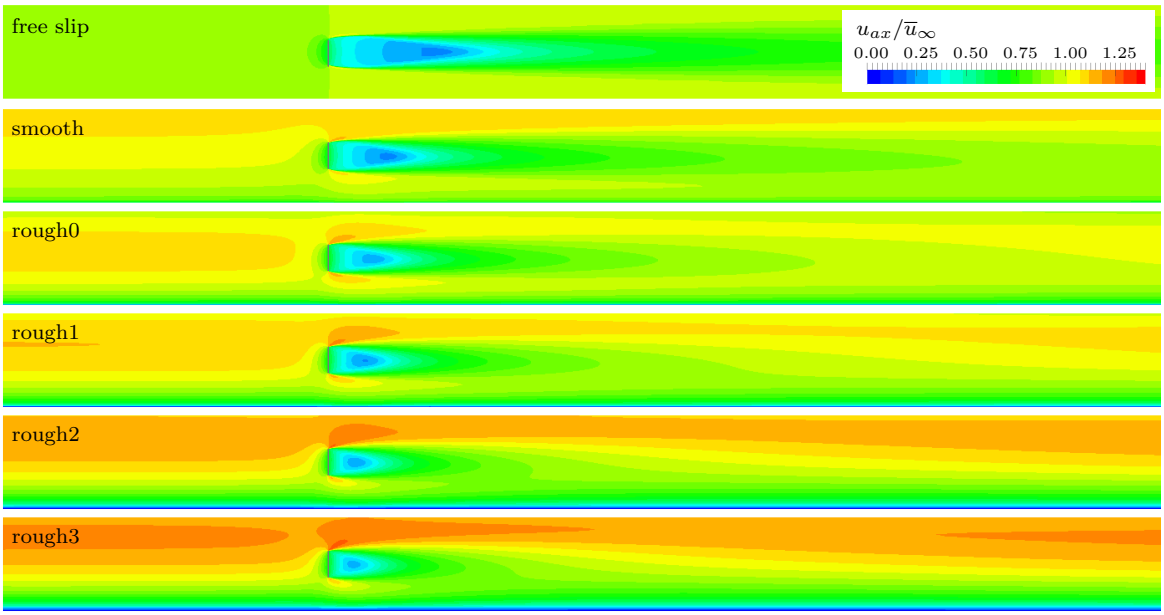

Figure A.5: Resulting flow fields for actuator disk in channel B2 with varying roughness

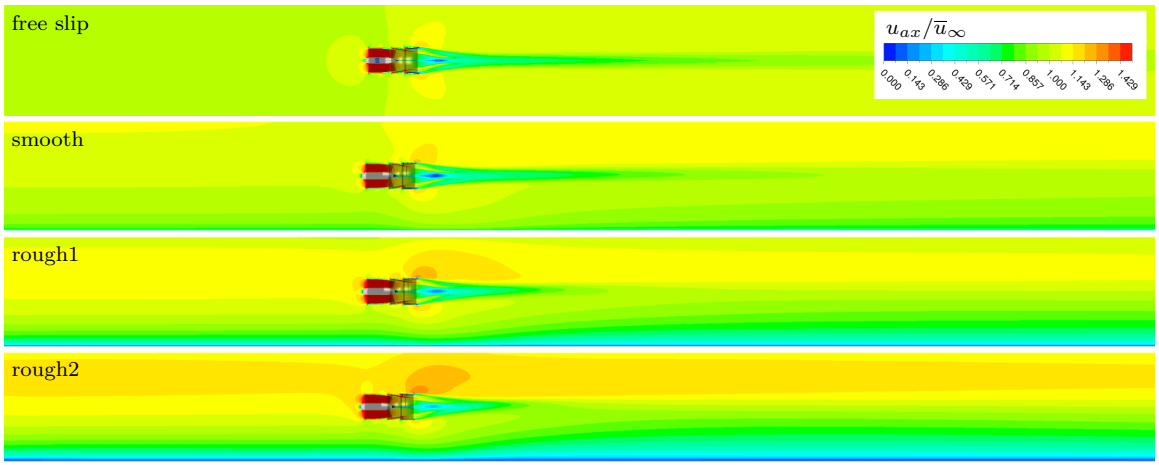

Figure A.6: Resulting flow fields for GenIHS in channel B2 with varying roughness

B Additional Information on Turbine Model

Figure B.1 shows the results for simulating a turbine through a fixed drag coefficient in the various academic channel geometries. It can be observed that for larger drag coefficients the velocity and thus the absolut drag in the turbine cell is highly depending on the the channel dimensions. This leads to the assumption that problems occuring in context of the dimensioning of the turbine cell are caused by the 2d blockage effect in the shallow water model.

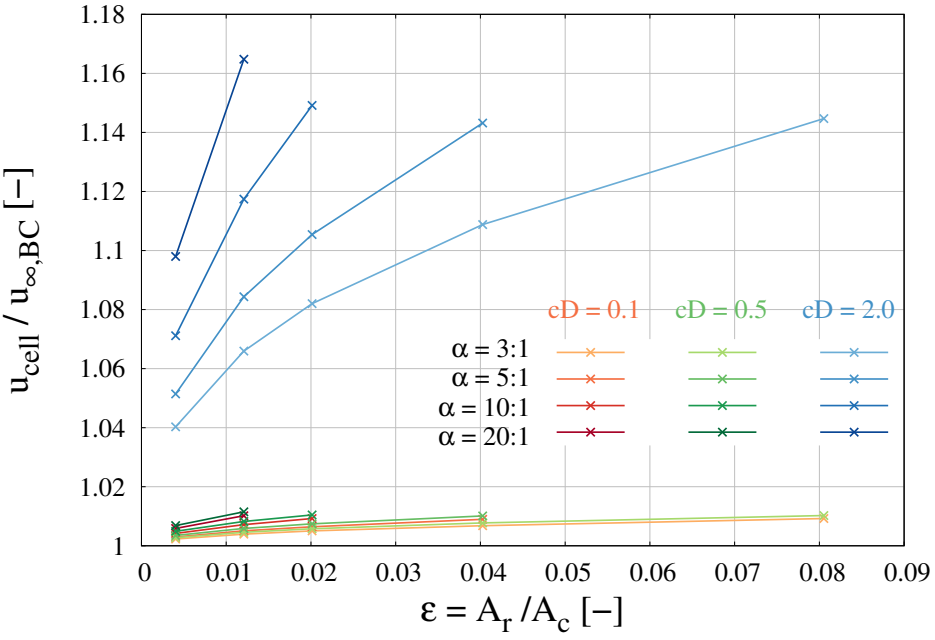

Figure B.1: Influence of channel dimensions on average velocity in turbine cell for different constant 2d drag coefficients

Listing B.1 provides the source code for the calculation of the correlation between velocity in the turbine cell u_{cell} and fictitious upstream undisturbed velocity $\overline{u}_{\infty}$ calculated by the solver for a sheared flow profile and the resulting determination of the upstream undisturbed velocity over the rotor height $\overline{u}_{t,\infty}$.

Listing B.1: Integration of disturbed velocity profile and correlation

```
//Integration boundaries
scalarField boundTup(cells_.size(), 0.0);
boundTup = (hhub_+Rtip_)/h;

scalarField boundTlow(cells_.size(), 0.0);
boundTlow = (hhub_-Rtip_)/h;

scalarField term1(cells_.size(), 0.0);
term1 = (-0.1 * pow(boundTlow,4.0)+0.13333* pow(boundTlow,3.0)+0.985*(boundTlow)
+ 0.215*(boundTlow) * log(boundTlow))
- (-0.1 * pow(VSMALL/h,4.0)+0.13333* pow(VSMALL/h,3.0) + 0.985*(VSMALL/h)
+ 0.215*(VSMALL/h) * log(VSMALL/h));

scalarField term2(cells_.size(), 0.0);
term2 = (-0.1 * pow(boundTup,4.0)+0.13333* pow(boundTup,3.0) + 0.985*(boundTup)
+ 0.215*(boundTup) * log(boundTup))
-(-0.1 * pow(boundTlow,4.0)+0.13333* pow(boundTlow,3.0)+0.985*(boundTlow)
+ 0.215*(boundTlow) * log(boundTlow));

scalarField term3(cells_.size(), 0.0);
term3 = (-0.1 * pow(h/h,4.0)+0.13333* pow(h/h,3.0) + 0.985*(h/h)
+ 0.215*(h/h) * log(h/h) )
- (-0.1 * pow(boundTup,4.0)+0.13333* pow(boundTup,3.0) + 0.985*(boundTup)
+ 0.215*(boundTup )* log(boundTup) );

//depth averaged upstream undisturbed velocity
scalarField U_Tinf0( mag(U) / (term1 + term2*(1.0-a) +term3)) ; // uncorrected
```

Figure B.1 and B.2 provide exemplary solver input files for the single rotor turbine model and the GenIHS turbine model. The files contain information on the channel or site as well as on the turbine.

Table B.1: Solver input data - single rotor turbine

Name	**Variable**	**Value**
Channel width	B_c	118.50 m
Channel cross section	A_c	4680.80 m^2
Hub height over bed	h_{hub}	4 m
Rotor radius	R_{tip}	2.45 m
Initial power coefficient	$c_{P,\infty}$	0.608
Initial induction factor	a_∞	0.35

Table B.2: Solver input data - GenIHS turbine (no considering struts, support structure and detailed blade geometry)

Name	**Variable**	**Value**
Channel width	B_c	118.50 m
Channel cross section	A_c	4680.80 m^2
Hub height over bed	h_{hub}	4 m
Diffuser exit area	A_d	46.7 m^2
Diffuser width	b_d	12.0 m
Diffuser height	h_d	4.0 m
Diffuser area ratio	γ	4.0
Initial diffuser power coefficient	$c_{P,d,\infty}$	0.43
Initial diffuser induction factor	$a_{d,\infty}$	0.224
Initial thrust ratio	τ_∞	0.224
Initial mass flow ratio	q_∞	1.95

C Additional Information on Site Evaluation

In the following different hydraulic data on the potential project area in Montreal are gathered. Figure C.1 shows the time resoled vertical velocity profile measured at three Stations in the potential project area in Montreal. The locations of the stations can be found in Figure 7.1c. Those data are used as basis for the sheared flow investigations.

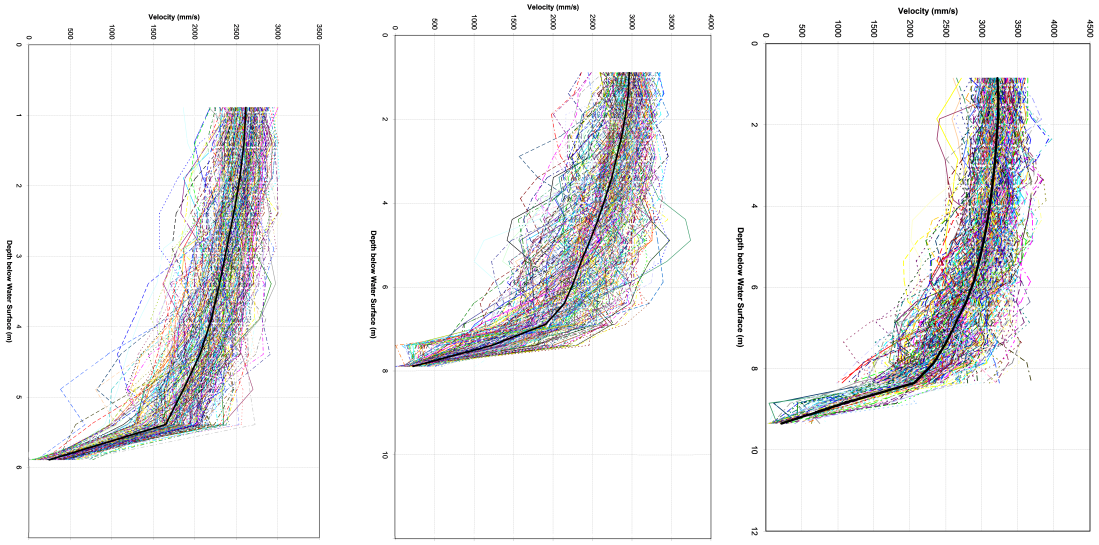

(a) Station 1 **(b)** Station 2 **(c)** Station 3

Figure C.1: Vertical velocity profiles gained from time resolved measurement at the potential project area in Montreal

Figure C.2 shows the annual duration curve for the river run-off of St. Lawrence River in the region of Montreal.

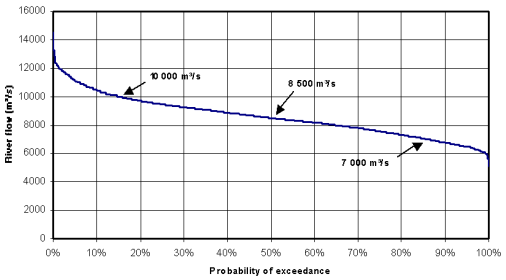

Figure C.2: Annual run-off duration curve of St. Lawrence River in Montreal

Figure C.3 provides ADCP measurements of the flow velocity in several river cross sections in direct comparison with the results of corresponding numerical flow simulation. The images supplement the results presented in Figure 7.6b.

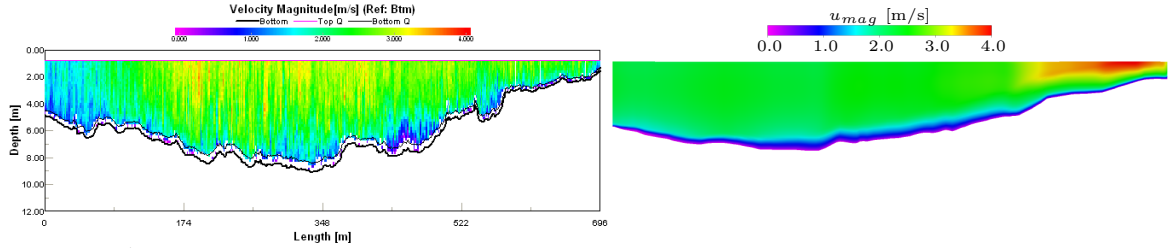

ADCP measurment 3D simulation

(a) Velocity distribution in Section10

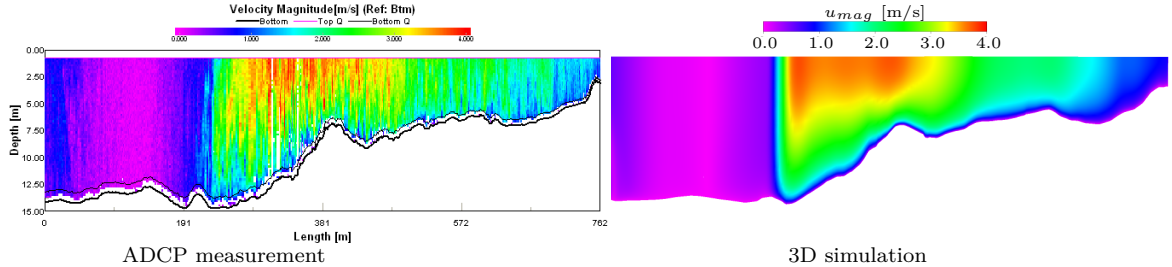

ADCP measurement 3D simulation

(b) Velocity distribution in Section11

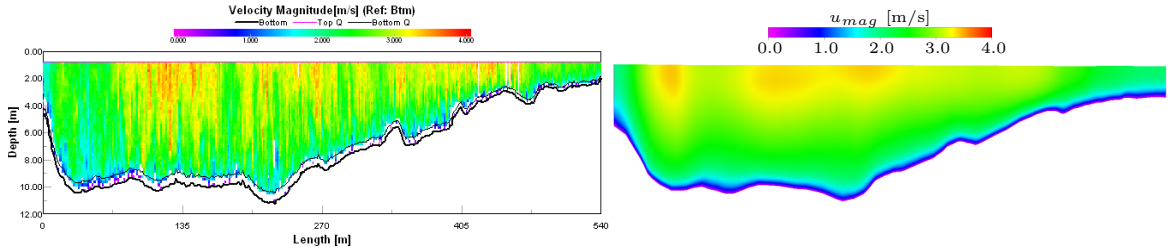

ADCP measurement 3D simulation

(c) Velocity distribution in Section13

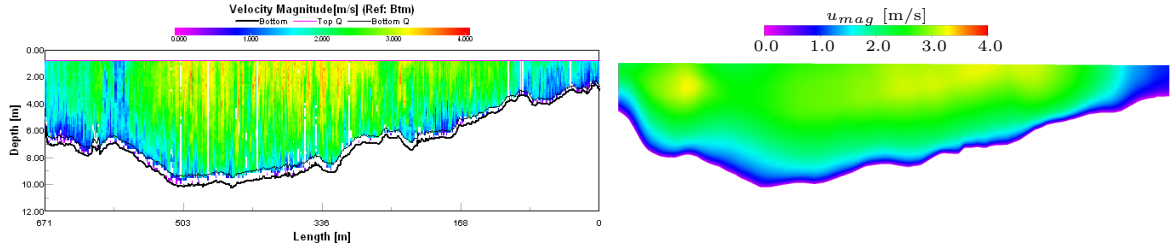

ADCP measurement 3D simulation

(d) Velocity distribution in Section14

Figure C.3: Comparison of ADCP measurements and 3d simulation results in several channel cross sections

D Additional Information on Investigation of GenIHS

During the GenIHS-design-process a mesh independence study was performed. The results are illustrated in Figure D.1. With regards to the large number of variants to be simulated with that mesh, the 13.5 M mesh was chosen to be of sufficient accuracy for this work, where the focus is more on getting a basic idea on different correlations than on a very exact prediction of the turbine performance. It can be seen, that this approach is conservative as, the turbine power is underestimated.

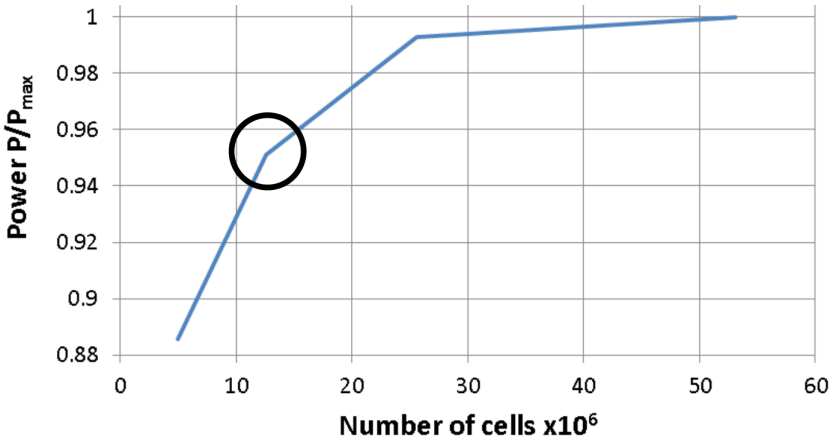

Figure D.1: Mesh independence study for the GenIHS geometry

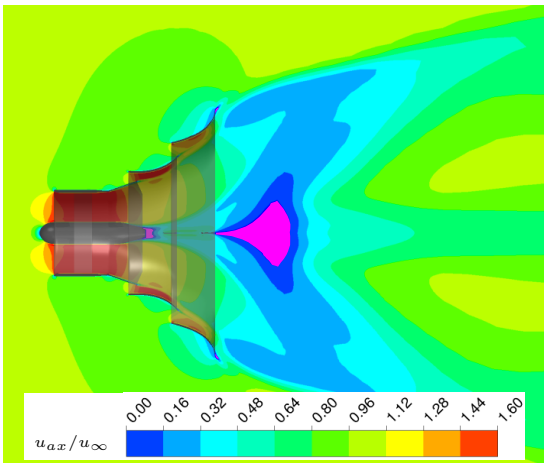

Figure D.2: Axial velocity field around GenIHS turbine in horizontal mid-plane (AD Approach)

Liste der bisher erschienenen IHS-Mitteilungen

Nr.	Jahr	Verfasser	Titel
1	1986		Beitrag zur 14. Sitzung des VDEW-Arbeitsausschusses „Meßmethoden in Wasserkraftanlagen”. ISBN 3-9802130-0-5
2	1989	Schneider, K. Eichinger, P.	Das Verhalten von Sicherheits-Drosselklappen. Modifikation des Standardcharakteristikenverfahrens zur Berechnung zeitlich zurückliegender Druckverläufe. ISBN 3-9802130-1-3
3	1989	Ruprecht, A.	Finite Elemente zur Berechnung dreidimensionaler, turbulenter Strömungen in komplexen Geometrien. ISBN 3-9802130-2-1
4	1990	Maurer, W.	Drehzahlregelung von Wasserturbinen mit Zustandsreglern. ISBN 3-9802130-3-X
5	1990	Acosta Del Carpio, H.	Das dynamische Verhalten von Kreiselpumpen niedriger spezifischer Drehzahl bei raschen Drehzahländerungen. ISBN 3-9802130-4-8
6	1990	Gronenberg, R.	Untersuchung des dynamischen Verhalten von Rückflußverhinderern unterschiedlicher Bauart. ISBN 3-9802130-5-6
7	1992	Eichinger, P.	Untersuchung des Reibungsverhaltens bei instationären Strömungsvorgängen in Rohrleitungen. ISBN 3-9802130-6-4
8	1993	Chihab, W. S.	Experimentelle und theoretische Untersuchung des Saugrohrs einer Kaplanturbine. ISBN 3-9802130-7-2
9	1994		Aktuelle Forschungsarbeiten des Instituts. ISBN 3-9802130-8-0
10	1994	Feyrer, R.	Kontinuierliche On-Line Berechnung der zulässigen Leistungsänderung in einem Pumpspeicherwerk. ISBN 3-9802130-9-9
11	1996	Zhang, Y.	Finite Elemente zur Berechnung instationärer Strömungen mit bewegten Wänden. ISBN 3-9804376-0-4
12	1997	Ginter, F.	Berechnung der instationären, turbulenten Strömung in hydraulischen Strömungsmaschinen. ISBN 3-9804376-1-2

Nr.	Jahr	Verfasser	Titel
13	1997		Beiträge zum Seminar „Kleinwasserkraft", Stuttgart, 10.10.97 ISBN 3-9804376-2-0
14	1998	Welzel, B.	Numerische Optimierung einer Axialturbine. ISBN 3-9804376-3-9
15	1999	Harbort, T.	Entwicklung eines echtzeitfähigen Simulationsprogramms zur Untersuchung instationärer Vorgänge in Wasserkraftwerken. ISBN 3-9804376-4-7
16	1999		Beiträge zum 2. Seminar „Kleinwasserkraft", Stuttgart, 01.10.99 ISBN 3-9804376-5-5
17	2000	Gentner, Ch.	Experimentelle und numerische Untersuchung der instationären Strömung in einer Axialturbine. ISBN 3-9804376-6-3
18	2000	Steibler, P.	Finite Element Methode zur numerischen Strömungsberechnung mit beliebigen Elementen. ISBN 3-9804376-7-1
19	2000	Lin, J.-C.	Überwachung von Wasserschlössern in Wasserkraftwerken mit Fuzzy-Control. ISBN 3-9804376-8-X
20	2000	Ott, Ch.	Entwurf und Simulation einer Staustufenregelung. ISBN 3-9804376-9-8
21	2001	Bauer, Ch.	Instationäre Berechnung einer hydraulischen Axialturbine unter Berücksichtigung der Interaktion zwischen Leit- und Laufrad. ISBN 3-9807322-0-7
22	2001	Liu, W.	Modeling of Swirling Turbulent Flows. ISBN 3-9807322-1-5
23	2002		Beiträge zum 3. Seminar „Kleinwasserkraft", Stuttgart, 05.10.01 ISBN 3-9807322-2-3
24	2001	Janetzky, B.	Ein Verfahren zur Berechnung instationärer Strömungen mit freier Oberfläche. ISBN 3-9807322-3-1
25	2002	Anz, R.	Systemidentifikation und Reglerselbsteinstellung in Wasserkraftanlagen. ISBN 3-9807322-4-X

Nr.	Jahr	Verfasser	Titel
26	2002	Maihöfer, M.	Effiziente Verfahren zur Berechnung dreidimensionaler Strömungen mit nichtpassenden Gittern. ISBN 3-9807322-5-8
27	2003		Beiträge zum 4. Seminar „Kleinwasserkraft“, Stuttgart, 19.09.03 ISBN 3-9807322-6-6
28	2003	Batrekhy, S.	Numerische und experimentelle Strömungsuntersuchungen an Rechen von Wasserkraftanlagen. ISBN 3-9807322-7-4
29	2005		Beiträge zum 5. Seminar „Kleinwasserkraft“, Stuttgart, 14.10.05 ISBN 3-9807322-8-2
30	2007	Helmrich, T.	Simulation instationärer Wirbelstrukturen in hydraulischen Maschinen. ISBN 978-3-9807322-9-1
31	2010	Lippold, F.	Zur Simulation von Fluid-Struktur-Wechselwirkungen mit flexiblen Kopplungsverfahren. ISBN 978-3-9812054-0-4
32	2011	Kirschner, O.	Experimentelle Untersuchung des Wirbelzopfes im geraden Saugrohr einer Modell-Pumpturbine. ISBN 978-3-9812054-1-1
33	2016	Ruopp, A.	Optimierung von symmetrischen Gezeitenströmungsturbinen und deren Analyse in großräumigen Gezeitenströmungsgebieten. ISBN 978-3-9812054-2-8
34	2016	Wang, H.	Very large eddy simulation for prediction of flow instabilities in turbomachinery. ISBN 978-3-9812054-3-5
35	2017	Neipp, A.	Ein- und zweistufige axiale Entspannungsturbine zur Energierückgewinnung. ISBN 978-3-9812054-4-2
36	2018	Stens, C.	Investigation of a fast transition from pump mode to generating mode in a reversible pump turbine. ISBN 978-3-9812054-5-9
37	2018	Krappel, T.	Turbulenzauflösende Strömungssimulation einer Francisturbine in Teillast. ISBN 978-3-9812054-6-6

Nr.	Jahr	Verfasser	Titel
38	2019	Schmidt, H.	Entwicklung eines Analyseverfahrens zur Kavitationsdetektion und Lokalisierung in hydraulischen Strömungsmaschinen. ISBN 978-3-9812054-7-3
39	2019	Schlipf, M.	Automatisierte Mehrzieloptimierung hydraulischer axialer Strömungsmaschinen. ISBN 978-3-9812054-8-0
40	2019	Brost, V.	Wiederaufbau des Stromnetzes mit einem Inselverbund aus Wasserkraftanlagen. ISBN 978-3-9812054-9-7
41	2019	Mössinger, P.	Numerische Untersuchung der Strömung bei transienten und instabilen Betriebszuständen von Francis-Turbinen. ISBN 978-3-9812054-00-9
42	2020	Tismer, A.	Entwicklung einer Softwareumgebung zur automatischen Auslegung von hydraulischen Maschinen mit dem Inselmodell. ISBN 978-3-948328-01-6
43	2020	Frey, A.	Untersuchung von periodischen und turbulenten Strömungsfluktuationen einer Francis-Turbine im Teillastbetrieb mit Laser-Doppler-Anemometrie. ISBN 978-3-948328-02-3
44	2020	Wack, J.	Numerical Investigation of the Full Load Instability in a Francis Turbine. ISBN 978-3-948328-03-0
45	2021	Hankeln, F.	Zur numerischen Berechnung des Betriebsverhaltens von Kreiselpumpen bei hydroabrasiver Erosion ISBN 978-3-948328-04-7
46	2022	Junginger, B.	Untersuchungen zum Einfluss des Laufradspalts einer schnellläufigen Axialturbine unter Verwendung skalenauflösender Turbulenzmodelle. ISBN 978-3-948328-05-4
47	2023	Junginger, J.	Feasibility of Transient Model Tests in a Closed-Loop Test Rig with the Example of a Reversible Pump Turbine. ISBN 978-3-948328-06-1

ISBN 978-3-948328-07-8